CELL-PHYSIOLOGICAL STUDY OF SALT TOLERANCE IN POACEAE

2021, September

TRAN THI HUONG SEN

Graduate School of Environmental and Life Science

(Doctor's Course)

OKAYAMA UNIVERSITY

DECLARATION

I hereby declare that my dissertation entitled:

"**CELL-PHYSIOLOGICAL STUDY OF SALT TOLERANCE IN POACEAE**"

has been composed by myself, that the work contained herein is my own except where explicitly stated otherwise in the text, and that this work has not been submitted for any other degree or processional qualification except as specified.

Parts of this work have been published in International Journal of Molecular Science.

Date

10th September 2021

Signature

Tran Thi Huong Sen

TABLE OF CONTENTS

CHAPTER 1

General introduction

Aquaporins (AQPs) are membrane channel proteins belonging to Major Intrinsic Protein (MIP) superfamily and present ubiquitously in all living organisms except thermophilic Archaea and intracellular bacteria (Afzal et al., 2016). They play an important role in plant water relations, in the transport of small neutral solutes, gasses, and metal ions. Plants contain the largest number and greatest diversity of aquaporin homologs with diverse tissue and subcellular localization patterns, gating properties, and solute specificity in all kingdoms of life. In saline conditions, excessive salt accumulation is detrimental to plant growth and limits crop productivity. This problem is often referred to as ionic toxicity, and for many cereals it is brought about by excessive Na^+ influx into roots followed by excess Na^+ accumulation, particularly in the aerial parts of the plants (Horie et al., 2012). Uptake of Na^+ at the root-soil boundary is conferred by multiple pathways involving a range of different types of membrane transporters and channels. The role of aquaporin in Na^+ uptake is a matter of debate at present. Therefore, it is very important to improve crop productivity by understanding the molecular mechanism of aquaporin involved in water and ion transport activity and physiological function throughout plant growth and development response to environmental stresses.

1.1. Aquaporin in plants and its functional

Aquaporin in plants comprise a large protein family known as major intrinsic protein (MIPs) and are classified in five subfamilies, i.e., plasma membrane intrinsic proteins (PIPs), tonoplast intrinsic proteins (TIPs), nodulin-26 like intrinsic proteins (NIPs), small basic intrinsic proteins (SIPs) and X-intrinsic proteins (XIPs) (Laloux et al., 2018) based on membrane localization and amino acid sequence. Each subfamily could be further divided into several subgroups. For example, PIPs have been divided two subgroups, PIP1 and PIP2. Each subgroup usually includes some isoforms, such as PIP1;1 and PIP2;1, which have specialized locations and functions (Figure 1.1) (Danielson and Johanson, 2008; Afzal et al., 2016; Fox et al., 2017). Aquaporins are key proteins in regulating water and ion transport, plant growth and development. Some aquaporins transport only water and others transport gases (carbon dioxide and ammonia), metalloids (boron, silicon and arsenic) or reactive oxygen species (hydrogen peroxide), ions transport (Uehlein et al., 2003; Loque et al., 2005; Ma et al., 2006; Takano et al., 2006; Dynowski et al., 2008; Kamiya et al., 2009; Hove1 et al., 2015; Mori et al., 2018; Xu et al., 2019). Some aquaporins were reported to permeate water molecules and ions across the plasma membrane (Byrt et al., 2017; Kourghi et al., 2017; Tran et al., 2020). The activity of PIPs is regulated transcriptionally and post transcriptionally (Katsuhara et al., 2003;

McGaughey et al., 2018). Recently, the ion-conducting AQPs (icAQPs) were demonstrated in heterologous expression systems or by incorporation of purified protein into membrane bilayers. These studies are developing our knowledge on the physiological meanings of aquaporins in plants development and the putative icAQPs isoforms were demonstrated in the general picture of plant in Figure 1.2 (Tyerman et al., 2021).

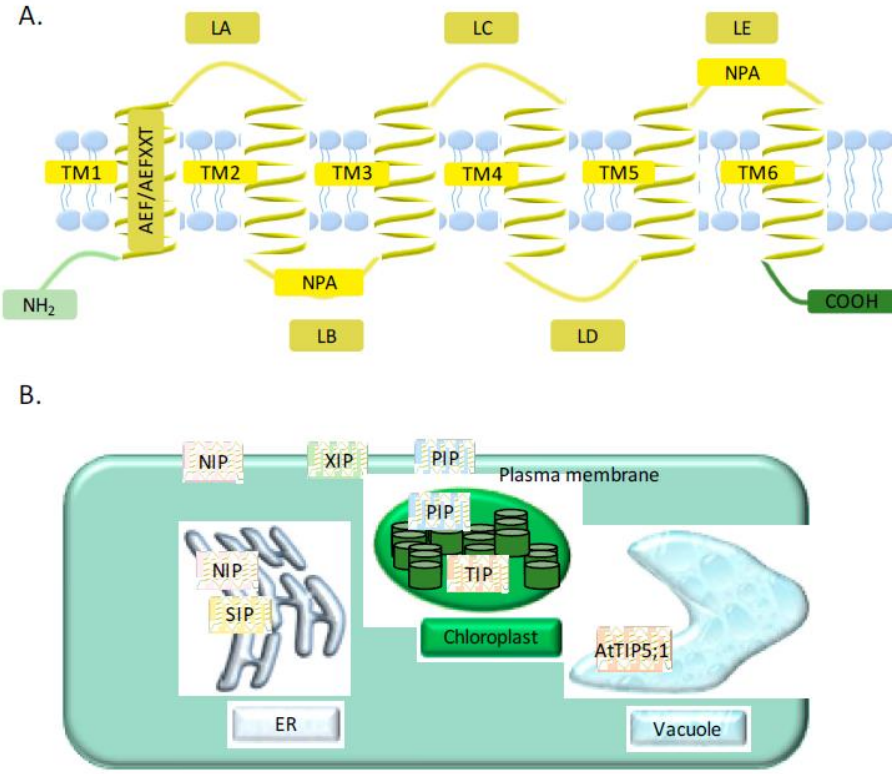

Figure 1.1. General structure and localization of aquaporins. (**A**) Major intrinsic protein (MIP) monomer includes six alpha helical transmembrane helices (TM1–TM6), five inter-helical loops (LA-LE), an AEF(Ala-Glu-Phe) or AEFXXT motif in the N-terminal domain and two highly conserved NPA (Asp-Pro-Ala) motifs; (**B**) General localization of aquaporins. Plasma membrane intrinsic proteins (PIPs), nodulin-26 like intrinsic proteins (NIPs), and uncategorized X intrinsic proteins (XIPs) are generally localized to the plasma membrane, and expressed on the entire cell surface. Small basic intrinsic proteins (SIPs) and some NIPs have been found localizing to endoplasmic reticulum (ER). Tonoplast intrinsic proteins (TIPs) are localized to tonoplast, the membrane of vacuole. Some PIPs and TIPs have been predicted to localized to the inner envelop and thylakoids, while AtTIP5;1 has been found to be located to tonoplast (Afzal et al., 2016).

All major intrinsic proteins, including AQPs, consist of six transmembrane helices with N and C-terminal facing the cytosol, five inter-helical loops (LA-LE), an AEF (Ala-Glu-Phe) or AEFXXT motif in the N-termial domain, and two highly conserved NPA (Asp-Pro-Ala) motifs (the “NPA box”) (Figure 1.1 and 1.4).

Besides their functions as water transporter, MIPs have been reported to transport atypical substrates, including ammonia, arsenite, boric acid, carbon dioxide, formamide, glycerol, hydrogen peroxide (H_2O_2), lactic acid, silicic acid, urea and ions. Two factors contributing to the substrate selectivity have been corroborated: the NPA box and amino acid residues in the Ar/R (aromatic/arginine) region. The NPA box contributes to the selectivity for water molecules (Forrest and Bhave, 2007), which are highly conserved in plant PIPs and TIPs. Alternative sequences in the NPA box occur only in the NIP or SIP groups (Ishibashi et al., 2000; Ishibashi et al., 2006). PIPs function as transporters of water, glycerol, H_2O_2, carbon dioxide, urea and ions (Figure 1.2) (Hanba et al., 2004; Matsumoto et al., 2009; Byrt et al., 2017; Kourghi et al., 2017; Xu et al., 2019; Tran et al., 2020, Tyerman et al., 2021). PIP aquaporins are also involved in abiotic stress responses (Matsumoto et al., 2009; Liu et al., 2013; Wang et al., 2018; Liu et al., 2020; Tran et al., 2020). The main role of TIPs has been described in the permeability of water and TIP localized at the tonoplasts. The water permeability of plant aquaporin was first demonstrated in a TIP from *Arabidopsis*. Further studies have shown that TIPs may control water exchange between cytosolic and vacuolar compartments, which implies that they have a role in regulating cell turgor. Besides its water permeating function, TIPs also play roles in glycerol, urea, and ammonia transport and abiotic stress response. Specific TIP isoforms of rice and maize or *Arabidopsis* also show differential responses to water stress, salt, and cold stress. NIPs are able to transport water, glycerol, ammonia, silicic acid, and other solutes between plant and bacterial symbionts. Compared to PIPs and TIPs, NIPs have lower water transport activity, but higher permeability to small organic molecules and mineral nutrients. The functions of NIPs include transporting beneficial and toxic metal molecules (Zhao et al., 2010; Zangi et al., 2012). For example, OsNIP2;1 not only functions as a silicic acid influx transporter (Ma et al., 2006) but is also involved in selenite uptake in rice (Ma et al., 2008). SIPs have moderate water transport activity and may also function in original pore conformation. XIPs work as multifunctional channels permeable to water, metalloids and ROS. For example, PtXIP2;1 exhibited a differential expression in leaves and stems under the stress of drought, salicylic acid, or wounding (Lopez et al., 2012).

In plants, AQPs are present in almost all organs including roots, leaves, stems, flowers, fruits, and seeds (Figure 1.2; Johanson et al., 2001; Chaumont et al., 2001). Plant species typically have a higher number of AQP genes than animals, ranking from 30 - 70. For instance, 55 in poplar (Gupta et al., 2009; Almeida-Rodriguez et al., 2010), 38 in rice (Sakura et al., 2005; Forrest and Bhave (2007), 35 in *Arabidopsis thaliana (*Johanson et al., 2001), 31 in maize (Chaumont et al., 2001), 34 in sweet orange (Martins et al., 2015), 47 in tomato (Reuscher et al., 2013), 66 in soybean (Ali et al., 2013) and 41 in sorghum (Reddy et al., 2015) have been identified.

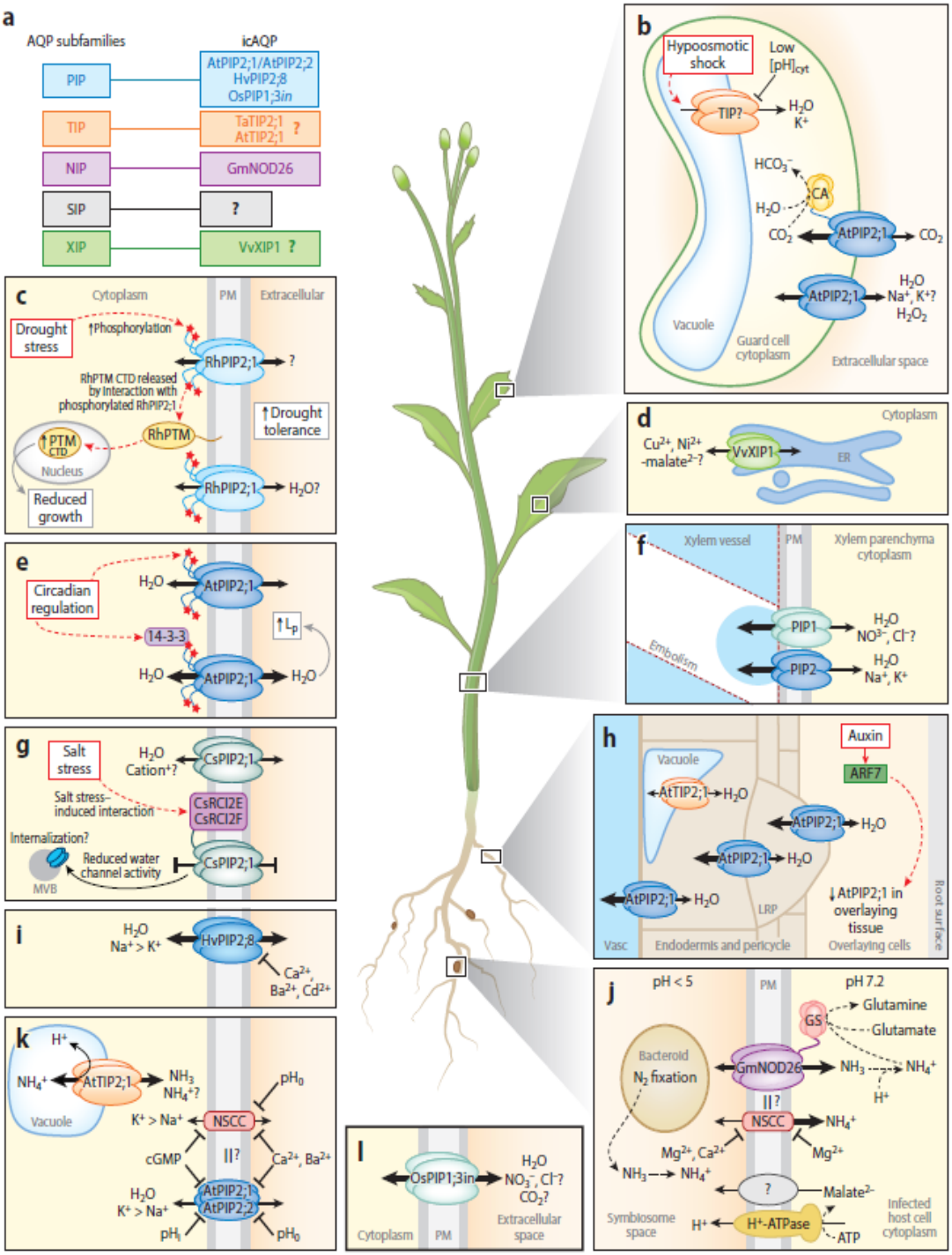

Figure 1.2. The diverse roles of multifunctional (putative) icAQPs. Plant AQPs are classified into five subfamilies: PIPs (PIP1 and PIP2), TIPs (5 groups), NIPs (7 groups), SIPs (2 groups), and the uncharacterized XIPs (4 groups) (Tyerman et al., 2021).

1.2. Regulation of AQPs

1.2.1. Regulation of aquaporin gene expression in plant

Gene expression is a process through which gene information is converted into protein. The first clues about aquaporin function in plants come from the study of the level of expression in different organs, tissues, or cell types according to the developmental stages and in response to different environmental conditions (Figure 1.2). Many studies comparing PIP and TIP aquaporin expression in different organs and conditions in various plant species have been published and have highlighted their involvement in the control of radial transcellular water transport but also in cell osmoregulation (Tyerman et al., 1999; Luu and Maurel, 2005; Hachez et al., 2006b; Kaldenhoff and Fischer, 2006; Forrest and Bhave, 2007; Maurel et al., 2008; Prado and Maurel, 2013). It is interesting to mention that, in general, PIP and TIP aquaporin expression seems to be more abundant in roots than in leaves (Alexandersson et al., 2005; Besse et al., 2011), but several isoforms are highly or exclusively expressed in leaf tissues (Sakurai et al., 2005; Azad et al., 2008).

The cell type localization of aquaporin expression can also provide clues about their physiological roles. For instance, expression of PIP aquaporins in roots and leaves has been correlated to the presence of apoplastic barriers, the exodermis and endodermis in roots or in suberized bundle sheath cells in leaves, suggesting an essential role in the transmembrane water diffusion and ion transport when its movement is hindered (Vandeleur et al., 2009; Prado and Maurel, 2013). The majority of AQPs present in plants are localized in either the tonoplast or the plasma membrane and some are possibly localized in the endomembranes. AQPs can also be found in the plasmalemmasomes and inside of the plasma membrane that extends into vacuole. The presence of AQPs in the plasmalemmasomes suggests that they may play a significant role in the osmotic balance and turgor maintenance of mesophyll cells (Frangne et al., 2001).

The abundance of AQPs is critical for understanding their function. Expression of AQPs may be altered by abiotic factors including drought, salinity, low temperatures, and wounding (Sakurai et al., 2005; Zhu et al., 2005; Alexander et al., 2005)

1.2.2. Regulation of AQPs by tetramerization

AQPs are capable of forming homo-tetramers and hetero-tetramers in the biological membranes (Fetter et al., 2004). Forming homo- or hetero-tetramer structures enables AQPs to be trafficked to cellular membranes and to function as channel transporters (Figure 1.3). Among the different PIP isoforms, PIP1 subgroup has lower water permeability and ion transport

compared to PIP2 isoforms (Chaumont et al., 2000; Matsumoto et al., 2009; Shibasaka et al., 2012; Liu et al., 2020; Byrt et al., 2017; Tran et al., 2020). However, PIP1 proteins may interact with PIP2 members by forming hetero-tetramer structures that can function as water channels (Fetter et al., 2004). Expressing PIP1s in combination with PIP2s can significantly improve the water permeability (Johansson et al., 1998; Tornroth-Horsefield et al., 2006; Liu et al., 2020) but inhibited ion transport (Byrt et al., 2017; Tran et al., 2020). For instance, OsPIP1;3 in rice has been shown to be no functional expressed alone; if it interacts with OsPIP2;2 and particularly of OsPIP2;4 but not OsPIP2;3 leading to water permeability significantly increased when they are co-expressed in *Xenopus* oocytes (Matsumoto et al., 2009; Liu et al., 2020). In addition, the combinations of OsPIP1;1/OsPIP2;1 (Liu et al., 2013) and in *Beta vulgaris* BvPIP1;1/BvPIP2;1 (Jozefkowicz et al., 2013) could significantly enhance PIP1 activities through their physical interactions with PIP2s. Also, SoPIP1 in spinach (*Spinacia oleracea*) has been shown to have low water permeability whereas its heterotetramer with PIP2 had relatively high water permeability (Johansson et al., 1998; Tornroth-Horsefield et al., 2006). Although hetero-tetramers usually provide greater stability and folding of the proteins resulting in highly efficient water transport across biological membranes, not all of the AQP subgroups are activated by forming hetero-tetramers (Fetter et al., 2004; Byrt et al., 2017; Tran et al., 2020).

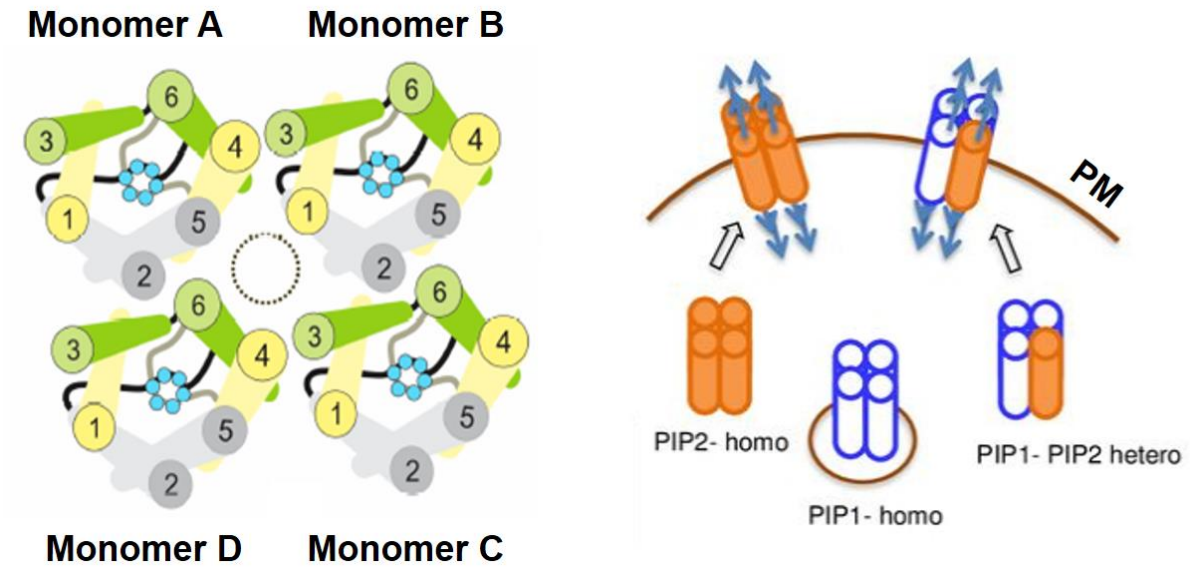

Figure 1.3. Illustration of the homo- and hetero-tetrameric organization of AQPs. Transmembrane segments (TM) are numbered from 1 to 6. The cytoplasmic loop B (black line), the extracellular loop E (gray line) and the highly conserved NPA motifs (light blue circles) are represented. The central pore is indicated by the dash-lined oval (left panel). Homo-and hetero-tetrameric organization between PIP1 and PIP2. PIP1-homo (while cylinder); PIP2-homo (orange cylinder). PM: Plasma membrane (right panel) (modified from Ozu et al., 2018).

The lack of expression clearly shows that hetero-tetramers may not be an important factor for the efficient water transport in all plant tissues, for example, *Zea mays Zm*PIP2;5 was

lacking in shoot tissues of maize (Chaumont et al., 2000). In fact, some PIP2s, TIPs and NIPs are functional when they are expressed alone in heterologous conditions. In some plants, PIP1s are not able to form tetramers individually, but when PIP1s are co-expressed with PIP2s, then only the PIP1s become active water channels and this proves that forming hetero-tetramer structures can be an important factor in activating or regulating plant AQPs. Generally, Loop E of AQPs is considered to control tetramer formation in plants (Fetter et al., 2004).

1.2.3. Regulation of phosphorylation and dephosphorylation through AQP gating

AQP gating involves opening and closing of the AQP water channel pore and phosphorylation and dephosphorylation of AQPs are considered to be important mechanisms regulating their activity (Qiu et al., 2020; Tran et al., 2020). Phosphorylation enhances AQP activity by keeping the AQP pores in the open state (Tornroth-Horsefield et al., 2006). Phosphorylation of plant AQPs can be directly involved in rapid channel gating. It has been confirmed that the loop B and the N- and C-terminal tails of AQPs are the important sites in water and ion channel regulation. A conserved phosphorylation site has been determined in the loop B and C-terminal of almost all plant PIPs (Azad et al., 2004; Qiu et al., 2020; Tran et al., 2020). In addition to the phosphorylation of N- or C-terminal serine, a serine residue located in the cytoplasmic loop close to the first NPA motif can also be phosphorylated. The serine residue is conserved in all plant PIPs and in some TIPs. When S115 of SoPIP2;1 is dephosphorylated, it also stabilizes the closed state; however, phosphorylation of this residue and other key serine residues at the loop D and C-terminal disrupts this stabilization and might induce an open state (Tornroth-Horsefield. et al., 2006). The role of phosphorylation in aquaporin activity has been investigated using kinases and phosphatases (Qiu et al., 2020; Tran et al., 2020).

1.3. Plasma membrane intrinsic proteins (PIPs)

The plasma membrane intrinsic protein constitutes the largest plant AQP subfamily with the molecular weight of around 30kDa. PIPs have been mainly localized at the plasma membranes and in organs characterized by large fluxes of water and substrates i.e roots, vascular tissues, guard cell. They have several basic amino acids at C-terminal domain. Among the 35 full-length aquaporins genes of the *Arabidopsis thaliana* genome, 13 encodes for PIPs (Gupta et al., 2009). Thirteen encode PIPs out of 38 aquaporins in rice (Sakurai et al., 2005; Forrest and Bhave, 2007), 40 aquaporins have been identified in barley, in which 19 encodes for PIPs (Hove et al., 2015).

A) Structure of PIP aquaporin

PIP channels present a main structural core of six transmembrane alpha helices and five connecting loops with N and C-terminal domains in the cytoplasmic side. The transmembrane helices are organized surrounding a single pore together with a seventh transmembrane region created by the insertion of loops B and E into the channel from opposite sides of the membrane. All PIP channels present the two main and conserved regions that determine their solute specificity: Asn-Pro-Ala (NPA) motif and the aromatic/arginine (Ar/R) selectivity filter (Figure 1.4). The main difference among PIP and other aquaporins is the length of loop D. This flexible structure is crucial for the open-closed transition found in PIP channels.

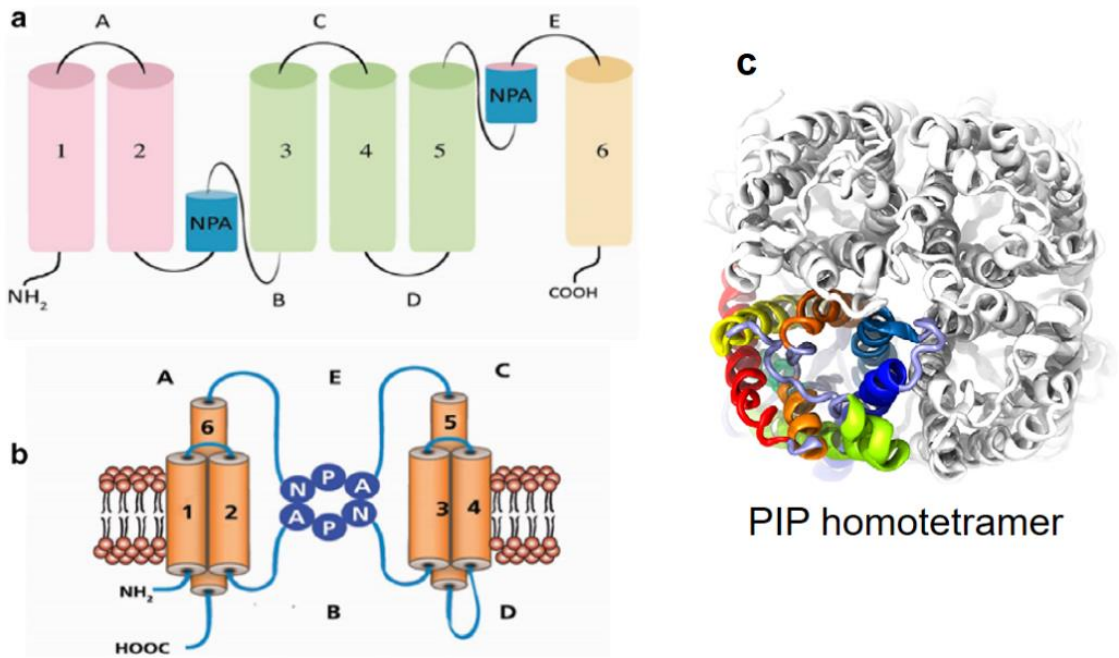

Figure 1.4. General PIPs aquaporin structure. Pore of the AQP is composed of two halves called as hemipores. **a)** PIPs consist of six transmembrane domains connected by five loops (A–E), with cytoplasmic N- and C-terminal. Locations of NPA (Asn-Pro-Ala) motifs are at the loops B and E. **b)** Functional AQP formed by the interaction of the two hemi-pores. **c)** Top view of a representative PIP homo-tetramer as built for molecular dynamics simulations (Kapilan et al., 2018; Fortuna et al., 2019).

B) Sub-family of PIP and its functional

PIP1s: Despite the fact that the amino acid sequences are similar in both PIP1 and PIP2 subgroups, their water transport ability and cellular functions are very different. In barley, the PIP1 subgroup has five members (PIP1;1 to PIP1;5), whereas the PIP2 subgroup has eight isoforms (PIP2;1 to PIP2;8). In rice, PIP2 have been detected additional 2PIPs (OsPIP2;9 and OsPIP2;10) recently (Maurel et al., 2007; Forest and Brave, 2007). PIP1 proteins have longer N-terminal but shorter C-terminal tails compared with PIP2. Most PIP1 channels are retained

in intracellular membranes, hence fail to be targeted to the plasma membrane, typically the endoplasmic reticulum (ER) when heterologously expressed in oocytes or yeast, or even in plant cells (Katsuhara et al., 2002; Liu et al., 2013; Liu et al., 2020) and are considered to show a low water permeability (Matsumoto et al., 2009; Ding et al., 2019). Some of the PIP1 proteins are not able to act independently and they must form hetero-tetramers with the PIP2 monomers to be able to facilitate water molecules (Chaumont et al., 2000; Liu et al., 2020; Shibasaka et al., 2012), however, there is also strong evidence demonstrating their importance in regulating water permeability. Some members of the PIP1 subgroup are also considered to be responsible for transporting glycerol, NO_3^-, CO_2 in addition to water (Hanba et al., 2004; Liu et al., 2020).

PIP2s: Aquaporins of the PIP2 subfamily are thought to be more efficient as water and ion channels than members of the PIP1 group and different isoforms of PIP2 are considered to be the main pathway for cell-to-cell water transport (Kaldenhoff et al., 2006). Many studies using *Xenopus* oocytes showed that overexpression of the PIP2s significantly increased the water permeability compared to the control and PIP1s as well as ion transport. Compared with PIP1s, PIP2 AQPs have a shorter N-terminal and a longer C-terminal ends with an additional stretch of 4–10 amino acids located in the first extra-cytosolic loop. These features can contribute to cell-to-cell water transport in roots, leaves, reproductive organs, and seeds.

1.4. PIPs aquaporin expression and their roles in response to abiotic stress

Numerous studies have confirmed that the abundance of AQPs is regulated by various developmental and environmental factors including biotic and abiotic stresses. Environmental stresses such as salinity, drought and low root temperature can quickly reduce water transport rates and changing ions concentration outside and inside of plant cells (Kapilan et al., 2018).

Many aquaporin isoforms show differential expression in response to abiotic stresses. Some are up-regulated, while others are down-regulated (Sakurai et al., 2005; Zhu et al., 2005; Alexander et al., 2005). Such differences in the regulation of aquaporins might contribute to increased resistance/susceptibility to specific stress. In this study, we focus on salt stress response of rice and barley aquaporins. Regulation of PIPs may help plants maintain water balance and ion influxes in plant cells under salt environment. Exposure to salinity stress immediately triggers an osmotic stress at a high salt concentration in the soil and resulted in a decreases the soil water potential. Following this rapid osmotic effect, high salt concentration also causes ion toxicity, nutritional disorders and oxidative stress which result in alteration of major physiological processes, such as photosynthesis, cell division and elongation, maintenance of membrane integrity, protein synthesis as well as energy and lipid metabolism

in the later phase of the salt stress. Together, these effects reduce plant growth, development and yield.

Among abiotic stresses, exposure to high salinity (NaCl) is one of serious issues limiting plant growth and development world-wide (Munns and Tester, 2008). Salt stress not only impacts the transcriptional regulation of *PIPs* but also alters the abundance of PIP proteins in the plasma membrane and their cycling between the plasma membrane and endosomal compartments including the trans-Golgi network and the early endosomes (TGN/EE) (Boursiac et al., 2005, 2008; Li et al., 2011; Luu et al., 2012; Hachez et al., 2014a). Salinity affects the expression of the PIP2 aquaporins in a time- and isoform-dependent manner. Changes in aquaporin regulation in response to changes in salinity are particularly interesting because previous studies have revealed that a significant proportion of the highly abundant AtPIP2;1 protein relocates from the plasma membrane in *Arabidopsis* roots to an internalized location, and this could account for the reduction in root hydraulic conductance that is observed under salinity (Prak et al., 2008). Targeting of PIPs to the plasma membrane and regulation of their internalization under salinity depends on the phosphorylation status of a serine (S283) in the C-terminal domain of AtPIP2;1 (Prak et al., 2008; Maurel et al., 2015). The regulation of PIPs in plants changes in response to salt treatments, and these changes might influence plant adaptation to salt stress (Liu et al., 2013; Alavilli et al., 2016; Ayadi, Brini and Masmoudi, 2019).

Anion and cation transport properties have been reported for subsets of plant PIPs when expressed and tested in heterologous systems. For example, the rice (*Oryza sativa*) OsPIP1;3, which is upregulated in roots under drought stress, has recently been shown to be able to transport nitrate anions when expressed in mammalian HEK293 cells, and to also function as a water channel (Liu et al., 2020). This aquaporin isoform is postulated to be a functional ortholog to the animal AQP6 that shows anion transport activity, though normally not water channel activity (Ikeda et al., 2002). Two *Arabidopsis* PIPs, AtPIP2;1 and AtPIP2;2 were reported to display non-selective cation conductance ($K^+ > Na^+$) when expressed in *Xenopus laevis* oocytes. These aquaporins have similar but not identical features to a human HsAQP1 ion and water channel aquaporin (Byrt et al., 2017; Kourghi et al., 2017; Qiu et al., 2020). It was hypothesized that AtPIP2;1 could account for the voltage-independent non-selective cation channels (viNSCC) in plants (Byrt et al., 2017) since the PIP2;1 and PIP2;2 cation conductance was inhibited by a low pH and by divalent cations (Byrt et al., 2017; Kourghi et al., 2017), which resemble the features observed for the viNSCCs observed in patch-clamp measurements on root protoplasts and roots (Tyerman et al., 1997; Demidchik et al., 2002; Essah et al., 2003). There

is also the similarity of inhibition of NSCCs and AtPIP2;1/AtPIP2;2 by cGMP (Isayenkov et al., 2019; Qiu et al., 2020). There are other features of voltage-independent NSCCs that remain to be tested on the ion conducting PIP2s, including the selectivity to different monovalent cations. It is also unknown how many of the PIP2 isoforms of a species may induce ion conductance.

Therefore, understanding the water and ion transport functions and significance of PIP aquaporins and their regulation in physiological processes under major environmental salinity stresses in rice and barley, then final identification of a master regulator controlling ion transport via aquaporin activity are necessary.

1.5. Summary of aquaporin subfamilies in rice and barley

In recent years, the function of plant AQPs has been extended from transport of water alone to the transport of other substrates and responding to diverse physiological processes and environmental stresses (reviewed in Maurel et al., 2008; Tyerman et al, 2021). Many studies have reported significant information exists on water permeability and ion transport activity of the AQP families, but a complete picture of plant AQPs function remains to be unraveled until now, especially in rice and barley aquaporins, two of the most important cereal crops.

Rice and barley are important food crops which belongs to grass family Poaceae, subfamily Pooideae and tribe Triticeae, which also include the larger cereal crop, wheat. However, barley is more adaptable and resilient than wheat (Zohary and Hopf, 2000). Aquaporins such as PIPs have crucial roles in water and ion uptake, its transmembrane transport, ion and osmotic mechanisms. Hence a deeper understanding of these genes in rice and barley will be essential for crop improvement through selective breeding and transgenic, both in rice and barley.

In rice (*Oryza sativa* L. cv. Nipponbare), 38 genes for aquaporin in the rice genome sequence have been identified as shown in Figure 1.5 (Sakurai et al., 2005; Forest and Brave, 2007). OsPIP2;4 and OsPIP2;5 were expressed predominantly in roots (Sakurai et al., 2005; Guo et al., 2006; Matsumoto et al., 2009), while 14 genes, including OsPIP2;7 and OsTIP1;2 were found in leaf blades (Sakurai et al., 2005). Eight genes, such as OsPIP1;1 and OsTIP4;1, were evenly expressed in leaf blades, roots and anthers. OsPIP2;4 or OsPIP2;5 revealed high water channel activity when expressed in yeast but not when OsPIP1;1 or OsPIP1;2 were expressed (Sakurai et al., 2005).

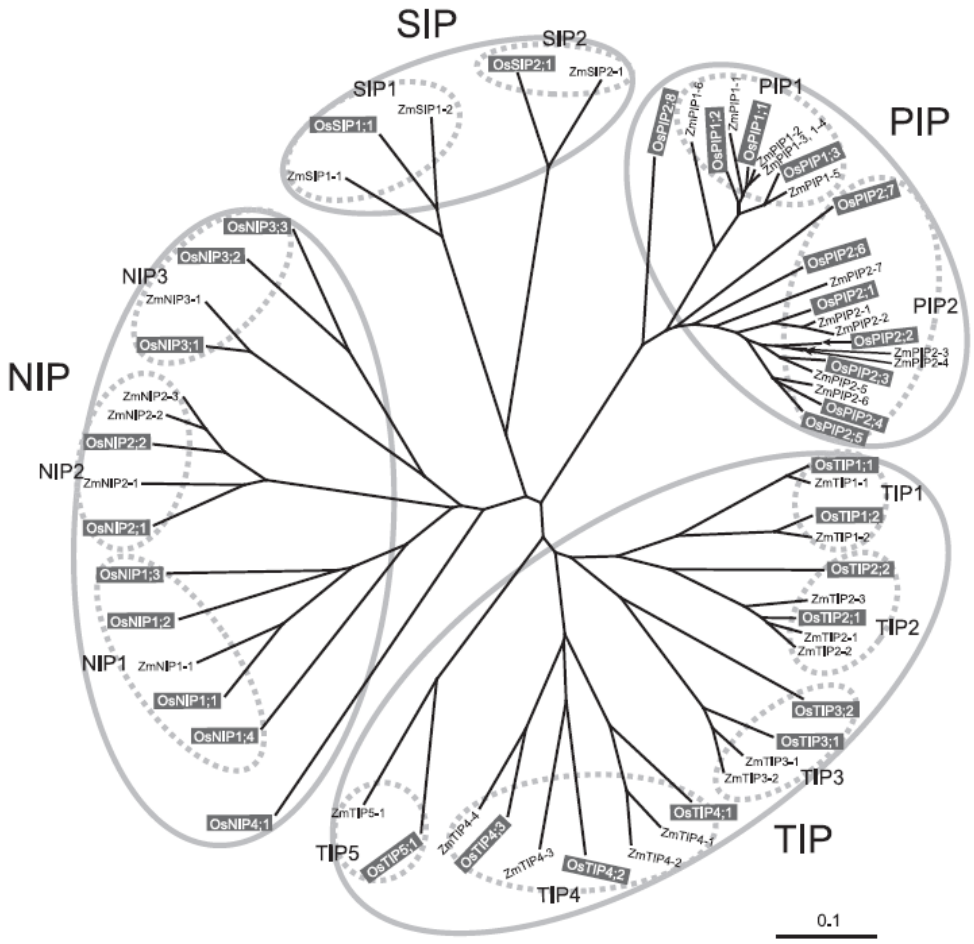

Figure 1.5. Phylogenetic analysis of the deduced amino acid sequences of rice aquaporins with those of Z. mays aquaporins. The accession numbers of Z. mays aquaporins are listed in Chaumont et al. (2001). The scale bar of 0.10 is equal to 10% sequence divergence (Sakurai et al., 2005).

Forest and Brave (2007) have indicated 38 MIP genes ranging in size from 669 to 1,113 bp and spread across all rice chromosomes except chromosome 11. The MIPs could be split into 13 PIPs, 10 TIPs, 13 NIPs, 2 SIPs. These results were similar to those of Sakurai et al. (2005), of the five additional genes (OsPIP2;9, OsPIP2;10, OsNIP1;5, OsNIP3;4, and OsNIP3;5) have been identified. The OsPIP members had sequence similarity (58.5 – 92.7%), while the members of the OsTIP, OsNIP and OsSIP subfamilies had a somewhat variable sequence similarity. For example, the sequence similarity among the OsTIP members was 35.8 – 72.0%. The OsPIP subfamily was divided into two groups including 3 PIP1s and 10 PIP2s (Table 1.1; Forest and Brave, 2007). OsPIP2;8 had a unique sequence and formed a long branch in the phylogenetic tree. However, we provisionally assigned OsPIP2;8 as a member of the PIP2 group because its sequence was similar to that of OsPIP2 members compared to sequences of OsPIP1s.

In barley genomes, 40 MIP genes are classified into four major sub-families (TIPs, PIPs, NIPs, SIPs) based of orthologs of rice. HvPIP2;8 clustered with OsPIP2;8 and the previously annotated HvPIP2;8 (Shibasaka et al., 2012) and was annotated as HvPIP2;9 as shown in Figure 1.6 (Hove et al., 2015).

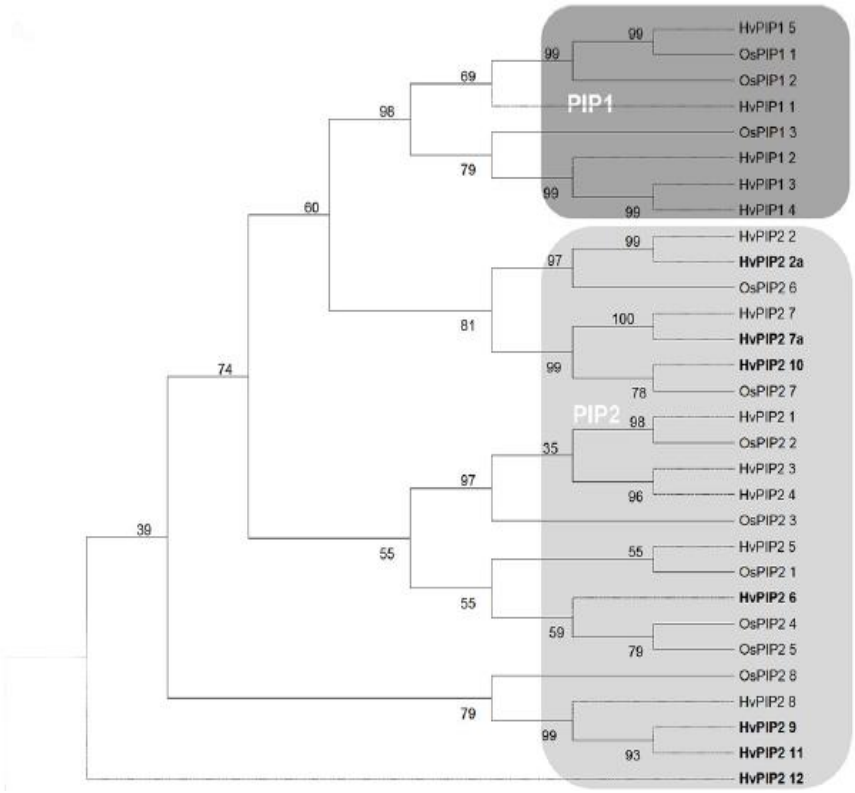

Figure 1.6. Phylogenetic trees of putative barley and rice PIPs aquaporin sequences. The different sub-families and groups are highlighted in different shades of grey. The AQPs annotated in this study are shown in bold. The branches corresponding to barley AQPs are shown as dashed lines while those for rice are solid lines (Hove et al., 2015)

The potential to transport urea (many PIPs, TIPs and NIPs) and boron (many HvPIPs but no TIPs) was widespread, but that for ammonia was restricted to some TIPs (HvTIP2;1, HvTIP2;2, HvTIP2;3), CO_2 to HvPIPs (all except HvPIP2;7), and silicon to NIPs (HvNIP2;1, HvNIP2;2). The potential to transport the signalling molecule H_2O_2 seemed restricted to the TIPs. NIPs had the most diverse predicted substrates, as found in other studies, including the potentially toxic arsenite.

In general, 38 AQPs in rice and 40 AQPs in barley are the large number aquaporins subfamilies were reported as shown in Table 1.1 and so far. Many studies have found the potential to transport water, gasses, ion and the neutral solutes transported by different AQPs. However, the ion influxes across the plasma membrane by HvPIPs and OsPIP2s response to abiotic stress have been poorly understood and still not all clearly until now.

Table 1.1. Summary of AQP subfamilies and localization in plant rice and barley cells

AQP subfamilies		Localization	No. of genes	
			Rice	**Barley**
PIP	Plasma membrane Intrinsic Protein	Plasma membrane (PM)	13	19
TIP	Tonoplast Intrinsic Protein	Tonoplast (Vacuolar membrane)	10	11
NIP	Nodulin 26-like Intrinsic Protein	Bacteroid membrane, Endoplasmic reticulum (ER), PM	13	8
SIP	Small basic Intrinsic Protein	ER membrane	2	2
Total			**38**	**40**

(Sakurai et al., 2005; Forest and Hove, 2007; Hove et al., 2015)

References

Alavilli H. Alavilli H., Awasthi J.P., Rout G. R., Sahoo L., Lee B., Panda S.K. **(2016)**. Overexpression of a barley aquaporin gene, HvPIP2;5 confers salt and osmotic stress tolerance in yeast and plants, *Front. Plant Sci.,* 7, 1–12. doi: 10.3389/fpls.2016.01566.

Afzal Z.T.C., Sun H.Y., Mukhtar M. S. **(2016)**. The roles of aquaporins in plant stress responses. Reviews. *J. Dev. Biol.,* 4 (9); doi:10.3390/jdb4010009

Alexandersson E., Fraysse L., Sjovall-Larsen S., Gustavsson S., Fellert M., Karlsson M., Johanson U., Kjellbom P. **(2005)**. Whole gene family expression and drought stress regulation of aquaporins. *Plant Mol. Biol.,* 59, 469–484.

Ali Z., Wang C.B., Xu L., Yi J.X., Xu Z.L., Liu X.Q., He X.L., Huang Y.H., Khan I.A., Trethowan, R. **(2013)**. Genome-wide sequence characterization and expression analysis of major intrinsic proteins in soybean (*Glycine max* L.). *PLoS ONE,* 8, e56312

Almeida-Rodriguez A.M., Cooke J.E.K., Yeh F., Zwiazek J.J. **(2010)**. Functional characterization of drought- responsive aquaporins in *Populus balsamifera* and *Populus simonii* × *balsamifera* clones with different drought resistance strategies. *Plant Physiol.*, 140, 321–333

Ayadi M., Brini F., Masmoudi K. **(2019)**. Overexpression of a wheat aquaporin gene, TdPIP2;1, enhances salt and drought tolerance in transgenic durum wheat cv. Maali, *Int. J. Mol. Sci.*, 20 (10). doi: 10.3390/ijms20102389.

Azad A.K., Sawa Y., Ishikawa T., Shibata H. **(2004)**. Characterization of protein phosphatase 2A acting on phosphorylated plasma membrane aquaporin of tulip petals. *Biosci. Biotechnol. Biochem.*, 68 (5), 1170–1174.

Boursiac Y., Chen S., Luu D.T., Sorieul M., van den Dries N., Maurel C. **(2005)**. Early effects of salinity on water transport in Arabidopsis roots. Molecular and cellular features of aquaporin expression. *Plant Physiol.*, 139, 790–805.

Boursiac Y., Boudet J., Postaire O., Luu D.T., Tournaire-Roux C., Maurel C. **(2008)**. Stimulus-induced downregulation of root water transport involves reactive oxygen species-activated cell signaling and plasma membrane intrinsic protein internalization. *Plant J.*, 56, 207–218

Besse M., Knipfer T., Miller A.J., Verdeil J.L., Jahn T.P., Fricke W. **(2011)**. Developmental pattern of aquaporin expression in barley (*Hordeum vulgare* L.) leaves. *J. Exp. Bot.*, 62, 4127–4142.

Byrt C.S., Zhao M., Kourghi M., Bose J., Henderson S.W., Qiu J., Tyerman S.D. **(2017)**. Non-selective cation channel activity of aquaporin AtPIP2;1 regulated by Ca^{2+} and pH. *Plant Cell Environ.*, 40, 802–815.

Chaumont F., Barrieu F., Jung R., Chrispeels M.J. **(2000)**. Plasma membrane intrinsic proteins from maize cluster in two sequence subgroups with differential aquaporin activity. *Plant Physiol.*,122, 1025–1034.

Chaumont, F., Barrieu, F., Wojcik, E., Chrispeels, M.J., Jung, R. **(2001)**. Aquaporins constitute a large and highly divergent protein family in maize. *Plant Physiol.*, 125, 1206–1215.

Danielson J.Å., Johanson U., **(2008)**. Unexpected complexity of the aquaporin gene family in the moss *Physcomitrella* patens. *BMC Plant Biol.*, 8 (45).

Demidchik V., Tester M. **(2002)**. Sodium fluxes through nonselective cation channels in the plasma membrane of protoplasts from Arabidopsis roots. *Plant Physiol.*, 128, 379–387.

Ding L., Uehlein N., Kaldenhoff R., Guo S., Zhu Y., Kai L. **(2019)**. Aquaporin PIP2;1 affects water transport and root growth in rice (*Oryza sativa* L.). *Plant Physiol. Biochem.*, 139, 152-160.

Dynowski M., Mayer M., Moran O., Ludewig U. **(2008)**. Molecular determinants of ammonia and urea conductance in plant aquaporin homologs. *FEBS Letters*, 582, 2458–2462.

Essah P.A., Davenport R., Tester M. **(2003)**. Sodium influx and accumulation in *Arabidopsis*. *Plant Physiol.*, 133, 307–318.

Fetter K., Van Wilder V., Moshelion M., Chaumont F. **(2004)**. Interactions between plasma membrane aquaporins modulate their water channel activity. *Plant Cell*,16, 215–228.

Forrest K.L., Bhave M. **(2007)**. Major intrinsic proteins (MIPs) in plants: A complex gene family with major impacts on plant phenotype. *Funct. Integr. Genomics*, 7, 263–289

Fox A.R., Maistriaux L.C., Chaumont F. **(2017)**. Toward understanding of the high number of plant aquaporin isoforms and multiple regulation mechanisms. *Plant Sci.*, 264, 179–187.

Fortuna C.A., Zerbetto De Palma G., Aliperti Car, L., Armentia L., Vitali V., Zeida A., Estrin D.A., Alleva K. **(2019)**. Gating in plant plasma membrane aquaporins: the involvement of leucine in the formation of a pore constriction in the closed state. *FEBS J.*, 286 (17), 3473–3487. doi: 10.1111/febs.14922.

Frangne N., Maeshima M., Schaffner A.R., Mandel T. Martinola E., Bonnemain J.L. **(2001)**. Expression and distribution of a vacuolar aquaporin in young and mature leaf tissues of *Brassica napus* in relation to water fluxes. *Planta.*, 212, 201–208.

Guo L., Zi Y. W., Lin H., Wei E. C., Chen J., Liu M., Zhang L.C., Li J.Q., Gu H. **(2006)**. Expression and functional analysis of the rice plasma-membrane intrinsic protein gene family, *Cell Research*, 16 (3), 277–286. doi: 10.1038/sj.cr.7310035.

Gupta A.B., Sankararamakrishnan R. **(2009)**. Genome-wide analysis of major intrinsic proteins in the tree plant *Populus trichocarpa*: characterization of XIP subfamily of aquaporins from evolutionary perspective. *BMC Plant Biol.*, 9, 134.

Hachez C., Zelazny E.F. **(2006)**. Chaumont modulating the expression of aquaporin genes in planta: a key to understand their physiological functions? *Biochem. Biophys. Acta.,* 1758,1142–1156.

Hachez C., Laloux T., Reinhardt H., Cavez D., Degand H., Grefen C., De Rycke R., Inze D., Blatt M.R., Russinova E., Chaumont F. **(2014a)**. Arabidopsis SNAREs SYP61 and SYP121 coordinate the trafficking of plasma membrane aquaporin PIP2;7 to modulate the cell membrane water permeability. *Plant Cell*, 26, 3132–3147.

Hanba Y.T., Shibasaka M., Hayashi Y., Hayakawa T., Kasamo K., Terashima I., Katsuhara M. **(2004)**. Overexpression of the barley aquaporin HvPIP2;1 increases internal CO_2 conductance and CO_2 assimilation in the leaves of transgenic rice plants. *Plant Cell Physiol.,* 45, 521–529.

Horie T., Karahara I., Katsuhara M. **(2012)**. Salinity tolerance mechanisms in glycophytes: An overview with the central focus on rice plants. *Rice*, 5, 1–18.

Hove R.M., Bhave M. **(2011)**. Plant aquaporins with non-aqua functions: Deciphering the signature sequences. *Plant Mol. Biol.,* 75, 413–430.

Hove R. M., Ziemann M., Bhave M. **(2015)**. Identification and expression analysis of the barley (*Hordeum vulgare* L.) aquaporin gene family. *Plos One,* 10 (6): e0128025. doi:10.1371/journal. pone.0128025.

Ikeda M., Beitz E., Kozono D., Guggino W.B., Agre P., Yasui M. **(2002)**. Characterization of aquaporin-6 as a nitrate channel in mammalian cells-Requirement of pore-lining residue threonine 63. *J. Biol. Chem.*, 277, 39873–39879.

Isayenkov S.V., Maathuis F.J.M. **(2019)**. Plant salinity stress: Many unanswered questions remain. *Front. Plant Sci.*, 10 (80).

Ishibashi K., Kuwahara M., KageyamanY., Sasaki, S., Suzuki, M., Imai, M. **(2000)**. Molecular cloning of a new aquaporin superfamily in mammals. *Int. Mol. Biol. Physiol.*, Springer: New York, NY, USA, 123–126.

Ishibashi K. **(2006)**. Aquaporin subfamily with unusual NPA boxes. *Biochim. Biophys. Acta Biomembr.*, 1758, 989–993.

Johansson I., Karlsson M., Shukla V., Chrispeels M., Larsson C., Kjellbom P. **(1998)**. Water transport activity of the plasma membrane aquaporin PM28A is regulated by phosphorylation. *Plant Cell,* 10, 451–460.

Johanson U., Karlsson M., Johansson I., Gustavsson S., Sjovall S., Fraysse L., Weig A.R., Kjellbom P. **(2001)**. The complete set of genes encoding major intrinsic proteins in arabidopsis provides a framework for a new nomenclature for major intrinsic proteins in plants. *Plant Physiol.*,126, 1358–1369.

Jozefkowicz C., RosiP., Sigaut L., Soto G., Pietrasanta L.I., Amodeo G., Alleva K. **(2013)**. Loop A is critical for the functional interaction of two *Beta vulgaris* PIP aquaporins. *PLOS ONE*, 8 (3), e57993.

Kaldenhoff R., Fisher M. **(2006)**. Aquaporins in plants. *Acta Physiol.*,187, 169–176.

Kamiya T., Tanaka M., Mitani N., Ma J.F., Maeshima M., Fujiwara T. **(2009)**. NIP1;1, an aquaporin homolog, determines the arsenite sensitivity of *Arabidopsis thaliana*. *J. Biol. Chem.*, 284, 2114–2120.

Kapilan R., Vaziri M., Zwiazek J.J. **(2018)**. Regulation of aquaporins in plants under stress. *Biol. Res.*, 51 (4).

Katsuhara, M., Akiyama, Y., Koshio, K., Shibasaka, M. and Kasamo, K. **(2002)**. Functional analysis of water channels in barley roots. *Plant Cell Physiol.*, 43, 885–893.

Katsuhara M., Koshio K., Shibasaka M., Hayashi Y., Hayakawa T., Kasamo K. **(2003)**. Over-expression of a barely aquaporin increased the shoot/root ratio and raised salt sensitivity in transgenic rice plants. *Plant Cell Physiol.*, 44, 1378–1383.

Kourghi M., Nourmohammadi S., Pei J.V., Qiu J., McGaughey S., Tyerman S.D., Yool A.J. **(2017)**. Divalent cations regulate the ion conductance properties of diverse classes of aquaporins. *Int. J. Mol. Sci.*, 18, 2323.

Li X., Wang X., Yang Y., Li R., He Q., Fang X., Luu D.T., Maurel C., Lin J. **(2011)**. Single-molecule analysis of PIP2;1 dynamics and partitioning reveals multiple modes of Arabidopsis plasma membrane aquaporin regulation. *Plant Cell*, 23, 3780–3797.

Liu C., Fukumoto T., Matsumoto T., Gena P., Frascaria D., Kaneko T., Katsuhara M., Zhong S., Sun X., Zhu Y., Iwasaki I., Ding X., Calamita G., Kitagawa Y. **(2013)**. Aquaporin OsPIP1;1 promotes rice salt resistance and seed germination, *Plant Physiol. Biochem.*, Elsevier Masson SAS, 63, 151–158. doi: 10.1016/j.plaphy.2012.11.018.

Liu S.Y., Fukumoto T., Gena P., Feng P., Sun Q., Li Q., Ding X.D. **(2020)**. Ectopic expression of a rice plasma membrane intrinsic protein (OsPIP1;3) promotes plant growth and water uptake. *Plant J.*,102, 779–796.

Lopez D., Bronner G.L., Brunel N., Auguin D., Bourgerie S., Brignolas F., Carpin S., Tournaire-Roux, C., Maurel C., Fumanal B. **(2012)**. Insights into populus XIP aquaporins: Evolutionary expansion, protein functionality, and environmental regulation. *J. Exp. Bot.*, 63, 2217–2230.

Loqué D., Ludewig U., Yuan L., Von Wirén N. **(2005)**. Tonoplast intrinsic proteins AtTIP2;1 and AtTIP2;3 facilitate NH_3 transport into the vacuole. *Plant Physiol.*, 137, 671–680.

Laloux T., Junqueira B., Maistriaux L.C., Ahmed J., Jurkiewicz A., Chaumont F. **(2018)**. Plant and Mammal Aquaporins: Same but Different. *Int. J. Mol. Sci.*, 19, 27

Luu D.T., Maurel C. **(2005)**. Aquaporins in a challenging environment: molecular gears for adjusting plant water status. *Plant Cell Environ.,* 28, 85–96.

Luu D.T., Martiniere A., Sorieul M., Runions J., Maurel C. **(2012)**. Fluorescence recovery after photobleaching reveals high cycling dynamics of plasma membrane aquaporins in Arabidopsis roots under salt stress. *Plant J.*, 69, 894–905.

Ma J.F., Tamai K., Yamaji N., Mitani N., Konishi S., Katsuhara M., Yano M. **(2006)**. A silicon transporter in rice. *Nature,* 440, 688–691.

Ma J.F., Yamaji N., Mitani N., Xu X.Y., Su Y.H., McGrath S.P., Zhao F.J. **(2008)**. Transporters of arsenite in rice and their role in arsenic accumulation in rice grain. *Proc. Natl. Acad. Sci*. USA, 105, 9931–9935

Martins C.D.P.S., Pedrosa A.M., Du D., Goncalves L.P., Yu Q., Gmitter F.G.Jr., Costa M.G.C. **(2015)**. Genome-wide characterization and expression analysis of major intrinsic proteins during abiotic and biotic stresses in sweet orange (*Citrus sinensis* L. Osb.). *PLoS ONE,* 10, e0138786.

Matsumoto T., Lian H.L., Su W.A., Tanaka D., Liu C.W. **(2009)**. Role of the aquaporin PIP1 subfamily in the chilling tolerance of rice. *Plant Cell Physiol*., 50, 216–229.

Maurel C. **(2007)**. Plant aquaporins: novel functions and regulation properties. *FEBS Lett.*, 581, 2227–2236.

Maurel C., Verdoucq L., Luu D.T., Santoni V. **(2008)**. Plant aquaporins: membrane channels with multiple integrated functions. *Annu. Rev. Plant Biol.*,59, 595–624

Maurel C., Boursiac Y., Luu D.T., Santoni V., Shahzad Z., Verdoucq L. **(2015)**. Aquaporins in plants. *Physiol. Rev.*, 95, 1321–1358.

McGaughey S.A., Qiu J., Tyerman S.D., Byrt C.S. **(2018)**. Regulating root aquaporin function in response to changes in salinity. *Ann. Plant Rev. Online,* 1, 381–416.

Mori I.C., Nobukiyo Y., Nakahara Y., Shibasaka M., Furuichi T., Katsuhara M. **(2018)**. A cyclic nucleotide-gated channel, HvCNGC2-3, is activated by the co-presence of Na^+ and K^+ and permeable to Na^+ and K^+ non-selectively, *Plants*, 7 (61); doi:10.3390/plants7030061.

Munns R., Tester M. **(2008)**. Mechanisms of salinity tolerance. *Ann. Rev. Plant Biol.*, 59, 651–681.

Ozu M., Galizia L., Acuña C., Amodeo G. **(2018)**. Review Aquaporins: more than functional monomers in a tetrameric arrangement, *Cells*, 7, 209; doi:10.3390/cells7110209)

Prak S., Hem S., Boudet J., Viennois G., Sommerer N., Rossignol M., Santoni V. **(2008)**. Multiple phosphorylations in the C-terminal tail of plant plasma membrane aquaporins: Role in subcellular trafficking of AtPIP2;1 in response to salt stress. *Mol. Cell. Proteom.*, 7, 1019–1030.

Prado K., Maurel C. **(2013)**. Regulation of leaf hydraulics: From molecular to whole plant levels. *Frontiers Plant Sci.,* 4, 1–14.

Qiu J., McGaughey S.A., Groszmann M., Tyerman S.D., Byrt C.S. **(2020)**. Phosphorylation influences water and ion channel function of AtPIP2;1. *Plant Cell Environ.*, in press.

Reddy P.S., Rao T.S.R.B., Sharma K.K., Vadez V. **(2015)**. Genome-wide identification and characterization of the aquaporin gene family in *Sorghum bicolor* (L.). *Plant Gene,* 1, 18–28.

Reuscher S., Akiyama M., Mori C., Aoki K., Shibata D., Shiratake K. **(2013)**. Genome-wide identification and expression analysis of aquaporins in tomato. *PLoS ONE*, 8, e79052.

Sakurai J., Ishikawa F., Yamaguchi T., Uemura M., Maeshima M. **(2005)**. Identification of 33 rice aquaporin genes and analysis of their expression and function. *Plant Cell Physiol.*, 46(9), 1568–1577. doi: 10.1093/pcp/pci172.

Shibasaka M., Sasano S., Utsugi S., Katsuhara M. **(2012)**. Functional characterization of a novel plasma membrane intrinsic protein2 in barley. *Plant Signal Behav.,* 7, 1648-1652. doi: 10.4161/psb.22294 PMID: 23073013 22

Takano J., WadaM., Ludewig U., Schaaf G., VonWirén N., Fujiwara T. **(2006)**. The Arabidopsis major intrinsic protein NIP5;1 is essential for efficient boron uptake and plant development under boron limitation. *The Plant Cell,* 18, 1498–1509.

Tornroth-Horsefield S., Wang Y., Hedfalk K., Johanson U., Karlsson M., Tajkhorshid E., Neutze R., Kjellbom P. **(2006)**. Structural mechanism of plant aquaporin gating. *Nature,* 439, 688–694.

Tran S. T. H., Horie T., Imran S., Qiu J., McGaughey S., Byrt C.S., Tyerman S.D., Katsuhara M. **(2020)**. A survey of barley PIPc aquaporin ionic conductance reveals Ca^{2+}-sensitive HvPIP2;8 Na^+ and K^+ conductance. *Int. J. Mol. Sci.*, 21 (19), 1–20. doi: 10.3390/ijms21197135.

Tyerman S.D., Skerrett M., Garrill A., Findlay G.P., Leigh R.A. **(1997)**. Pathways for the permeation of Na^+ and Cl^- into protoplasts derived from the cortex of wheat roots. *J. Exp. Bot*., 48, 459–480.

Tyerman S.D., Bohnert H.J., Maurel C., Steudle E., Smith J.A. **(1999)**. Plant aquaporins: their molecular biology, biophysics and significance for plant water relations. *J. Exp. Bot.*, 50, 1055–1071.

Tyerman S.D., McGaughey S.A., Qiu J., Yool A.J., Byrt C.S **(2021)**. Adaptable and multifunctional ion-conducting aquaporins. *Annu. Rev. Plant Biol.*, 72:703–736

Uehlein N., Lovisolo C., Siefritz F., Kaldenhoff R. **(2003)**. The tobacco aquaporin NtAQP1 is a membrane CO_2 pore with physiological functions. *Nature,* 425, 734–737.

Vandeleur R.K., Mayo G., Shelden M.C., Gilliham M., Kaiser B.N., Tyerman S.D. **(2009)**. The role of plasma membrane intrinsic protein aquaporins in water transport through roots: Diurnal and drought stress responses reveal different strategies between isohydric and anisohydric cultivars of grapevine. *Plant Physiol.,* 149, 445–460.

Wang X., Gao F., Bing J., Sun W., Feng X., Ma X., Zhou Y., Zhang G. **(2019)**. Overexpression of the Jojoba aquaporin gene, ScPIP1, enhances drought and salt tolerance in transgenic Arabidopsis. *Int. J. Mol. Sci.,* 20, 153; doi:10.3390/ijms20010153

Xu F., Wang K., Yuan W., Xu W., Liu S., Kronzucker J.H., Chen G., Miao R., Zhang M., Ding M., Xiao L., Kai L., Zhang J., Zhu Y. **(2019)**. Overexpression of rice aquaporin OsPIP1;2 improves yield by enhancing mesophyll CO_2 conductance and phloem sucrose transport. *J. Exp. Bot.,* 70 (2), 671–681.

Zangi R., Filella M. **(2012)**. Transport routes of metalloids into and out of the cell: A review of the current knowledge. *Chemico Biol. Interact.,* 197, 47–57.

Zhao X.Q., Mitani N., Yamaji N., Shen R.F., Ma J.F. **(2010)**. Involvement of silicon influx transporter OsNIP2;1 in selenite uptake in rice. *Plant Physiol.,* 153, 1871–1877.

Zhu C., Schraut D., Hartung W., SchÃffner A.R. **(2005)**. Differential responses of maize MIP genes to salt stress and ABA. *J. Exp. Bot.,* 56, 2971–2981.

Zohary D., Hopf M. **(2000)**. Domestication of plants in the old world: the origin and spread of cultivated plants in West Asia, Europe, and the Nile Valley, 3rd edn. New York, Oxford University Press.16

CHAPTER 2

Ca^{2+}- sensitive and non-selective Na^{+}/K^{+} channel activity of a barley aquaporin HvPIP2;8

2.1. Introduction

Barley (*Hordeum vulgare* L.) is an important grain crop worldwide and is relatively salt tolerant compared to other crops and *Arabidopsis* (Munns et al., 2008; Ismail et al., 2017). In barley, the analysis of an expressed sequence tag (EST) database and subsequent cDNA cloning have led to the identification five HvPIP1s and fourteen HvPIP2s (Figure 1.6) (Hove et al., 2015). HvPIP2;8 forms a different clade with other HvPIPs (Figure 2.1A) (Shibasaka et al., 2012).

Robust water transport activity of HvPIP2;1 to HvPIP2;5 and HvPIP2;8 have been demonstrated using the heterologous expression system of *X. laevis* oocytes (Horie et al., 2011; Shibasaka et al., 2012). HvPIP1;3 showed a relatively weak water transport activity, and all the other HvPIP1s showed no water channel activity when expressed alone in oocytes (Horie et al., 2011). HvPIPs can influence the root hydraulic conductivity of barley, and the phosphorylation status and membrane internalization of the HvPIPs are implicated in the response of barley roots to salinity/osmotic stress (Horie et al., 2011; Kaneko et al., 2015; Knipfer et al., 2011; Besse et al., 2011; Coffey et al., 2011). Previous studies have revealed that there are multiple transporters influencing plasma membrane monovalent cation conductance in barley (Amtmann et al., 1997; Chen et al., 2007).

On the other hand, PIP1 and PIP2 isoforms can interact to form hetero-tetramers (Bienert et al., 2018). This interaction influences the movement of the PIP1 members to the plasma membrane (Zelazny et al., 2007; Bienert et al., 2018), which also influences water transport, substrate selectivity, and pH dependency compared to the PIP2 homo-tetramers (Otto et al., 2010; Byrt et al., 2017; Vitali et al., 2019). The cation transporting AtPIP2;1 was reported to show reduced cation transport when co-expressed with AtPIP1;2 in *X. laevis* oocytes (Byrt et al., 2017), and this also resulted in increased water transport, as has been reported previously for several PIP1/PIP2 combinations (Zelazny et al., 2007; Vandeleur et al., 2023; Horie et al., 2011). Here, the barley PIP2s (from HvPIP2;1 to HvPIP2;8 except HvPIP2;6) and PIP1s (HvPIP1;1 to HvPIP1;5) are surveyed to test for ion transport activity when expressed in *X. laevis* oocytes by two electrode voltage clamp (TEVC) experiments. In this study, we provide evidence that HvPIP2;8, an abundantly expressed aquaporin that shows water channel activity (Shibasaka et al., 2012) and only shows cation conductance among other HvPIP2s. The

HvPIP2;8 cation selectivity, divalent cation sensitivity, interaction with PIP1 isoforms were examined, as well as the HvPIP2;8 expression patterns in different barley cultivars.

HvPIP2;8 structure was characterized by Shibasaka et al., 2012. Particularly, HvPIP2;8 presents six transmembrane domains, and two NPA motifs. Furthermore, following highly conserved amino acid residues, which are considered to be involved in the regulation of activation, $Ser^{280,}$ and Ser^{285} via phosphorylation, His^{206}, Lys^{199}, Arg^{200}, and Arg^{203} in Loop D, and Asp^{13}, Asp^{16}, Glu^{18}, Asp^{27}, Asp^{30}, Asp^{38}, and Glu^{41} in acidic N-terminal, via cytosolic pH, are also present in HvPIP2;8. Interestingly, HvPIP2;8 exhibits three histidine residues in Loop C, which are not conserved in other members (Figure 2.1B) (Shibasaka et al., 2012).

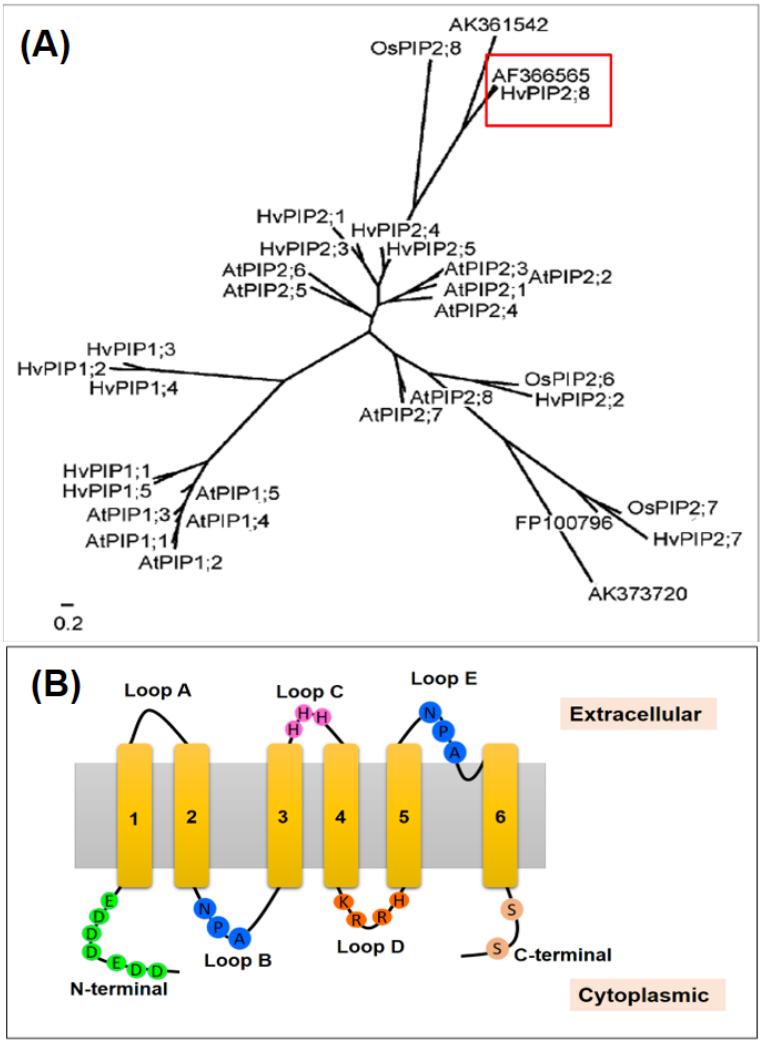

Figure 2.1. Phylogenetic analysis and predicted protein structure. A) Phylogenetic tree of the plasma membrane intrinsic protein (PIP) from barley (*H. vulgare* cv Harunanijo), *Arabidopsis thaliana*, and rice (*O. sativa* cv Nipponbare). The scale bar indicates 0.2 substitutions per site. **B)** Predicted structure of HvPIP2;8 (modified from Shibasaka et al., 2012).

2.2. Materials and methods

2.2.1. Plant materials and growth conditions

For sterilization, the seeds of barley (*Hordeum vulgare* L., cv. Haruna-Nijo, cv. K305, cv. I743) were treated with 10% H_2O_2 for 10 min. After 1 day, seeds were immersed in distilled water with aeration, and the germinated seeds were transplanted and hydroponically cultured with aeration in 3.5 L pots with 0.25 mM $CaSO_4$ for 2 days, and then for more days after replacing the medium with the hydroponic solution as described previously (Katsuhara et al., 2002). With aeration, all pots were in the dark for first 1 day, and then for a 12 h dark/12 h light cycle with fluorescent lamps of 150 photons μmol m^{-2} s^{-1} in an air conditioned room (23 ± 0.5°C). Salt stress (100 mM or 200 mM NaCl) was treated with 5-day-old seedlings by adding 20.5 g and 40.9 g NaCl to the 3.5 L of hydroponic solution, respectively.

2.2.2. Extraction of RNA and gene expression analysis by RT-PCR and real-time quantitative PCR (qPCR)

Shoots and roots were sampled from hydroponically grown barley plants at 5, 6, or 10 days old (control), and 1 or 5 days after the treatment of 100 mM or 200 mM NaCl. Samples were rinsed and immediately frozen in liquid nitrogen. Total RNA was extracted using a mortar and pestle and the RNeasy Plant Mini Kit (Qiagen, Hilden, Germany). cDNA was synthesized using the Rever Tra Ace kit (Toyobo, Osaka Japan). cDNA fragments of *HvPIP2;8* (GenBank accession number AK356299) and Elongation factor 1α (*EF1α*, GenBank accession number Z50789) as an internal control were amplified with a set of specific primers listed in Table 2.1:

Table 2.1. Gene-specific primer pairs used in the RT-PCR and qPCR experiments

Gene name	Forward primer (5′-3′)	Reverse primer (5′-3′)
HvPIP2;8 (full length)	GGAGATCTAGCTTCATGACTATGGCCG	CCAGATCTAAGTAGCTAGACGGCG
HvPIP2;8 (RT-PCR)	ACACAAGCGCCAGACCGACG	GCCAGGTTGATGCTACGGCGG
HvPIP2;8 (qPCR)	TTGGGGAGACCAGTGGATCT	GCCAGGTTGATGCTACGGCGG
HvEF1α	GATAGTTGTTTTAGTCGCTTGGGTTATT	CACCAACACAACCGAACGATAC

Absolute quantification was performed in the qPCR analysis using the 7300 real-time PCR machine (Applied Biosystem, Foster City, CA, USA) with PCR conditions of 50°C for 2

min, 95 °C for 10 min, 33 cycles of 95 °C for 15 s, and 58 °C for 1 min to analyze the expression level of *HvPIP2;8*. Transcript copy numbers were quantified from three technical replications, and two biological independent experiments were conducted.

2.2.3. Preparation of HvPIP cRNAs

The coding region of each *HvPIP* (from *Hordeum vulgare* cv. Haruna-Nijo) was cloned into the vector pXβG-ev1 (Horie et al., 2011; Shibasaka et al., 2012). Each construct was linearized and cRNAs were synthesized using the mMESSAGE mMACHINE T3 kit (Ambion, Austin, TX, USA), with a final concentration of 1μg/μL.

2.2.4. Expression of HvPIPs in *X. laevis* oocytes

Oocytes were obtained from adult female *X. laevis* frogs and placed in a modified Barth's solution (MBS: 88 mM NaCl, 1 mM KCl, 2.4 mM $NaHCO_3$, 1.5 mM Tris-HCl (pH 7.6), 0.3 mM $Ca(NO_3)_2 \cdot 4H_2O$, 0.41 mM $CaCl_2 \cdot 4H_2O$, 0.82 mM $MgSO_4 \cdot 7H_2O$, 10 μg mL^{-1} penicillin sodium salt, and 10 μg mL^{-1} streptomycin sulfate). The lobes were torn apart and treated with 1 mg mL^{-1} collagenase B (type B, Boehringer Mannheim, Germany) in Ca-free MBS for 1.5 h. Isolated oocytes were washed several times and incubated in MBS for 1 day at 20 °C before the microinjection.

Each oocyte was injected with 10 ng of *HvPIP2* cRNA. As for *HvPIP1s*, 40 ng of each cRNA was injected. Oocytes were injected with nuclease-free water as a negative control in all experiments. Injected oocytes were incubated for 24 h to 48 h at 20 °C in MBS or a low Na^+ Ringer solution until the electrophysiological experiments were performed. The experiments using frog oocytes were approved by the Animal Care and Use Committee, Okayama University (approval number OKU-2017271), which follows the related international and domestic regulations.

2.2.5. Electrophysiology

Two-electrode voltage clamp (TEVC) was performed using *X. laevis* oocytes injected with water or cRNA. Borosilicate glass pipettes (Harvard Apparatus, GC150TF-10, 1.5 mm O.D. × 1.17 mm I.D.) for voltage and current injecting electrodes were pulled and filled with 3 M KCl. A bath clamp system was used to minimize the effect of series resistance in the bath solution. The bath current and voltage sensing electrodes consisted of a silver–silver chloride electrode connected to the bath by a 3% agar with 3 M KCl bridges. All bath solutions contained high external calcium concentration (1.8 mM $MgCl_2$, 1.8 mM Mannitol, 1.8 mM $CaCl_2$, 10 mM HEPES, pH 7.5 with Tris) or low external calcium concentration (1.8 mM $MgCl_2$, 1.8 mM EGTA (ethylene glycol-bis (β- aminoethyl ether)-N, N, N', N'-tetraacetic acid), 1.8 mM $CaCl_2$, 10 mM HEPES, pH 7.5 with Tris), otherwise mentioned. Osmolality of the bath solutions was adjusted to 200 mosmol kg^{-1} with supplemental mannitol. Free Ca^{2+}

concentration in the bath solution was calculated using https://somapp.ucdmc.ucdavis.edu/pharmacology/bers/ maxchelator/CaMgATPEGTA-NIST-Plot.htm. Divalent cations (Ca^{2+}, Mg^{2+}, Ba^{2+} and Cd^{2+}) and monovalent cations (Na^{+}, K^{+}, Li^{+}, Cs^{+} and Rb^{+}) were added as chloride salts or gluconate salts. Each oocyte was carefully pierced with the voltage and current electrodes and the membrane voltage was allowed to stabilize. Conductance responses were monitored through the experiments by the repeat of steps from −120 mV to +30 mV with 2 s steady states and 5 s intervals. The recording was performed and analyzed with an Axoclamp 900A amplifier and Clampex 9.0 software (Molecular Devices, CA, USA) at room temperature (20 – 22 °C).

Biological replication included testing of different oocytes from different batches harvested from different frogs, and the oocyte and batch replication was three or more; the representative result from one or more oocyte batch from each experiment was included in the figures.

2.2.6. Water transport activity assay in *X. laevis* oocytes

The coding regions of *HvPIP1;1; HvPIP1;2; HvPIP1;3; HvPIP1;4; HvPIP1;5* and *HvPIP2;8* cDNA were sub-cloned into the pXβG-ev1 expression vector. The constructs were linearlized with *PstI*, and capped cRNA were synthesized using the mMESSAGE mMACHINE T3 *in vitro* transcription kit (Ambion). Oocytes were isolated from adult female *X. laevis* frogs and maintained as described in part 2.2.4. Oocytes were injected with 50 nL of a cRNA solution containing 10 ng of *HvPIP2;8* and co-expressed 10 ng of *HvPIP2;8* and 40 ng of each *HvPIP1s* as described above. As a negative control, nuclease-free water-injected oocytes were used. Osmotic permeability (P_{os}) was calculated from the increase in volume with time (n = 7 to 10) using the following equation:

$$P_{os} = V_o \, (d \, (V/V_o)/dt) \, / \, S \times V_w \, (Osm_{in} - Osm_{out})$$

Where: V_o is the initial oocyte volume (mm^3); $d\,(V/V_o)/dt$ is the rate of initial relative cell volume change (mm^3s^{-1}); S is the initial surface area (mm^3); V_w is the partial molar volume of water $18cm^3mol^{-1}$; $Osm_{in} - Osm_{out}$ is the change in osmolality.

2.2.7. Statistical analysis

Statistical analysis was conducted using SPSS statistics software (version 20). Analysis of variance was identified by one-way ANOVA followed by the least significant difference (LSD) test at the 0.05 level; or one-way ANOVA followed by Duncan's multiple comparisons test.

2.3. Results

2.3.1. Ion transport activity was observed for HvPIP2;8 in test screening for barley PIP2 ionic conductance

To test HvPIP ion transport activity, two electrode voltage clamp (TEVC) experiments were conducted using *X. laevis* oocytes expressing HvPIP2s (from HvPIP2;1 to HvPIP2;8). This revealed that only the expression of HvPIP2;8 elicited large bidirectional and voltage-independent currents in the bath solution, containing 86.4 mM NaCl and 9.6 mM KCl, and 30 µM free Ca^{2+} (low Ca^{2+} condition) (Figure 2.2A). Small currents were observed in the *HvPIP2;1*-injected oocytes in low Ca^{2+} conditions, and in some experiments these currents were greater than the currents recorded for the water-injected controls (Table 2.2). When the bath solution contained a high Ca^{2+} concentration, 1.8 mM Ca^{2+}, the HvPIP2;8-associated currents were smaller than in low Ca^{2+} conditions (Figure 2.2B). The HvPIP2;8-associated ionic conductance was 36.46 and 14.50 µS in low and high external free Ca^{2+} conditions, respectively, and these values were significantly higher than the ionic conductance of the water-injected oocytes (3.31 and 3.44 µS, respectively). HvPIP2;2, HvPIP2;3, HvPIP2;4, HvPIP2;5, and HvPIP2;7 did not elicit ionic conductance that was not significant to that of the water-injected oocytes (Figure 2.2A, B, Table 2.2).

The ionic conductance induced by HvPIP2;8 was further examined in response to various concentrations of Ca^{2+} supplemented in the bath solution containing 86.4 mM NaCl and 9.6 mM KCl. Interestingly, the ionic conductance was gradually inhibited in accordance with increasing concentration of external free Ca^{2+} (Figure 2.2C, D). This result suggested a negative correlation between the HvPIP2;8-mediated ionic conductance and the external free Ca^{2+} concentrations. In all experiments, no shift of the reversal potential was observed at high or low external calcium concentrations (Table 2.3), indicating that the channel was not permeable to Ca^{2+}.

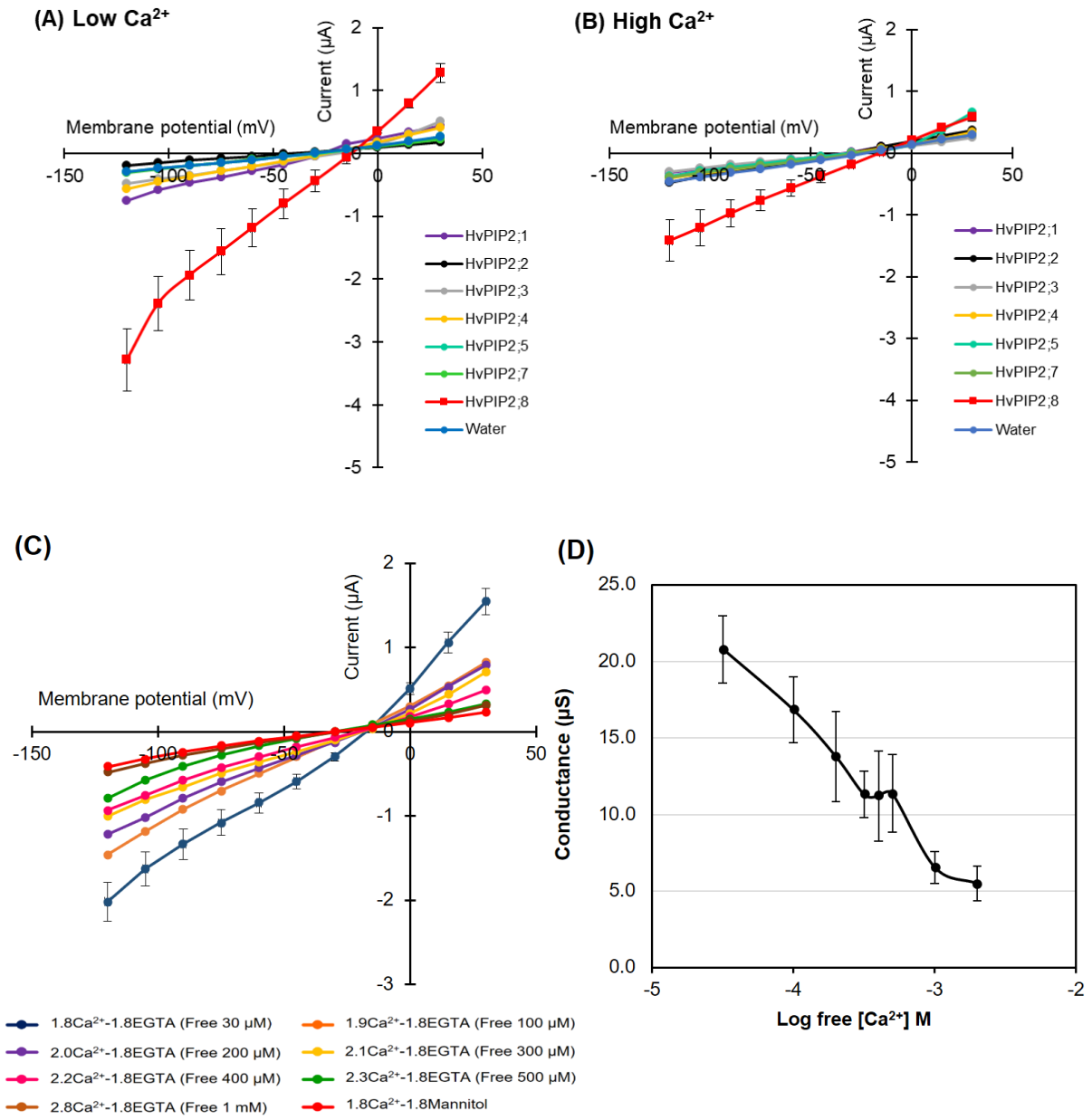

Figure 2.2. Electrophysiological survey to test for HvPIP2 ion transport (**A**, **B**) Current–voltage relationships of *X. leavis* oocytes expressing each *HvPIP2* in the presence of 86.4 mM NaCl and 9.6 mM KCl with 30 µM Ca^{2+} (**A**) or 1.8 mM Ca^{2+} (**B**). A total of 10 ng of each *HvPIP2* cRNA or water (control) was injected into *X. laevis* oocytes. **(C)** The inhibition of Na^{+} transport by external free Ca^{2+} concentration in *HvPIP2;8* expressed in *X. laevis* oocytes. **(D)** Relationships between the external free Ca^{2+} concentration and HvPIP2;8-mediated Na^{+} conductance in the presence of 86.4 mM NaCl and 9.6 mM KCl (R^2 = 0.93) in (C). The free Ca^{2+} concentrations are given in methods. A step pulse protocol of −120 mV to +30 mV with a 15 mV increment was applied on every oocyte. Ionic conductance was calculated based on the data obtained from V = −75 mV to −120 mV of the membrane potential. Data are the means ± SE (n = 5 for A, C, D and n = 7 for B).

Table 2.2. Ionic conductance of oocytes injected HvPIP2s or water (control) in the presence of 86.4 mM NaCl and 9.6 mM KCl

Ionic conductance (μS)	Water (control)	HvPIP2s						
		2;1	2;2	2;3	2;4	2;5	2;7	2;8
Low Ca^{2+} (30 μM)	3.33 ± 0.6^{ns}	8.34 ± 2.1^{ns}	5.52 ± 0.4^{ns}	5.30 ± 0.8^{ns}	6.66 ± 1.5^{ns}	4.76 ± 0.6^{ns}	4.08 ± 0.8^{ns}	36.46 ± 5.5*
High Ca^{2+} (1.8 mM)	3.44 ± 2.4^{ns}	3.38 ± 0.4^{ns}	2.44 ± 1.4^{ns}	3.58 ± 0.6^{ns}	4.45 ± 0.6^{ns}	3.24 ± 2.3^{ns}	3.79 ± 0.8^{ns}	14.50 ± 4.5*

Ionic conductance was calculated based on the data obtained from V = −75 mV to −120 mV of the membrane potential in Figure 2.2A, B. Data are means ± SE (n = 5 - 7), ns (not significant); * (*P < 0.05*) using one-way ANOVA with Duncan's multiple comparisons test.

Table 2.3. Reversal potential of ion currents in oocytes expressing HvPIP2;8

Reversal potential (mV)	86.4 mM NaCl + 9.6 mM KCl	86.4 mM KCl + 9.6 mM NaCl
High Ca^{2+}	10.60 ± 1.02	12.21 ± 0.97
Low Ca^{2+}	10.30 ± 1.10	12.33 ± 1.05

Free external Ca^{2+} was calculated as about 30 μM in low Ca^{2+} and 1.8 mM in high Ca^{2+} solutions. Data are means ± SE.

2.3.2. HvPIP2;8 monovalent alkaline cation selectivity

Current–voltage relationships for the HvPIP2;8-expressing oocytes were recorded in the presence of 96 mM Na^+, K^+, Rb^+, Cs^+, or Li^+ (as chloride salt; Figure 2.3A). When the oocytes were bathed in a 96 mM Li^+, Rb^+, or Cs^+ solution, the HvPIP2;8-associated currents did not differ from the background currents recorded for the water-injected control oocytes; ionic conductance was only detected for the HvPIP2;8-expressing oocytes when bathed in either a Na^+- or K^+-containing solution (Figure 2.3A, B).

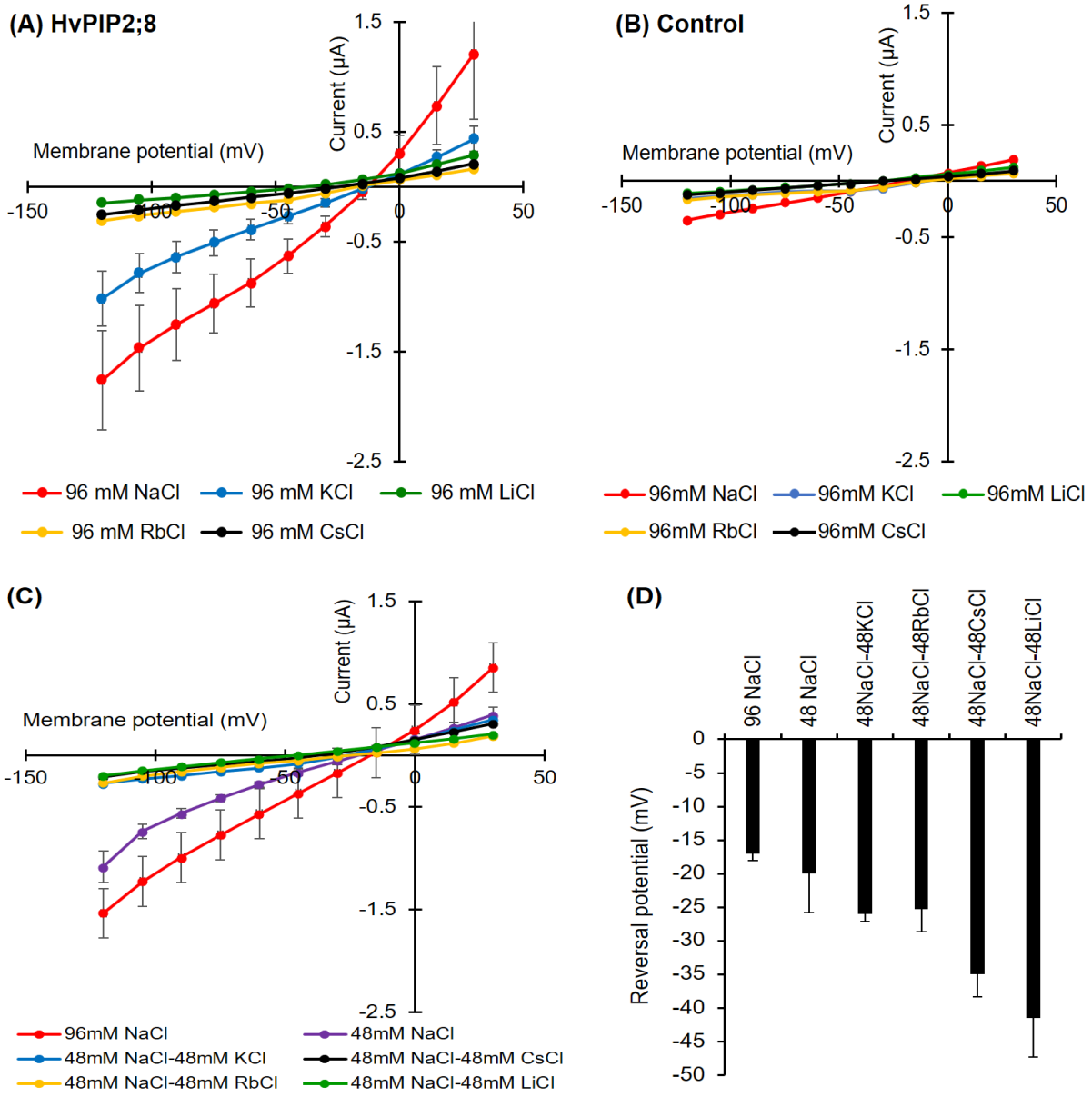

Figure 2.3. Monovalent alkaline cation selectivity of HvPIP2;8 and the effect of the interaction of K^+ and Na^+ on HvPIP2;8-mediated ion conductance activity. Current–voltage relationships obtained from oocytes either expressing HvPIP2;8 (**A**) or injected with water (**B**). HvPIP2;8 displays a different monovalent alkaline cation selectivity. Oocytes were successively immersed in bath solutions with a high calcium condition, supplemented with Na^+, K^+, Cs^+, Rb^+, and Li^+ (as chloride salts) at the concentration of 96 mM. (**C**) Inhibition of HvPIP2;8-mediated Na^+ transport by monovalent alkaline cations in the presence of 48 mM NaCl with 48 mM of each alkaline cation. **(D)** Reversal potentials of currents flowing through HvPIP2;8 in the presence tested of 48 mM NaCl with 48 mM each alkaline cation in D. The total concentration of (Na + K) was constantly 96 mM. *X. laevis* oocytes were injected with 10 ng of *HvPIP2;8* cRNA for the recording of the conductance in every experiment. Data are the means ± SE (n = 7 to 8 for A, n = 5 for B, n = 4 to 5 for C, and n = 5 to 6 for D).

HvPIP2;8-associated currents were then measured in the presence of solutions with combinations of different monovalent cations. Current–voltage relationships were obtained from HvPIP2;8 expressed in oocytes bathing in 48 mM Na^+ solutions in the co-presence of either 48 mM K^+, Cs^+, Rb^+, or Li^+ (as chloride salt). Smaller HvPIP2;8-associated currents were observed in Na^+ solutions when other monovalent cations were added to the solution (Figure 2.3C). A positive shift in the reversal potential was observed in 96 mM NaCl solutions relative to 48 mM NaCl solutions, consistent with HvPIP2;8 mediating Na^+ transport (Figure 2.3C, D). However, in the presence of solutions containing 48 mM KCl and 48 mM NaCl, there were smaller currents than in solutions with only 48 mM NaCl (Figure 2.3C).

The ion permeability ratios were calculated from the reversal potential shift according to the modified Goldman equation where the permeability of Cl^- was ignored:

$$E_{rev} = -\frac{RT}{F} ln\left(\frac{P_k[K^+]_{in} + P_{Na}[Na^+]_{in}}{P_k[K^+]_{out} + P_{Na}[Na^+]_{out}}\right)$$

Where E_{rev} is the reversal potential (mV);

R is the gas constant (8.31 J/K);

T is the absolute temperature (Kelvin);

F is the Faraday constant (9.654 x 10^4 C/mol);

P_k is the selectivity for that ion (k);

$[K^+]_{out}$: the extracellular concentration of the K^+;

$[K^+]_{in:}$ the intracellular concentration of the K^+;

$[Na^+]_{out}$: the extracellular concentration of the Na^+;

$[Na^+]_{in:}$ the intracellular concentration of the Na^+;

RT/F is approximately 25.26 mV at the experimental temperature (20 °C)

The intracellular concentration of ions must be kept constant. Therefore, the Goldman equation is modified as follows:

$$\text{In } x = \frac{P_k}{P_{Na}}, \text{then}$$

$$E_{rev} = -58log\left(\frac{Constant}{x[K^+]_{out} + [Na^+]_{out}}\right)$$

Considering Table 2.3, HvPIP2;8-injected oocytes were bathed in 86.4 mM NaCl and 9.6 mM KCl or 86.4 mM KCl and 9.6 mM NaCl solutions in high external free Ca^{2+} (free 1.8 mM Ca^{2+}) condition, the reversal potential for Na^+ (E_{Na+}) in the oocyte was −10.6 mV and the reversal potential for K^+ (E_{K+}) was −12.2 mV. In the presence of solutions with combination of different

monovalent cations with 48 mM Na^+ solutions in the co-presence of either 48 mM Cs^+, Rb^+, or Li^+ (as chloride salt), the measured reversal potential was −35 mV, −25.2 mV, or −41.5 mV, respectively (Figure 2.3C, D). The reversal potential 96 mM NaCl solution was −17 mV. Then, the Goldman equation suggested the stoichiometry of the HvPIP2;8-transporter, as Table 2.4.

Table 2.4. Ion permeability ratios of HvPIP2;8

ion	**Na^+**	**K^+**	**Rb^+**	**Cs^+**	**Li^+**
P_{ion}/P_{Na}	1	0.92	0.43	≈ 0	≈ 0

Thus, the ion permeability ratios from Table 2.4 indicate that HvPIP2;8 drives in 1 Na^+ to ~ 1 K^+ with something preference of Na^+ to K^+, that is consistent with higher Na^+ conductance than K^+ conductance as observed (Figure 2.4C).

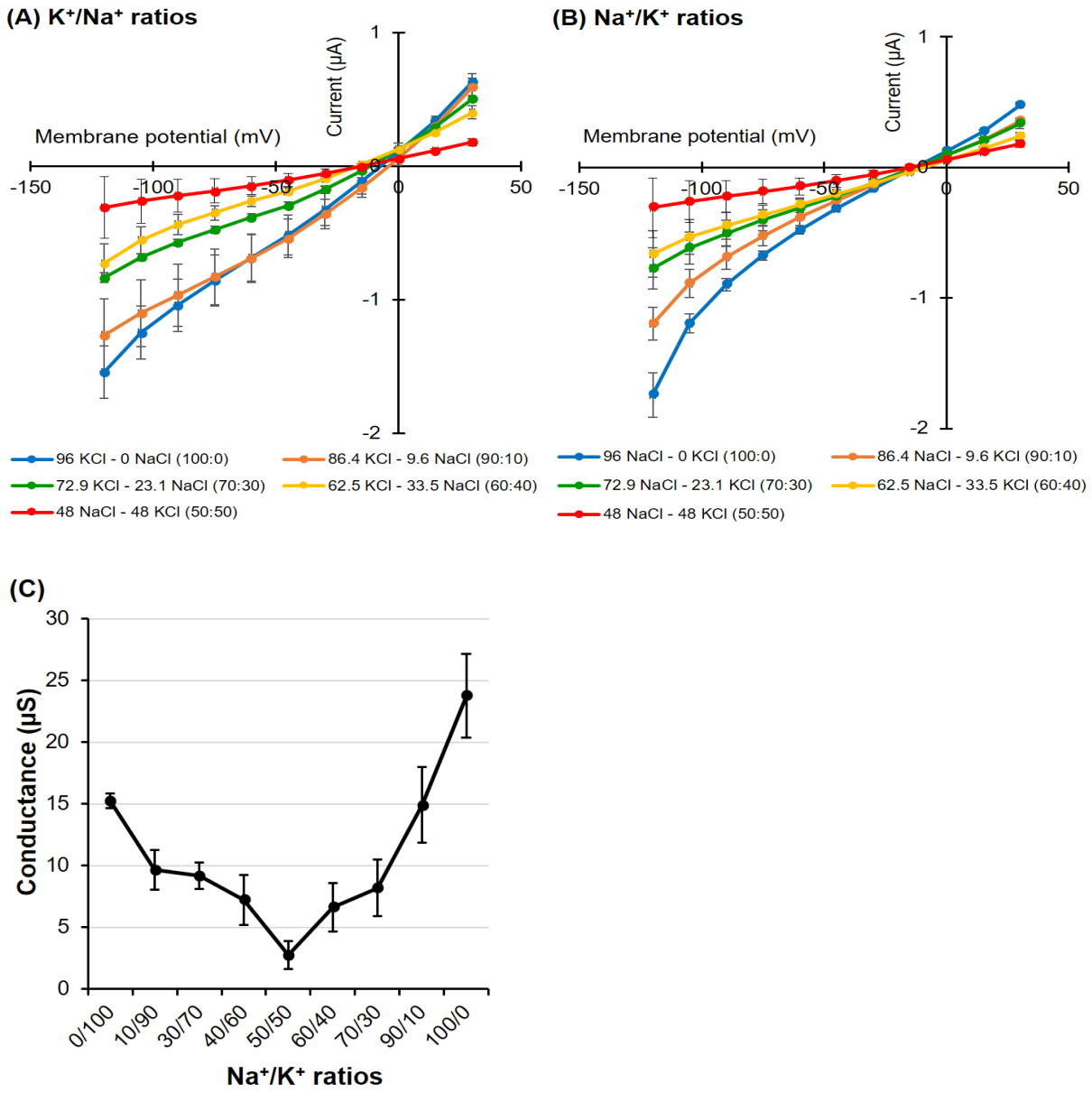

Figure 2.4. Interaction K^+ with Na^+ cations through HvPIP2;8-transporter. (A) Effect of external Na^+ cation on K^+ permeability. **(B)** Effect of external K^+ cation on Na^+ permeability through HvPIP2;8-transporter. **(C)** The effect of external Na^+/K^+ concentration ratios on the conductance of HvPIP2;8-expressing oocytes from V (membrane potential) = −75 mV to −120 mV. The total concentration of (Na + K) was constantly 96 mM. Na^+ and K^+ external concentration (chloride salt) were 9 different ratios bath solutions with high calcium condition contained a background (1.8 mM $MgCl_2$, 1.8 mM $CaCl_2$, 1.8 mM Mannitol, 10mM HEPES pH 7.5 with Tris). Steady-state current-voltage curves of *X. laevis* oocytes injected with 10 ng of cRNA per oocyte from the same batch. Data are means ± SE, n = 5 to 6.

The use of solutions that included different combinations of Na^+ and K^+ concentrations revealed that an external Na^+: K^+ ratio of 50:50 limited the ionic conductance of the HvPIP2;8-expressing oocytes; the magnitude of the currents in the 50:50 ratio solutions was 88.4% and 81.9% of the magnitude of the currents in a 100:0 or 0:100 Na^+: K^+ ratio solution, respectively

(Figure 2.4A-C). These observations indicated that the Na^+ permeability of HvPIP2;8 appears to be highly dependent on the external K^+ concentration.

2.3.3. HvPIP2;8 was not permeable to Cl^-

The effect of the presence of the external anion Cl^- on HvPIP2;8 ion transport was tested using Na-gluconate and Choline-Cl solutions (96 mM each). Similar current–voltage relationships for HvPIP2;8-expressing oocytes were observed regardless of whether there was Cl^- or gluconate solutions used in the bath (Figure 2.5A), and there was no shift in the reversal potential (−9 mV) for the different solutions, indicating that the HvPIP2;8-induced currents were not affected by Cl^-. In the presence of 96 mM Choline-Cl, the HvPIP2;8-expressing oocytes elicited minor currents (−0.68 ± 0.42 µA at −120 mV), comparable to those of the water-injected control oocytes (−0.39 ± 0.03 µA at −120 mV), which was significantly different to the currents observed in the presence of 96 mM NaCl (Figure 2.5B). These results indicated that the HvPIP2;8-associated Na^+-induced currents across the plasma membrane of the oocytes were not affected by the external Cl^- concentration.

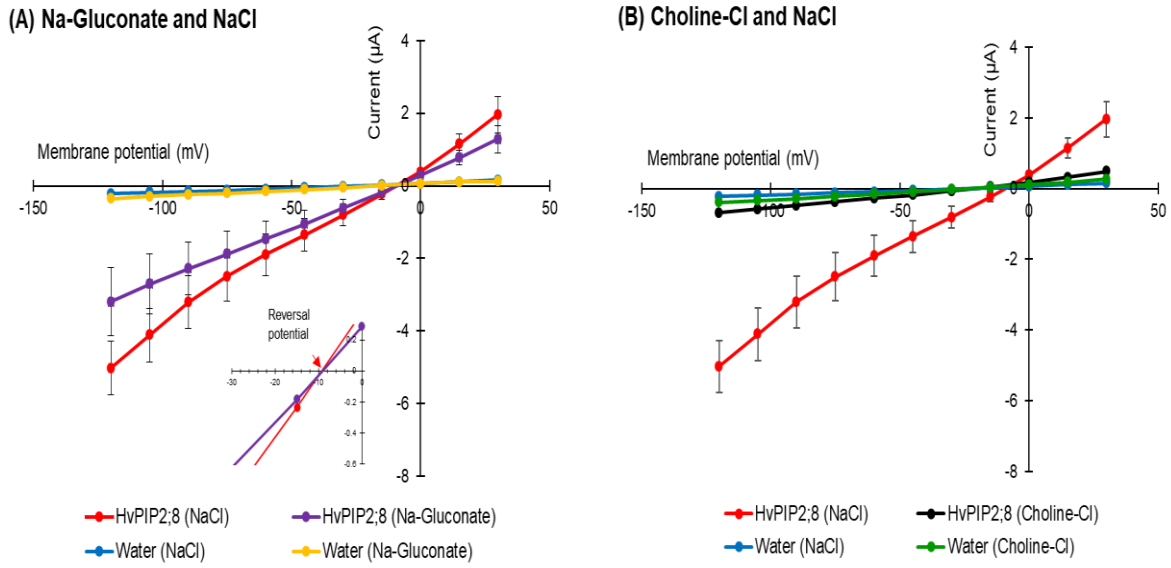

Figure 2.5. HvPIP2;8-mediated Na^+ transport is Cl^- independent. (A) Current–voltage relationships obtained from oocytes either expressing HvPIP2;8 or injected with water in the presence of either 96 mM NaCl or 96 mM Na-gluconate. Inset: Expanded current voltage curves around the reversal potential. **(B)** Current–voltage relationships obtained from oocytes either expressing HvPIP2;8 or injected with water in the presence of either 96 mM NaCl or 96 mM Choline-Cl. All solutions contained 30 µM Ca^{2+}. *X. laevis* oocytes were injected with 10 ng of *HvPIP2;8* cRNA. Data are the means ± SE (n = 7 to 8).

2.3.4. Effects of divalent cations on HvPIP2;8-mediated ion transport activity

The effect of different divalent cations on the ion conductance activity of HvPIP2;8 was tested. Maximal ionic conductance associated with HvPIP2;8 was observed when the oocytes were bathed in a divalent cation-free saline (86.4 mM NaCl, 9.6 mM KCl, 10 mM HEPES, pH 7.5 with Tris, and osmolality was adjusted to 200 mosmol Kg^{-1} with supplemental mannitol). However, the HvPIP2;8 channel was inhibited by the extracellular application of 1.8 mM Ba^{2+}, Cd^{2+}, or Ca^{2+} (Figure 2.6A). In contrast, the application of 1.8 mM $MgCl_2$ gave rise to a weaker inhibitory effect on the HvPIP2;8-mediated ion currents (Figure 2.6A, B).

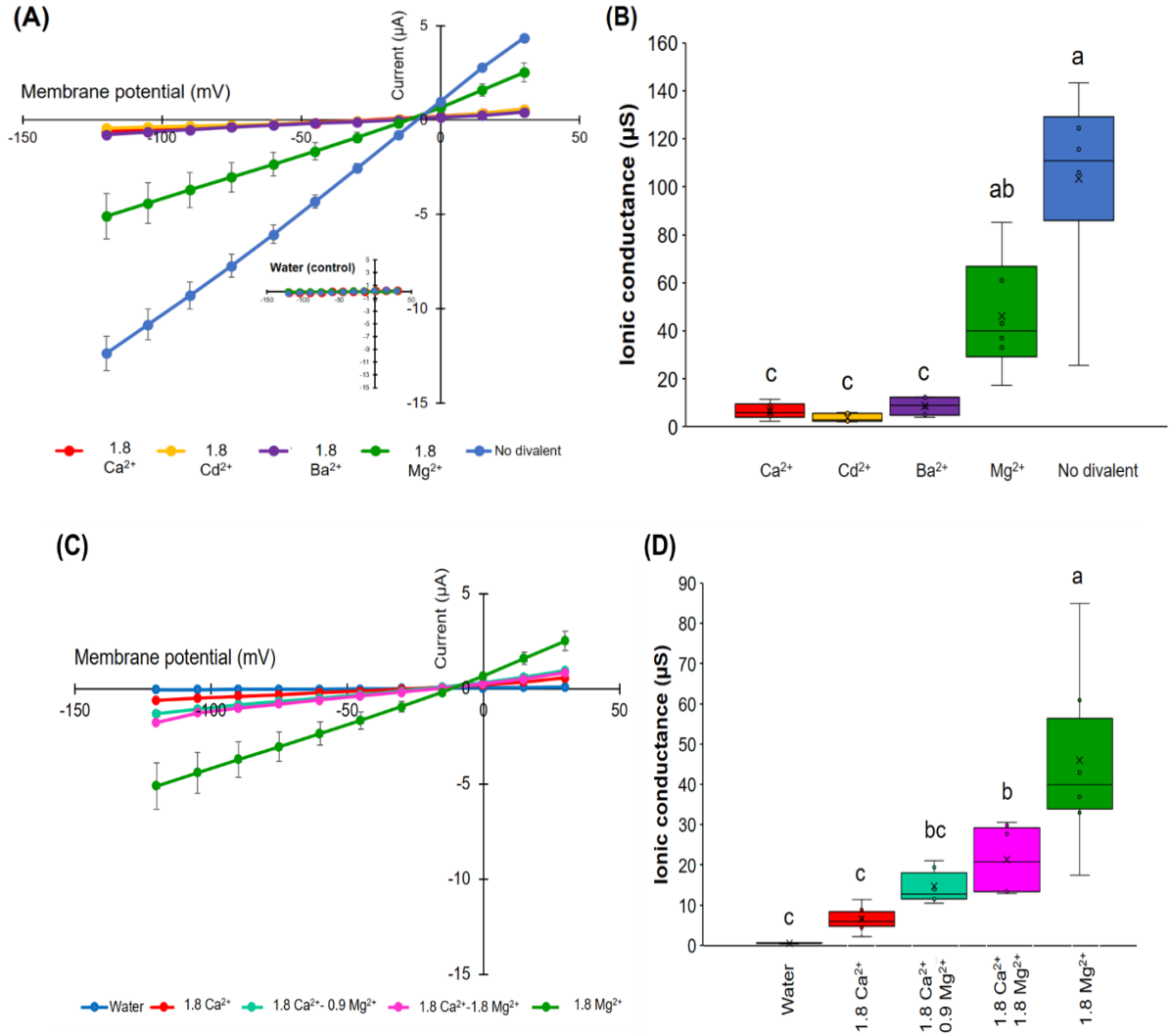

Figure 2.6. Effects of divalent cations on the ion current responses in oocytes expressing HvPIP2;8. (A) Effect of divalent cations on the ion currents of the HvPIP2;8-transporter; bath solutions with a high 1.8 mM Ca^{2+} background calcium conditions were successively replaced with either 1.8 mM Ca^{2+}, Ba^{2+}, Cd^{2+}, and Mg^{2+} (as chloride salts), at concentrations of 86.4 mM NaCl and 9.6 mM KCl. **(B)** Box plot summary of the ionic conductance presented in (A); the ionic conductances were calculated from V = −75 mV to −120 mV. **(C)** Relief of Ca^{2+} inhibition by the addition of Mg^{2+} on the ion current responses in oocytes expressing HvPIP2;8; note the different range of the Y-axis from the plot in (A). **(D)** Box plot summary of the ionic conductance presented in (C). Steady-state current–voltage curves of the *X. laevis* oocytes injected with 10 ng of cRNA per oocyte were

recorded. Currents from the oocytes injected with water were the negative controls from the same batch. Significant differences ($P < 0.05$) are indicated by different letters using one-way ANOVA with Duncan's multiple comparisons test. Data are the means ± SE of three independent experiments, (n = 6 for A, B).

An increase in the $MgCl_2$ concentration in the presence of 1.8 mM $CaCl_2$ tended to partially cancel out the inhibitory effect of Ca^{2+} in relation to the ion channel activity (Figure 2.6C, D). These results indicate that there may be a competitive interaction between Ca^{2+} and Mg^{2+}, which influences HvPIP2;8-mediated ion channel activity and the presence of more external Mg^{2+} can partially relieve the inhibitory effect of high Ca^{2+} on HvPIP2;8 ionic conductance.

2.3.5. Co-expression of HvPIP2;8 with HvPIP1s limited HvPIP2;8 ion transport activity

I examined the effect of the co-expression of HvPIP1s (HvPIP1;1 to HvPIP1;5) with HvPIP2;8 in relation to ionic conductance. When expressed alone, each HvPIP1 displayed similar currents to the water-injected controls (Figure 2.7A, C). However, when each HvPIP1 was co-expressed with HvPIP2;8, the large HvPIP2;8-associated currents were not observed in any of the co-expression combinations examined, whereas when HvPIP2;8 was expressed alone, the HvPIP2;8-associated currents were significant as expected (Figure 2.7B, D). These results indicate that HvPIP1s might be interacting with HvPIP2;8 and that this either prevents, or significantly reduces (for HvPIP1;3 and HvPIP1;4), the HvPIP2;8 ion channel activity, but not effect to water permeability (Figure 2.8). The inhibitory effect on the ionic current may not attribute to the hindrance of expression or localization of HvPIP2;8 in oocytes, since water permeability was not apparently hampered.

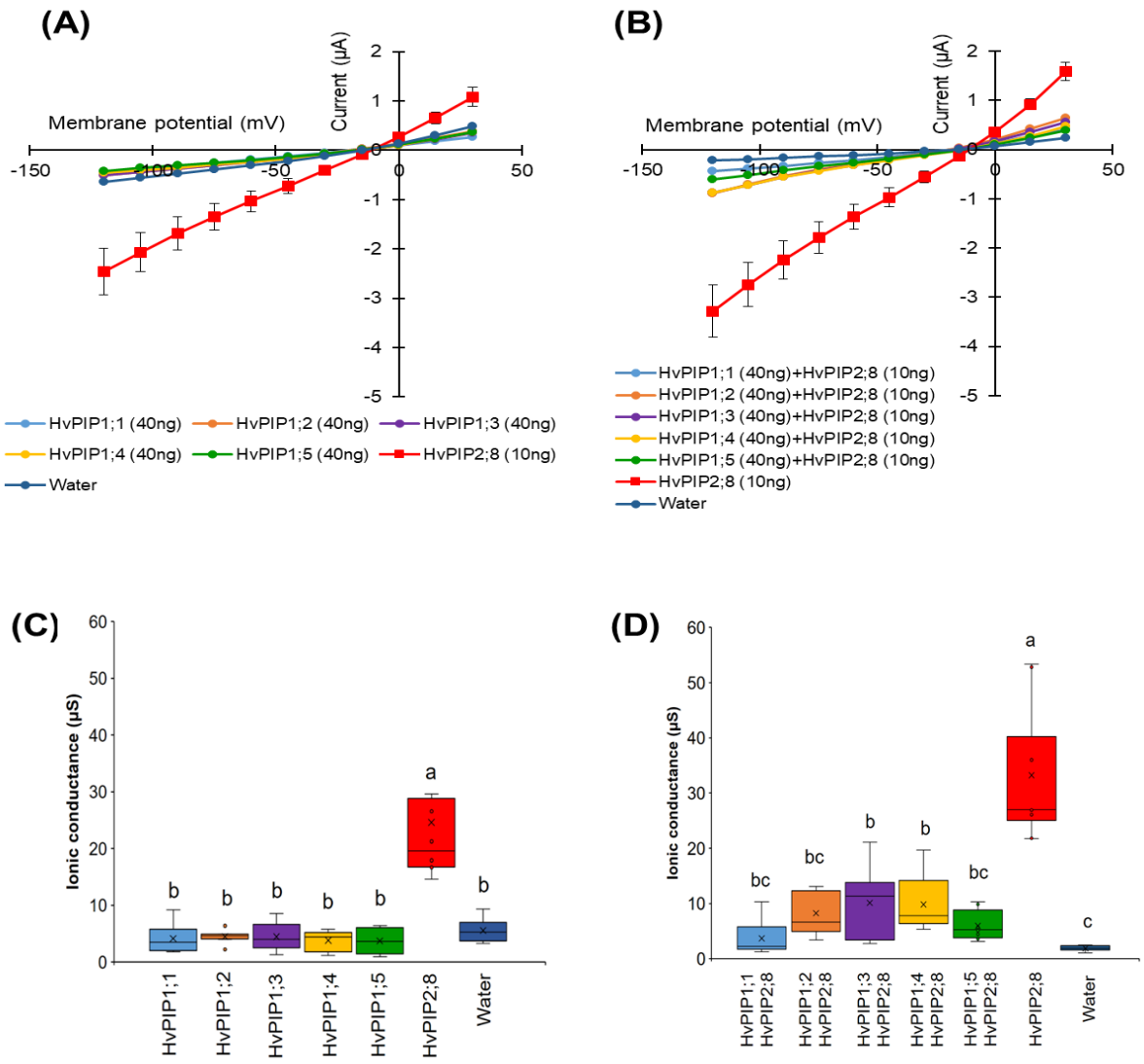

Figure 2.7. Co-expression of HvPIP1s and HvPIP2;8 reduces HvPIP2;8-dependent currents in *X. laevis* oocytes. (A) Current–voltage relationships obtained from oocytes either expressing HvPIP2;8 alone, each HvPIP1 alone, or injected with water; each HvPIP1 of the five HvPIP1s did not show ion channel activity when expressed alone. **(B)** Co-expression of HvPIP2;8 with each HvPIP1 largely inhibited the ion channel activity of HvPIP2;8. **(C, D)** Box plot summary of the ionic conductance for data shown in (A) and (B), respectively. Oocytes were injected with 10 ng cRNA of *HvPIP2;8*, 40 ng cRNA of each HvPIP1 in both the solo- and co-expression analyses. The bath solution included 86.4 mM NaCl, 9.6 mM KCl, 1.8 mM $MgCl_2$, 1.8 mM EGTA, 1.8 mM $CaCl_2$, 10 mM HEPES, and a pH 7.5 with Tris, and therefore the free Ca^{2+} concentration was 30 µM. Significant differences ($P < 0.05$) are indicated by different letters using one-way ANOVA with Duncan's multiple comparisons test. Data are the means ± SE (n = 8).

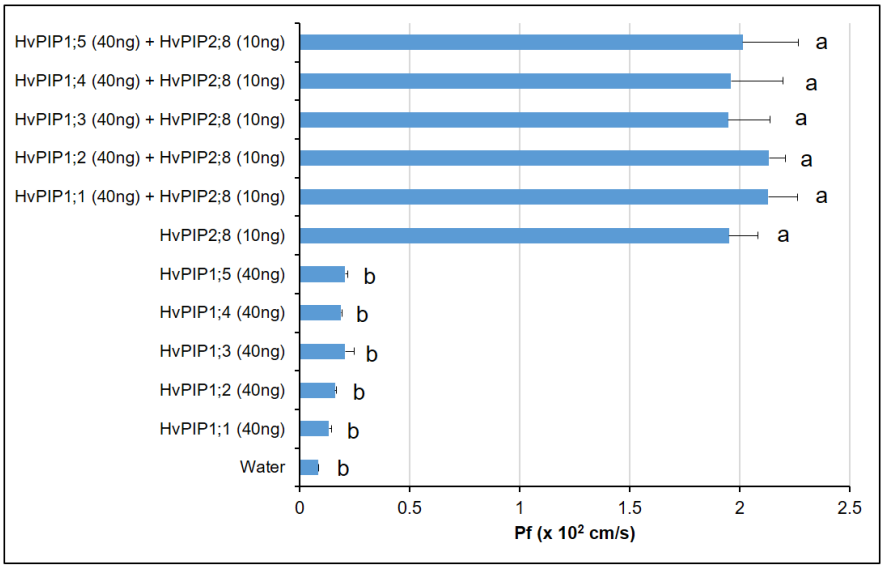

Figure 2.8. Water transport activity of co-expression HvPIP1s with HvPIP2;8. The amounts and kind of cRNAs injected were shown on the left of the graph. Significant differences *(P < 0.05*) are indicated by different letters using one-way ANOVA with Duncan's multiple comparisons test. Data are means ± SE (n = 7 to 10).

2.3.6. Expression of HvPIP2;8 in barley

Previously, *HvPIP2;8* was observed to be stably expressed in shoots, roots, pistils, and leaves (Shibasaka et al., 2012). In this study, to further explore the transcript regulation of *HvPIP2;8*, qPCR was used to assess expression in salt-treated and control shoot and root samples from the barley cultivar K305 and Haruna-Nijo (Figure 2.9B, C).

In roots of both cultivars, the transcript levels remained stable in both the salt-treated and control samples (Figure 2.9). However, the transcript level was different in shoots among different salt-sensitive and salt-tolerant cultivars. In K305, the transcript levels of *HvPIP2;8* were increased in shoots after 1 day and higher level after 5 days exposed to salt stress at 200 mM NaCl treatment relative to the controls (Figure 2.9A, B). However, in shoots from Haruna-Nijo plants, *HvPIP2;8* transcripts were more abundant in the salt-treated samples than the control samples after 1 day of either the 100 mM or 200 mM NaCl treatment. After 5 days of NaCl treatment, the *HvPIP2;8* transcripts were less abundant in the shoots than they were at 1 day after NaCl treatment (Figure 2.9A, C). Whereas, in the salt-sensitive cultivar, I743, there was no difference in the abundance of *HvPIP2;8* in the salt- and control-treated in both shoots and roots samples (Figure 2.9A). This indicates that the *HvPIP2;8* gene expression in shoots of barley cultivars might vary depending on cultivar and environmental conditions. This finding could be explain further biological function of HvPIP2;8 in plants.

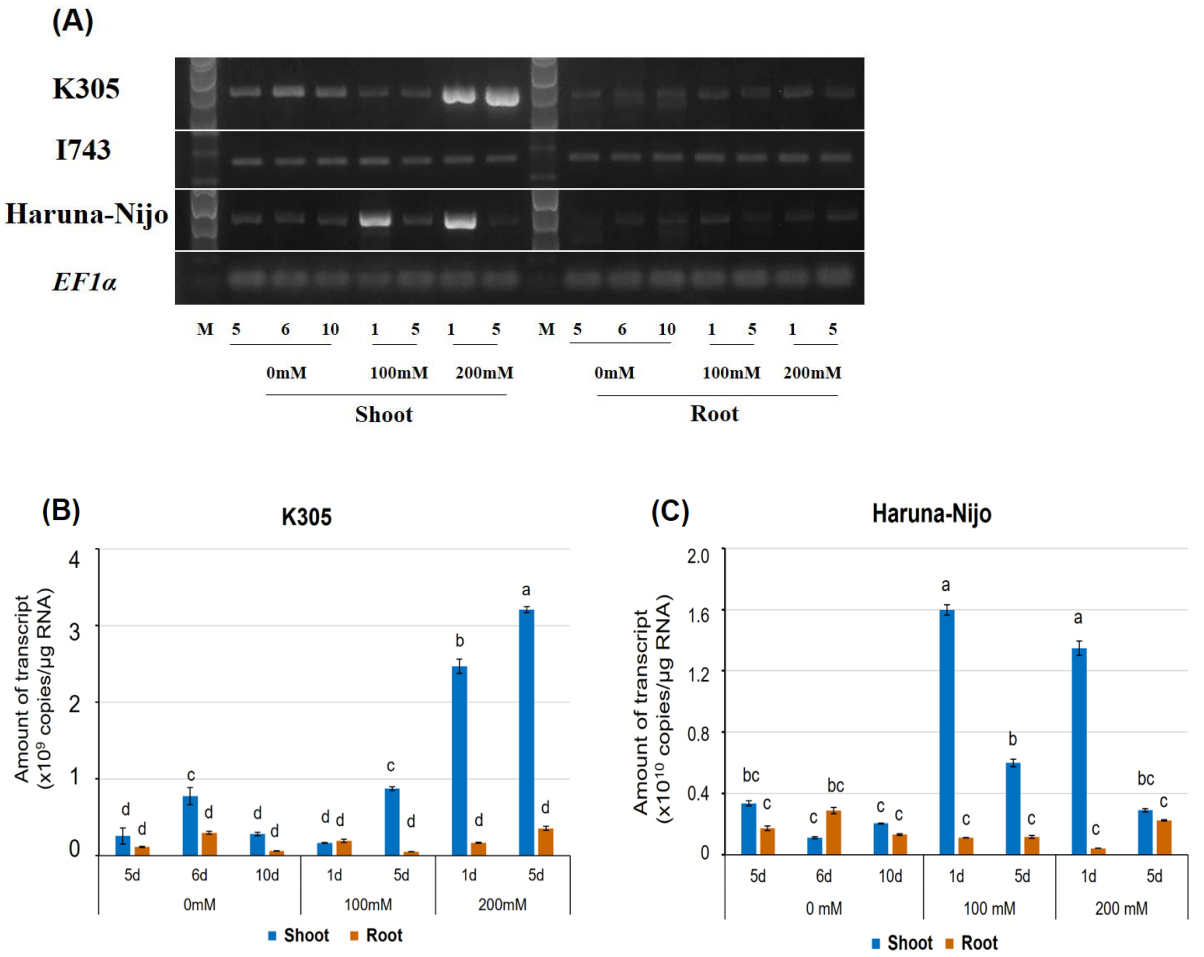

Figure 2.9. The expression level of the *HvPIP2;8* transcripts in barley cultivars. (A) Expression analysis of HvPIP2;8 using RT-PCR, internal standard EF1α fragments were amplified, M, DNA size marker, representative result was shown in 3 replications. **(B, C)** expression level of the *HvPIP2;8* transcripts in K305 and Haruna-Nijo, respectively. Five-day-old barley seedlings were prepared by hydroponic culture and further grown on the culture solution with or without NaCl (100 mM or 200 mM) for 1 day or 5 days. Transcript levels of *HvPIP2;8* in shoots and roots were investigated by absolute quantification. Absolute amounts of transcripts (copies/µg RNA) were displayed. Significant differences *($P < 0.05$)* are indicated by different letters using one-way ANOVA with Duncan's multiple comparisons test. Data are the means ± SE, and n = 3.

2.4. Discussion

HvPIP2;8 has dual function as both water and cation channel, where the channel characteristics can be influenced by K^+ and divalent cation activity, protein phosphorylation, and protein interactions. The *HvPIP2;8* transcript levels can be influenced by salt treatments. I observed that *Xenopus* oocytes expressing HvPIP2;8 displayed significant ionic conductance relative to the controls and relative to the oocytes expressing any of the six other HvPIP2s and five HvPIP1 proteins. Previous studies have demonstrated water channel activity for HvPIP2;1, HvPIP2;2, HvPIP2;3, HvPIP2;4, HvPIP2;5, and HvPIP2;7 when expressed in oocytes,

indicating that the low or absent ionic conductance associated with expression of these proteins is unlikely to relate to miss-folding or miss-targeting (Horie et al., 2011; Besse et al., 2011).

HvPIP2;8-associated ionic conductance was inhibited by external Ca^{2+}, Cd^{2+}, and Ba^{2+}, but less so by Mg^{2+} (Figure 2.6B). HvPIP2;8 was permeable to both Na^+ and K^+, and the Na^+ permeability of HvPIP2;8 was inhibited in the presence of external K^+, but not external Cl^-. Co-expression of HvPIP2;8 and HvPIP1 proteins reduced the HvPIP2;8-induced ionic conductance with differences between the PIP1 isoforms; HvPIP1;3 and HvPIP1;4 co-expressed with HvPIP2;8 still maintained a higher ionic conductance than the water-injected controls (Figure 2.7D). The salt-tolerant and salt-sensitive barley lines differed in their response to salt treatments, such that the salt tolerant cultivars tested displayed an increase in the abundance of *HvPIP2;8* transcripts within the first day after the salt treatments.

In saline conditions, excessive salt accumulation is detrimental to plant growth and limits crop productivity. This problem is often referred to as ionic toxicity, and for many cereals it is brought about by excessive Na^+ influx into roots followed by excess Na^+ accumulation, particularly in the aerial parts of the plants (Horie et al., 2012). Uptake of Na^+ at the root–soil boundary is conferred by multiple pathways involving a range of different types of membrane transporters and channels. For example, OsHKT2;1, one of the high-affinity K^+ transporter family proteins in rice, mediates direct Na^+ absorption from the outer environment of roots when the rice plant faces K^+ starvation conditions (Horie et al., 2007). The roles of some important Na^+ transporters, such as the SOS1, NHX, and HKT families, which contribute to salt-stress resistance, have been well characterized (Ismail et al., 2017). However, some pathways for Na^+ influx into plant roots remain unresolved at the molecular level, although we assume owing to electrophysiological studies that non-selective cation channels (NSCC) mediate significant Na^+ influx into roots following salinity stress (Ismail et al., 1997; Tyerman et al., 1997; Demidchik et al., 2002; Essah et al., 2003). Candidates for NSCCs include cyclic nucleotide-gated channels (CNGCs) and glutamate receptors (GLRs), but confirmation of the molecular identity of the NSCC will require further research (Davenport et al., 2000; Mori et al., 2018). In the future, determining the structure and the role of unidentified Na^+ permeable transporters/channels in plants that contribute to NSCC activity, including Na^+ permeable aquaporins, will help us to understand the complete picture of Na^+ transport and homeostasis during salinity stress.

Aquaporins are well known for their function as water channels (Knipfer et al., 2011; Besse et al., 2011; Coffey et al., 2011; Chaumont et al., 2014). Previous research has revealed that heterologous expression of AtPIP2;1, categorized as a plasma membrane-localized

aquaporin in *Arabidopsis thaliana*, is associated with non-selective cation conductance, and this ion channel function is sensitive to Ca^{2+} as well as AtPIP2;2 (Byrt et al., 2017; Kourghi et al., 2017). In the present study, I used TEVC experiments to screen *X. laevis* oocytes expressing barley HvPIPs and the control. It revealed significant HvPIP2;8-associated ion channel activity under low Ca^{2+} condition. Among the set of 12 HvPIPs tested, HvPIP2;8 stood out in relation to conferring ion channel activity in oocytes (Figure 2.2A, 2.7A). It is also noteworthy that all the plant aquaporins so far shown to conduct cations in the *Xenopus* oocytes show different characteristics in terms of cation selectivity and divalent cation inhibition. The human AQP1, which has an ion channel function, also shows differences in channel characteristics relative to AtPIP2;1 and AtPIP2;2 (Kourghi et al., 2017). This would strongly suggest that the aquaporins are not triggering a native *Xenopus* channel to be activated or recruited to the membrane.

As HvPIP2;8 has been demonstrated to conduct water and ion when expressed in oocytes (Shibasaka et al., 2012; Figure 2.2), I hypothesize that this aquaporin function as a channel that mediates both water and ion transport in plants. The Na^+ channel activity associated with HvPIP2;8 was sensitive to external Ca^{2+} concentrations (Figure 2.2A-D), and the IC_{50} of the channel was calculated to be approximately 401 μM (https://www.aatbio.com/tools/ic50-calculator), which was similar to the Ca^{2+} sensitivity of the AtPIP2;1 ionic conductance (IC_{50} = 321 μM; Byrt et al., 2017). The inhibition by Ca^{2+} is not total since even at 1.8 mM there is still a significant ion conductance (Figure 2.6D). The analysis of alkali monovalent cations selectivity revealed that HvPIP2;8 mediated not only Na^+ but also K^+ transport, although HvPIP2;8 did not mediate Rb^+, Cs^+, or Li^+ transport (Figure 2.3A, B). However, these monovalent cations, and K^+, blocked the Na^+ channel activity of HvPIP2;8 when the same amount of each cation was included in the bath solutions (Figures 2.3C, D and 2.4A-C). Inhibition or activation of Na^+ transport activity by the presence of similar or greater concentrations of external K^+ in the TEVC bath solution has been observed for different types of high-affinity K^+ transport (HKT)-type sodium transporters. For example, *Triticum aestivum* TaHKT1;5-D and *Triticum monococcum* TmHKT1;5-A encode dual affinity Na^+-transporters and their dual affinity Na^+ transport was inhibited by raising the external K^+ concentration (Byrt et al., 2008; Xu et al., 2018); whereas, for OsHKT2;2, extracellular K^+ stimulated the OsHKT2;2-mediated Na^+ transport (Yao et al., 2010). Additional research is needed to model how different monovalent ions interact with the pore lining residues of the ion channel aquaporins towards understanding the K^+ inhibition effect on the HvPIP2;8 Na^+ channel activity.

The influence of divalent cations on the HvPIP2;8-mediated Na^+ currents was complicated. The application of 1.8 mM Ba^{2+}, Ca^{2+}, or Cd^{2+} inhibited the HvPIP2;8 ionic

conductance (Figure 2.6A, B). The application of the same amount of Mg^{2+} in the bath solution did not have an equivalent inhibitory influence on the ionic conductance (just an approximately 63% reduction compared to no divalent control: Figure 2.6A, B). However, an increase in the Mg^{2+} concentrations in the presence of Ca^{2+} seemed to ameliorate the inhibitory effect of the Ca^{2+} (Figure 2.6C, D). The competitive interaction between Ca^{2+} and Mg^{2+} might be due to a higher affinity for Mg^{2+} than for Ca^{2+}. Alternatively, Mg^{2+} might interact with the same binding site as Ca^{2+}. Previous research revealed that the AtPIP2;1 and AtPIP2;2 ionic conductance was significantly inhibited by 100 µM and 10 µM extracellular free Ca^{2+}, respectively, and the ionic conductance was also significantly inhibited by the addition of Ba^{2+} and Cd^{2+} (Kourghi et al., 2017). There was also an interaction between Ca^{2+} inhibition and Ba^{2+} relief of block for AtPIP2;1 (Kourghi et al., 2017) that is similar to the interaction seen here for Ca^{2+} and Mg^{2+}. The determination of specific interaction sites for divalent cations in the structure of HvPIP2;8 will be essential to understanding the characteristics observed.

A previous study and my result showed that co-expression of HvPIP2;8 with HvPIP1;2 in *X. laevis* oocytes did not enhance the water transport activity compared to that of the expression of HvPIP2;8 alone (Shibasaka et al., 2012; Figure 2.8). In contrast, Horie et al., (2011) observed that co-expression of HvPIP1;2 with other HvPIP2s (2;1 to 2;5) increased the water permeability. This indicates that heteromerization of each HvPIP2 and HvPIP1;2 could modulate water channel activity differently. I observed here that co-expression of HvPIP2;8 with the HvPIP1s, including HvPIP1;2, significantly decreased the ionic conductance relative to expression of HvPIP2;8 alone (Figure 2.7), indicating that the HvPIP2;8-mediated ion channel activity might be negatively regulated through heteromerization. Some isoforms retained some ion conductance when co-expressed (HvPIP1;3 and HvPIP1;4). A previous study revealed that when AtPIP2;1 was co-expressed with AtPIP1;2 the water permeability was greater than when AtPIP2;1 or AtPIP1;2 was expressed alone (Byrt et al., 2017). However, the ionic conductance of AtPIP2;1 could be suppressed to the level of the water-injected controls when AtPIP2;1 was co-expressed with AtPIP1;2, indicating that the ionic conductance was not associated with higher water permeability (Byrt et al., 2017). However, this was done at high external Ca^{2+} concentration and it remains to be seen if the same result would be obtained at lower external Ca^{2+}. Together, these results reveal that the activity for water and ion channel PIPs could be differently regulated by independent mechanisms. At present, the mechanism of HvPIP1-dependent decreases in the ion transport activity of HvPIP2;8 is still unknown. Elucidating the underlying molecular mechanisms will be important to understand the functions of HvPIP2;8 as a Na^{+}-permeable ion channel.

In barley, the *HvPIP2;8* gene expresses in both roots and shoots (Figure 2.9). Interestingly, *HvPIP2;8*-expression in shoots was upregulated in response to salt stress (Figure 2.9). An RT-PCR analysis revealed that the upregulation trend for *HvPIP2;8* transcript abundance was observed in salt-tolerant barley, but not detected in a salt-sensitive barley cultivar (Figure 2.9A). These observations, and the characteristics of the HvPIP2;8 observed by TEVC experiments, led me to wonder whether HvPIP2;8 could play a positive role in shoot tissues to help cope with salt stress. I observed that the external free Ca^{2+} concentrations have a significant impact on the ion channel activity of HvPIP2;8 (Figures 2.2 and 2.6). It is well known that Ca^{2+} plays key roles in ameliorating Na^{+} toxicity under salt stress (Hyder et al., 1965). In addition, changes in free Ca^{2+} have important signaling roles, particularly in response to stress conditions (Sanders et al., 2002; Choi et al., 2014). The implications of Ca^{2+} sensitivity could be different depending on what kind of physiological role HvPIP2;8 has in planta: for example, if the HvPIP2;8 mediated the Na^{+} influx into the cytosol of mesophyll cells in leaves, then a Ca^{2+}-dependent inhibitory effect might be a positive feature as it could prevent excess Na^{+} influx. It is also possible that HvPIP2;8 might be an entry point for Na^{+} influx in root surface cells under salt stress when there is a low external Ca^{2+}. This could have physiological relevance in relation to regulating monovalent ion transport in conditions where K^{+} is abundant relative to when Na^{+} is in excess, such as in saline conditions. Water and ion transport are involved in the regulation of cell expansion, and aquaporins that can transport both ions and water could also potentially have key functions in cell expansion processes (Liam et al., 2004; Martinez-Ballesta et al., 2018). To understand the physiological roles of HvPIP2;8, it will be necessary to phenotype the barley control and mutant or transgenic lines that significantly vary in the abundance of HvPIP2;8. It will also be essential to determine the specific location and abundance of the HvPIP2;8-protein in both roots and shoots in control and salt-stressed conditions.

References

Amtmann A., Laurie S., Leigh R., Sanders D. **(1997)**. Multiple inward channels provide flexibility in Na^+/K^+ discrimination at the plasma membrane of barley suspension culture cells. *J. Exp. Bot.*, *48*, 481–497.

Besse M., Knipfer T., Miller A.J., Verdeil J.L., Jahn T.P., Fricke W. **(2011)**. Developmental pattern of aquaporin expression in barley (*Hordeum vulgare* L.) leaves. *J. Exp. Bot.*, *62*, 4127–4142.

Bienert M.D., Diehn T.A., Richet N., Chaumont F., Bienert G.P. **(2018)**. Heterotetramerization of plant PIP1 and PIP2 aquaporins is an evolutionary ancient feature to guide PIP1 plasma membrane localization and function. *Front. Plant Sci.*, *9*, 15.

Byrt C.S. **(2008)**. Genes for sodium exclusion in wheat. Ph.D. Thesis, University of Adelaide, Adelaide, Australia. Available online: https://digital.library.adelaide.edu.au/dspace/handle/2440/56208 (accessed on).

Byrt C.S., Zhao M., Kourghi M., Bose J., Henderson S.W., Qiu J., Tyerman S. **(2017)**. Non-selective cation channel activity of aquaporin AtPIP2;1 regulated by Ca^{2+} and pH. *Plant Cell Environ.*, *40*, 802–815.

Chaumont F., Tyerman S.D. **(2014)**. Aquaporins: highly regulated channels controlling plant water relations. *Plant Physiol.*, *164*, 1600–1618.

Chen Z., Pottosin I.I., Cuin T.A., Fuglsang A.T., Tester M., Jha D., Zepeda-Jazo I., Zhou M., Palmgren M.G., Newman I.A. **(2007)**. Root plasma membrane transporters controlling K^+/Na^+ homeostasis in salt-stressed barley. *Plant Physiol.*, *145*, 1714–1725.

Choi W.G., Toyota M., Kim S.H., Hilleary R., Gilroy S. **(2014)**. Salt stress induced Ca^{2+} waves are associated with rapid, long-distance root-to-shoot signaling in plants. *Proc. Natl. Acad. Sci. USA*, *111*, 6497–6502.

Coffey O., Bonfield R., Corre F., Althea Sirigiri J., Meng D., Fricke W. **(2018)**. Root and cell hydraulic conductivity, apoplastic barriers and aquaporin gene expression in barley (*Hordeum vulgare* L.) grown with low supply of potassium. *Ann. Bot.*, *122*, 1131–1141.

Davenport R.J., Tester M. **(2000)**. A weakly voltage-dependent, nonselective cation channel mediates toxic sodium influx in wheat. *Plant Physiol.*, *122*, 823–834.

Demidchik V., Tester M. **(2002)**. Sodium fluxes through nonselective cation channels in the plasma membrane of protoplasts from Arabidopsis roots. *Plant Physiol.*, *128*, 379–387.

Essah P.A., Davenport R., Tester M. **(2003)**. Sodium influx and accumulation in Arabidopsis. *Plant Physiol.*, *133*, 307–318.

Grondin A., Rodrigues O., Verdoucq L., Merlot S., Leonhardt N., Maurel C. **(2015)**. Aquaporins contribute to ABA-triggered stomatal closure through OST1-mediated phosphorylation. *Plant Cell, 27*, 1945–1954.

Horie T., Costa A., Kim T.H., Han M.J., Horie R., Leung H.Y., Miyao A., Hirochika H., An G., Schroeder I.J. **(2007)**. Rice OsHKT2;1 transporter mediates large Na^+ influx component into K^+-starved roots for growth. *EMBO J., 26,* 3003–3014.

Horie T., Kaneko T., Sugimoto G., Sasano S., Panda S.K., Shibasaka M., Katsuhara M. **(2011)**. Mechanisms of water transport mediated by PIP aquaporins and their regulation via phosphorylation events under salinity stress in barley roots. *Plant Cell Physiol., 52*, 663–675.

Horie T., Karahara I., Katsuhara M. **(2012)**. Salinity tolerance mechanisms in glycophytes: An overview with the central focus on rice plants. *Rice, 5,* 1–18.

Hove R.M., Ziemann M., Bhave M. **(2015)**. Identification and expression analysis of the barley (*Hordeum vulgare* L.) aquaporin gene family. *PLoS ONE, 10,* 1–21.

Hyder S.Z., Greenway H. **(1965)**. Effects of Ca^{2+} on plant sensitivity to high NaCl concentrations. *Plant Soil, 23,* 258–260.

Ikeda M., Beitz E., Kozono D., Guggino W.B., Agre P., Yasui M. **(2002)**. Characterization of aquaporin-6 as a nitrate channel in mammalian cells–Requirement of pore-lining residue threonine 63. *J. Biol. Chem., 277,* 39873–39879.

Isayenkov S.V., Maathuis F.J.M. **(2019)**. Plant salinity stress: Many unanswered questions remain. *Front. Plant Sci., 10,* 80.

Ismail A.M., Horie T. **(2017)**. Genomics, physiology, and molecular breeding approaches for improving salt tolerance. *Annu. Rev. Plant Biol., 68,* 405–434.

Kaneko T., Horie T., Nakahara Y., Tsuji N., Shibasaka M., Katsuhara M. **(2015)**. Dynamic regulation of the root hydraulic conductivity of barley plants in response to salinity/osmotic stress. *Plant Cell Physiol., 56,* 875–882.

Katsuhara M., Akiyama Y., Koshio K., Shibasaka M., Kasamo K. **(2002)**. Functional analysis of water channels in barley roots. *Plant Cell Physiol., 43,* 885–893.

Katsuhara M., Koshio K., Shibasaka M., Hayashi Y., Hayakawa T., Kasamo K. **(2003)**. Over-expression of a barely aquaporin increased the shoot/root ratio and raised salt sensitivity in transgenic rice plants. *Plant Cell Physiol., 44,* 1378–1383.

Katsuhara M., Shibasaka M. **(2007)**. Barley root hydraulic conductivity and aquaporins expression in relation to salt tolerance. *Soil Sci. Plant Nutr., 53,* 466–470.

Katsuhara M., Hanba Y.T., Shiratake K., Maeshima M. **(2008)**. Expanding roles of plant aquaporins in plasma membranes and cell organelles. *Funct. Plant Biol., 35,* 1–14.

Knipfer T., Besse M., Verdeil J.L., Fricke W. **(2011)**. Aquaporin-facilitated water uptake in barley (*Hordeum vulgare* L.) roots. *J. Exp. Bot.*, *62*, 4115–4126.

Kourghi M., Nourmohammadi S., Pei J.V., Qiu J., McGaughey S., Tyerman S.D., Yool A.J. **(2017)**. Divalent cations regulate the ion conductance properties of diverse classes of aquaporins. *Int. J. Mol. Sci.*, *18*, 2323.

Laloux T., Junqueira B., Maistriaux L.C., Ahmed J., Jurkiewicz A., Chaumont F. **(2018)**. Plant and mammal aquaporins: same but different. *Int. J. Mol. Sci.*, *19*, 27.

Liam D., Davies J. **(2004)**. Cell expansion in roots. *Curr. Opin. Plant Biol.*, *7*, 33–39.

Liu S.Y., Fukumoto T., Gena P., Feng P., Sun Q., Li Q., Ding X.D. **(2020)**. Ectopic expression of a rice plasma membrane intrinsic protein (OsPIP1,3) promotes plant growth and water uptake. *Plant J*., *102*, 779–796.

Martinez-Ballesta M.C., Garcia-Ibañez P., Yepes-Molina L., Rios J.J., Carvajal M. **(2018)**. The expanding role of vesicles containing aquaporins. *Cells*, *7*, 179.

McGaughey S.A., Qiu J., Tyerman S.D., Byrt C.S. **(2018)**. Regulating root aquaporin function in response to changes in salinity. *Ann. Plant Rev. Online*, *1*, 381–416.

Mori I.C., Nobukiyo Y., Nakahara Y., Shibasaka M., Furuichi T., Katsuhara M. **(2018)**. A cyclic nucleotide-gated channel, HvCNGC2-3, is activated by the co-presence of Na^+ and K^+ and permeable to Na^+ and K^+ non-selectively. *Plants*, *7*, 61.

Munns R., Tester M. **(2008)**. Mechanisms of salinity tolerance. *Ann. Rev. Plant Biol.*, *59*, 651–681.

Maurel C., Boursiac Y., Luu D.T., Santoni V., Shahzad Z., Verdoucq L. **(2015)**. Aquaporins in plants. *Physiol. Rev.*, *95*, 1321–1358.

Otto B., Uehlein N., Sdorra S., Fischer M., Ayaz M., Belastegui-Macadam X., Kaldenhoff R. **(2010)**. Aquaporin tetramer composition modifies the function of tobacco aquaporins. *J. Biol. Chem.*, *285*, 31253–31260.

Rodrigues O., Reshetnyak G., Grondin A., Saijo Y., Leonhardt N., Maurel C., Verdoucq L. **(2017)**. Aquaporins facilitate hydrogen peroxide entry into guard cells to mediate ABA- and pathogen-triggered stomatal closure. *Proc. Natl. Acad. Sci. USA*, *114*, 9200–9205.

Sanders D., Pelloux J., Brownlee C., Harper J.F. **(2002)**. Calcium at the crossroads of signaling. *Plant Cell*, *14*, S401–S417.

Shibasaka M., Sasano S., Utsugi S., Katsuhara M. **(2012)**. Functional characterization of a novel plasma membrane intrinsic protein2 in barley. *Plant Sigal. Behav*., *7*, 1648–1652.

Tyerman S.D., Skerrett M., Garrill A., Findlay G.P., Leigh R.A. **(1997)**. Pathways for the permeation of Na^+ and Cl^- into protoplasts derived from the cortex of wheat roots. *J. Exp. Bot*., *48*, 459–480.

Vandeleur R.K., Mayo G., Shelden M.C., Gilliham M., Kaiser B.N., Tyerman S.D. **(2009)**. The role of plasma membrane intrinsic protein aquaporins in water transport through roots: diurnal and drought stress responses reveal different strategies between isohydric and anisohydric cultivars of grapevine. *Plant Physiol*., *149*, 445–460.

Vitali V., Jozefkowicz C., Fortuna A.C., Soto G., Flecha F.L.G., Alleva K. **(2019)**. Cooperativity in proton sensing by PIP aquaporins. *FEBS J*., *286*, 991–1002.

Wang C., Hu H., Qin X., Zeise B., Xu D., Rappel W.J., Schroeder J.I. **(2015)**. Reconstitution of CO_2 regulation of SLAC1 anion channel and function of CO_2-permeable PIP2,1 aquaporin as CARBONIC ANHYDRASE4 interactor. *Plant Cell*, *28*, 568–582.

Xu B., Hrmova M., Gilliham M. **(2018)**. High affinity Na^+ transport by wheat HKT1, 5 is blocked by K^+. *BioRxiv*. Available online: https://www.biorxiv.org/content/10.1101/280453v2.abstract (accessed on).

Yao X., Horie T., Xue S., Leung H.Y., Katsuhara M., Brodsky D.E., Wu Y., Schroeder J.I. **(2010)**. Differential sodium and potassium transport selectivities of the rice OsHKT2;1 and OsHKT2;2 transporters in plant cells. *Plant Physiol.*, *152*, 341–355.

Yool A.J., Weinstein A.M. **(2002)**. New roles for old holes: Ion channel function in aquaporin-1. *News Physiol. Sci*., *17*, 68–72.

Zelazny E., Borst J.W., Muylaert M., Batoko H., Hemminga M.A., Chaumont F. **(2007)**. FRET imaging in living maize cells reveals that plasma membrane aquaporins interact to regulate their subcellular localization. *Proc. Natl. Acad. Sci. USA*, *104*, 12359–12364.

CHAPTER 3

Ion transport activity through a rice aquaporin OsPIP2;4 and its physiological role

3.1. Introduction

In rice (*Oryza sativa* L. cv. Nipponbare), 38 genes for aquaporin in the rice genome sequence have been identified as shown in Figure 1.5 (Sakurai et al., 2005; Forest and Brave, 2007). Their expression levels in leaf blades, roots and anthers of rice, in which, OsPIP2;4 and OsPIP2;5 were expressed predominantly in roots (Sakurai et al., 2005; Guo et al., 2006; Matsumoto et al., 2009), while 14 genes, including OsPIP2;7 and OsTIP1;2 were found in leaf blades (Sakurai et al., 2005). Eight genes, such as OsPIP1;1 and OsTIP4;1, were evenly expressed in leaf blades, roots and anthers. OsPIP2;4 or OsPIP2;5 revealed high water channel activity when expressed in yeast but not when OsPIP1;1 or OsPIP1;2 were expressed (Sakurai et al., 2005).

Water permeability, anions and cations selectivity have been reported for subsets of PIPs aquaporin when expressed in yeast cells *(Saccharomyces cerevisiae)* and *X. laevis* oocytes. For instance, robust water transport activity via OsPIP2;1, OsPIP2;3, OsPIP2;4, OsPIP2;5 have been demonstrated in yeast. OsPIP1;1, OsPIP1;2, OsPIP1;3 displayed only a slight or barely detectable increase in P_f with a range similar to controls (Matsumoto et al., 2009; Ding et al., 2019). The expression levels of some OsPIPs (OsPIP1;3, OsPIP2;4, OsPIP2;5) were found to be increased in roots in drought stress conditions (Verma et al., 2020). Root OsPIP1;3 is upregulated by osmotic stress in *indica* (20% polyethylene glycol) but does not change in *japonica*. Similar feature was observed in OsPIP1;2, OsPIP2;1, and OsPIP2;5. OsPIP1;3 which is upregulated in roots under drought stress, has recently been shown to be able to transport nitrate anions when expressed in mammalian HEK293 cells, and also showed function as water channel in co-expression with OsPIP2;2 (Liu et al., 2020). On the other hand, OsPIP2;4 and OsPIP2;7 are involved in mediating B transport in rice and provide tolerance via efflux of excess B from root and shoot tissues (Kumar et al., 2014). The OsPIP2;4-overexpresing lines of Gizal178 recovered their leaf relative water content faster than those of the wild type in the afternoon and showed improved gas exchange parameters, water use effiency, and grain yield, as a result of improved root hydraulic conductivity (Lp_r) and xylem sap flow but did not in IR64 similar to the wild type under drought condition (Nada and Abogadallah, 2020). OsPIPs can influence the root hydraulic conductivity of rice, and membrane internalization of the OsPIPs are implicated in the response of rice roots to chilling, drought, salinity/osmotic stress (Matsumoto

et al., 2009; Ding et al., 2019, Verma et al., 2020; Nada and Abogadallah, 2020). The regulation of PIPs in plants changes in response to salt treatments, and these changes might influence plant adaptation to salt stress (Liu et al., 2013; Alavilli et al., 2016; Ayadi, Brini and Masmoudi, 2019).

PIP1 and PIP2 isoforms share about 80% amino acid identity. The main differences between both groups are found in the length and amino acid composition of the N- and C-terminal and the loop A (Chaumont et al., 2001). Most PIP1 and PIP2 isoforms physically interact and assemble in hetero-tetramers to modulate their subcellular localization and channel activity when they are co-expressed in oocytes, yeasts, and plants. The cation transporting AtPIP2;1 was reported to have decreased ion transport when co-expressed with AtPIP1;2 but increased water transport in *X. laevis* oocytes (Byrt et al., 2017). Recently, the co-expression of HvPIP2;8 and HvPIP1;2 did not affect to water permeability but significantly decrease ion transport activity when compared with HvPIP2;8-expressed alone in oocytes (Shibasaka et al, 2012; Tran et al., 2020).

Two closely related members of the PIP2 group from *Arabidopsis*, AtPIP2;1 and AtPIP2;2 ($K^+ > Na^+$) as well as a barley aquaporin HvPIP2;8 ($Na^+ > K^+$) display nonselective voltage-independent cation conductance when expressed in *X. laevis* oocytes (Byrt et al., 2017; Tran et al., 2020). It was hypothesized that AtPIP2;1, HvPIP2;8 could account for the voltage-independent non-selective cation channels in plants and ion transport activity were inhibited by extracellular Ca^{2+} concentration and others divalent cation (Byrt et al., 2017; Kourghi et al., 2017; Tran et al., 2020). However, it is also still unknown how many of the PIP isoforms may induce ion conductance. Their features of voltage-independent NSCCs remain to be tested on the ion conducting PIPs.

In this study, the rice OsPIP2s (from OsPIP2;1 to OsPIP2;8) and OsPIP1s (OsPIP1;1 to OsPIP1;3) are explored to test ion transport activity when expressed in *X. laevis* oocytes using two electrode voltage clamp (TEVC) experiments. Combination with previous studies, we provide clearly evidence that *OsPIP2;4*, an abundantly expressed aquaporin localized at the plasma membrane, young root epidermis and root exodermis that shows water channel activity also elicited cation. The OsPIP2;4 aquaporin cations selectivity, Ca^{2+}-sensitive levels, interaction with OsPIP1s in hetero-tetramer formation, as well as tissue localization and its physiological role in plants were examined. All of these results provide a clear overview of the function of OsPIP2;4 aquaporin and its role in regulating ion transport activity.

3.2. Materials and methods

3.2.1. Preparation of OsPIP cRNAs

The coding region of each *OsPIP* (from *Oryza sativa* L. cv. Nippobare) was cloned into the vector pXβG-ev1. Each construct was linearized and cRNAs were synthesized using the mMESSAGE mMACHINE T3 kit (Ambion, Austin, TX, USA), with a final concentration of 1μg/μL.

3.2.2. Expression of OsPIPs in *X. laevis* oocytes

Oocytes were obtained from adult female *X. laevis* frogs and placed in a modified Barth's solution (MBS: 88 mM NaCl, 1 mM KCl, 2.4 mM $NaHCO_3$, 1.5 mM Tris-HCl (pH 7.6), 0.3 mM $Ca(NO_3)_2{\cdot}4H_2O$, 0.41 mM $CaCl_2{\cdot}4H_2O$, 0.82 mM $MgSO_4{\cdot}7H_2O$, 10 μg mL^{-1} penicillin sodium salt, and 10 μg mL^{-1} streptomycin sulfate). The lobes were torn apart and treated with 1 mg mL^{-1} collagenase B (type B, Boehringer Mannheim, Germany) in Ca-free MBS for 1.5 h. Isolated oocytes were washed several times and incubated in MBS for 1 day at 20 °C before the microinjection.

Oocytes were injected with 10 ng of *OsPIP2s* cRNA and 40 ng of *OsPIP1s* cRNA. Oocytes were injected with nuclear-free water as a negative control in all experiments. Injected oocytes were incubated for 24 h to 48 h at 20°C in MBS or a low Na^+ Ringer solution until the electrophysiological experiments were performed. The experiments using frog oocytes were approved by the Animal Care and Use Committee, Okayama University (approval number OKU-2017271), which follows the related international and domestic regulations.

3.2.3. Electrophysiology

Two-electrode voltage clamp (TEVC) was performed using *X. laevis* oocytes injected with water or cRNA as described in Chapter 2.

Monovalent cations (Na^+, K^+, Li^+, Cs^+ and Rb^+) were added as chloride salts or gluconate salts. Each oocyte was carefully pierced with the voltage and current electrodes and the membrane voltage was allowed to stabilize. Ionic currents were monitored through the experiments by the repeat of steps from −120 mV to +30 mV with 2 s steady states and 5 s intervals. Ionic conductance $(\Delta I/\Delta V)$ was obtained from data between V = −120mV and −75 mV. The recording was performed and analyzed with an Axoclamp 900A amplifier equipped with a Digidata 1440A and Clampex 9.0 software (Molecular Devices, CA, USA) at room temperature (20 – 22°C).

3.2.4. Water transport activity assay in *X. laevis* oocytes

The coding regions of *OsPIP1;1; OsPIP1;2; OsPIP1;3* and *OsPIP2;4* cDNA were sub-cloned into the pXβG-ev1 expression vector. The constructs were linearlized with *PstI*, and capped cRNA were synthesized using the mMESSAGE mMACHINE T3 *in vitro* transcription kit (Ambion). Oocytes were isolated from adult female *X. laevis* frogs and maintained as described in part 2.2.4 (Chapter 2). Oocytes were injected with 50 nL of a cRNA solution containing 10 ng of *OsPIP2;4* and co-expressed 10 ng of *OsPIP2;4* and 40 ng of each *OsPIP1s* as described above. As a negative control, nuclease-free water-injected oocytes were used. The osmotic water permeability coefficient of oocytes was measured according to the procedures described in part 2.2.6 of Chapter 2.

3.2.5. Plant material and growth condition

Rice plants (*Oryza sativa* L. cv. Nipponbare) were used in this study. Seeds were sterilized in one time by using NaClO and Tween-20, then shaking for 50 minutes and the washed with mili Q water template for five times. For germination, 15 seeds were placed on the mesh in the sterilized pot with 70 mL of 1 mM $CaSO_4$ + 10 mM KCl and placed in the dark condition until seed germinated. Plants were grown in a normal environment growth chamber. The temperature was maintained at 28°C and 25°C in 12-h light (250 µmol s^{-1} m^{-2} illumination) and 12-h dark, respectively. Seven-days-old seedlings were transferred to 3.5 L pots and grown hydroponically with the solutions containing 4 mM KNO_3, 1mM $NH_4H_2PO_4 \cdot 2H_2O$, 1 mM $CaCl_2 \cdot 2H_2O$, 1 mM $MgSO_4 \cdot 7H_2O$, and micronutrients (1 ppm Fe, 0.5 ppm B, 0.5 ppm Mn, 0.05 ppm Zn, 0.02 ppm Cu, and 0.01 ppm Mo). The pH of the nutrient solution was adjusted to 5.5 with NaOH. 15-days old plants were used for cDNA isolation.

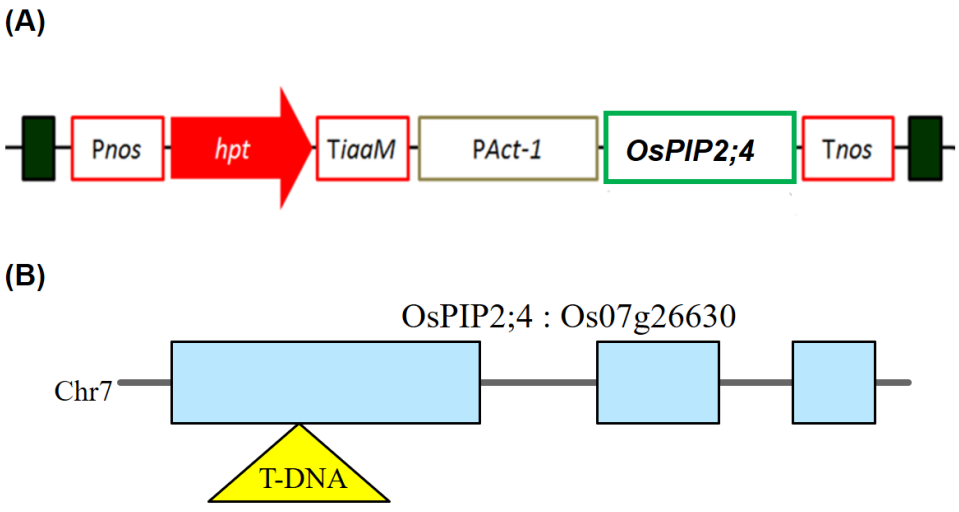

Figure 3.1. Vector construction of transgenic rice plants

(A) Vector construction of over expression (OE) and (B) T-DNA insertion of transgenic rice lines.

A T-DNA insertion mutant of rice used in this study, PFG_1C-08304.L (*O. sativa* L. cv. Howayoung), was found at the Rice Functional Genomic Express Database (http://signal.salk.edu/cgi-bin/RiceGE). A T-DNA was inserted in the first exon of *OsPIP2;4* (Os07g26630) in this mutant (knockout, KO). For overexpression (OE), the entire coding region of *OsPIP2;4* was inserted into the expression vector under the control of an actin promoter (Figure 3.1A). Transformation and selection were performed as described (Hakata et al., 2010).

For the preparation of rice plants in the reproductive growth stage, seedlings of wild types and transgenic plants were transferred to plastic pots filled with the paddy-field soil and grown in greenhouse with three replications. When the plants started heading, salt-stress treatments were initiated with 10 L of tap water containing 25 mM NaCl for two weeks. A stepwise 25 mM increase in NaCl concentration in 10 L of tap water was performed as follows: twice for 50 mM NaCl for two weeks, two twice for 75 mM NaCl for two weeks, and twice for 100 mM NaCl for two weeks, and once for 150 mM NaCl for a week. Plants were kept in salt stress condition afterwards until grain harvest. For the analyses of the growth stage-dependent gene expression and ion contents, roots and shoots were harvested at the same time. In brief, 3-week-old wild types (WT) and transgenic plants were prepared by hydroponic culture, then expression of *OsPIP2;4* in transgenic and wild types plants were checked by polymerase chain reaction (PCR) before transplanted to the paddy field in greenhouse. Indicated samples were obtained from the plants at reproductive growth stages.

3.2.6. Expression of *OsPIP2;4* by real-time quantitative PCR (qPCR)

For spatial expression of *OsPIP2;4*, two week-old seedlings of cultivar Nipponbare were separated into roots, stems, leaf sheaths and leaf blades. To further investigate the spatial expression of *OsPIP2;4* in subdivided roots, the roots were separated into different segment (0-5, 5-15 from the root tips). For expression aerial tissues at reproductive growth stage, samples were harvested after finishing time of salt treatment.

Each sample was harvested and immediately frozen in liquid nitrogen. Total RNA was extracted using a mortar and pestle and RNeasy Plant Mini Kit (Qiagen, Hilden, Germany). cDNA was synthesized using Rever Tra Ace kit (Toyobo, Osaka, Japan). cDNA fragment of *OsPIP2;4* (GeneBank accession number AK072632) was amplified with a set of specific primers (Table 3.1). Absolute quantification was performed in the qPCR conditions of 50^{o}C for 2min, 95^{o}C for 10min, 40 cycles of 95^{o}C for 15s, and 56^{o}C (for Nipponbare, Howayoung, Knockout (KO) samples) or 61^{o}C (for Overexpressing sample) for 1min to analyze the

expression level of *OsPIP2;4*. Transcript copy numbers were quantified from technical replications, and two biological independent experiments were conducted.

Table 3.1. Gene-specific primer pairs used in the qPCR experiments

Gene name	Forward primer (5′-3′)	Reverse primer (5′-3′)	T_m (°C)
Nipponbare, Howayoung (WT) and Knockout line (KO)			
OsPIP2;4	ACCTCTCTCAAGCAGCTTAG	GACTCGATTGGTTTGCAAGAA	56
Overexpressing line (OE1)			
OsPIP2;4	GCTGTACCACCAGGTCATCCTC	GATACAGCTGAACTACGCGTTGC	61

3.2.7. Immunostaining of OsPIP2;4

To examined the tissue localization of *OsPIP2;4*, immunostaining experiment were conducted using rice roots. Rice plants (*Oryza sativa* L. cv. Nipponbare) were grown in a hydroponic culture and are placed in a growth chamber under the temperature was maintained at 28°C and 25°C in 12-h light (250 μmol s^{-1} m^{-2} illumination) and 12-h dark, respectively for 8 days. Five mm root tip was used to immunocytochemical analysis using the anti-*OsPIP2;4* anti-serum (rabbit) raised against the synthetic oligopeptide corresponding to TDAAVNGADAAC in *OsPIP2;4* (Eurofins, Tokyo, Japan). Fluorescence of the secondary antibody (Alexa Fluor 546 goat anti-rabbit IgG; Molecular Probes, Eugene, OR, USA) was observed with confocal laser scanning microscopy (Keyence BZ-X700).

3.2.8. Measurements of ion contents in rice tissues

For the measurement of ion contents in rice tissues/organs, each sample was harvested and washed with ultrapure water twice. All samples were dried at 70 °C for 3 - 5 days, and the samples were digested with ultrapure nitric acid for a few days (Kanto Chemical, Japan). Digested samples were boiled at 95 °C for 10 min three times, and ion contents were determined using an inductively coupled plasma optical emission spectrometer (ICP-OES; SPS3100, SII Nano Technology Inc., Japan).

3.2.9. Statistical analysis

Statistical analysis was conducted using SPSS statistics software (version 20). Analysis of variance was identified by one-way ANOVA followed by the least significant difference (LSD) test at the *0.05* level; or one-way ANOVA followed by Duncan's multiple comparisons test.

3.3. Results

3.3.1. Sequence and structure analyses of OsPIP2;4

The genomic sequence of OsPIP2;4 (Genenome sequence accession number AP004668) contains 1215 bp including untranslated regions (UTR), and the full length of its complementary DNA (cDNA) is 861 bp, encoding a polypeptide of 286 amino acids.

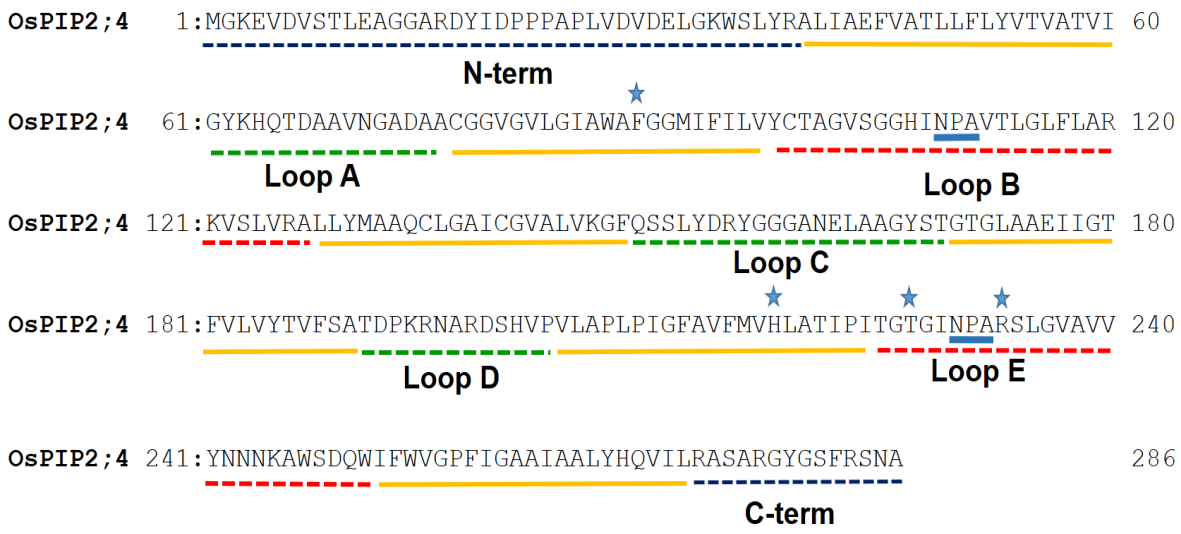

Figure 3.2. Deduced amino acid sequences of OsPIP2;4 proteins. Sequences alignment of OsPIP2;4 with two conserved NPA motifs underlined in blue in loop B and loop E are underlined with dotted red lines, Ar/R filter is pointed with stars; loop A, C, D are underlined with dotted green lines, six tranmembranes are underlined with yellow line, N- and C-terminal tails are underlined with dotted dark blue.

3.3.2. Ion selectivity of OsPIP2;4 expressed in *X. laevis* oocytes

3.3.2.1. Ion transport activity examined among rice PIP2s

At first, ion transport activity among OsPIP2s (from OsPIP2;1 to OsPIP2;8) was examined by using *X. laevis* oocytes. Only the expression of OsPIP2;4 in the oocytes elicited large bidirectional and voltage-independent currents in the bath solution, containing 86.4 mM NaCl and 9.6 mM KCl, and 30 µM free Ca^{2+} (low Ca^{2+} condition) (Figure 3.3A). In addition, The oocytes expressing OsPIP2;5 showed lower inward current than those expressing OsPIP2;4 but showed higher currents than those of the other OsPIP2. In contrast, the OsPIP2;4-associated currents were inhibited by high external Ca^{2+} concentration (1.8 mM Ca^{2+}) as well as OsPIP2;5 (Figure 3.3B). The OsPIP2;4-associated ionic conductance was 25.22 µS between V = –120 mV and –75 mV, and this value was significantly higher than the ionic conductance of other OsPIP2s in low external free Ca^{2+} condition but not in high external free Ca^{2+} (Figure 3.3C). OsPIP2;1, OsPIP2;2, OsPIP2;3, OsPIP2;6, OsPIP2;7 and OsPIP2;8 did not elicit ion conductance that was not significantly different to that of the water-injected oocytes in both low

and high external Ca^{2+} concentration. OsPIP2;5 only showed smaller ionic conductance 6.45 µS compared with OsPIP2;4 and significantly different with other OsPIP2s in low external free Ca^{2+} condition but did not different with OsPIP2;4 and other OsPIP2s in high external Ca^{2+} concentration using the same bath oocytes (Figure 3.3D).

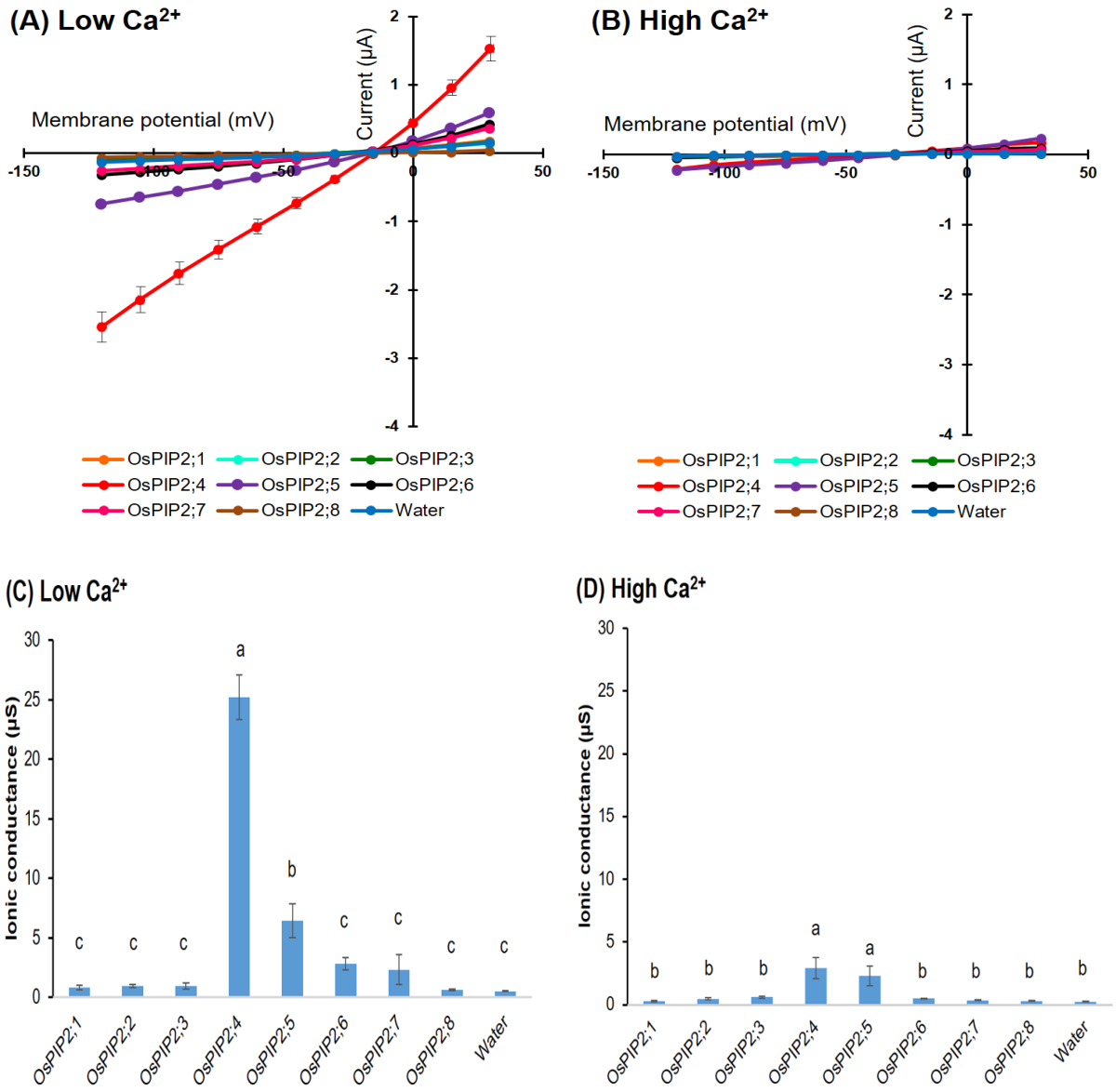

Figure 3.3. Electrophysiological survey of the ion transport activity among OsPIP2s. (A) Current-voltage relationships of *X. leavis* oocytes expressing each *OsPIP2* in the presence of 86.4 mM NaCl; 9.6 mM KCl with 30 µM Ca^{2+} **(A)** or 1.8 mM Ca^{2+} **(B)**. 10 ng of each *OsPIP2* cRNA or 50 nL water (control) was injected to *X. laevis* oocytes. Data are means ± SE (n = 6 for A, n = 5 for B). **C and D)** Ionic conductance of oocytes injected OsPIP2s or water in the presence of 86.4 mM NaCl and 9.6 mM KCl in low and high external free Ca^{2+} in A and B, respectively. Ionic conductance was calculated based on the data obtained from V = –75 mV to –120 mV of the membrane potential in Figure 3.3A, B. Significant differences ($P < 0.05$) are indicated by different letters using one-way ANOVA with Duncan's multiple comparisons test.

I then examined inhibitory effect of external free Ca^{2+} to ion permeable through OsPIP2;4 in bath solution various concentration of Ca^{2+}. Interestingly, the ionic conductance induced by OsPIP2;4 was gradually inhibited in response to increment of external free Ca^{2+} concentration (Figure 3.4B). This result indicated that Na^+- and K^+-dependent inward currents and ionic conductance of OsPIP2;4 were inhibited by high external free Ca^{2+} concentrations (in presence from 1.0 to 1.8 mM free Ca^{2+}) (Figure 3.4A).

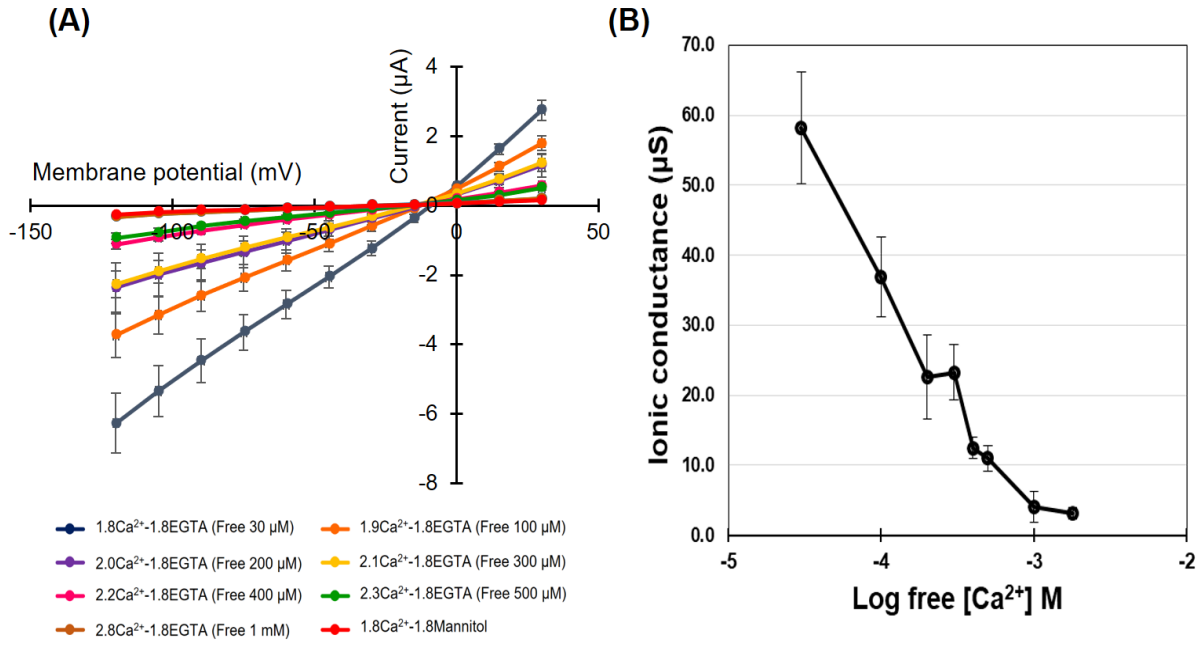

Figure 3.4. The inhibition of Na^+ transport by external free Ca^{2+} concentration in OsPIP2;4 expressed in *X. laevis* oocytes. A) The background solution contained (1.8 mM $MgCl_2$, 1.8 mM EGTA, 1.8 mM $CaCl_2$, 10 mM HEPES pH 7.5 with Tris) for external free 30 μM Ca^{2+} to 1 mM Ca^{2+} concentration; and (1.8 mM $MgCl_2$, 1.8 mM Mannitol, 1.8 mM $CaCl_2$, 10 mM HEPES pH 7.5 with Tris) for external free 1.8 mM Ca^{2+} concentration as control. Steady-state current-voltage curves of *X. laevis* oocytes injected with 10 ng of cRNA per oocyte from the same batch. **B)** Relationships between the external free Ca^{2+} concentration and OsPIP2;4-mediated Na^+ conductance in the presence of 86.4 mM NaCl; 9.6 mM KCl ($R^2 = 0.92$). Free Ca^{2+} concentrations are given in M. A step pulse protocol of −120 mV to +30 mV with a 15 mV increment was applied on every oocyte. Ionic conductance was calculated based on the data obtained from V = −75 mV to −120 mV of the membrane potential. Data are means ± SE (n = 6).

3.3.2.2. OsPIP2;4-transporter is selective more K^+ than Na^+

To explore OsPIP2;4 permeability of Na^+ and K^+, inward currents of the oocytes expressing OsPIP2;4 were compared with the bat solution containing 0 to 96 mM NaCl or KCl under low external free Ca^{2+} condition (30 µM free Ca^{2+}). The results showed that dose dependent increase in inward currents was observed with Na^+ or K^+ concentrations and ionic conductance was the highest at 96 mM Na^+ or K^+ concentration.

Furthermore, the reversal potential in the presence of Na^+ or K^+ was calculated and showed positive shift depending on increasing Na^+ or K^+ concentrations. OsPIP2;4 conductance showed larger in K^+ than in Na^+ solution, suggesting that OsPIP2;4 selectivity well transport K^+ rather than Na^+ (Figure 3.5 and Figure 3.6).

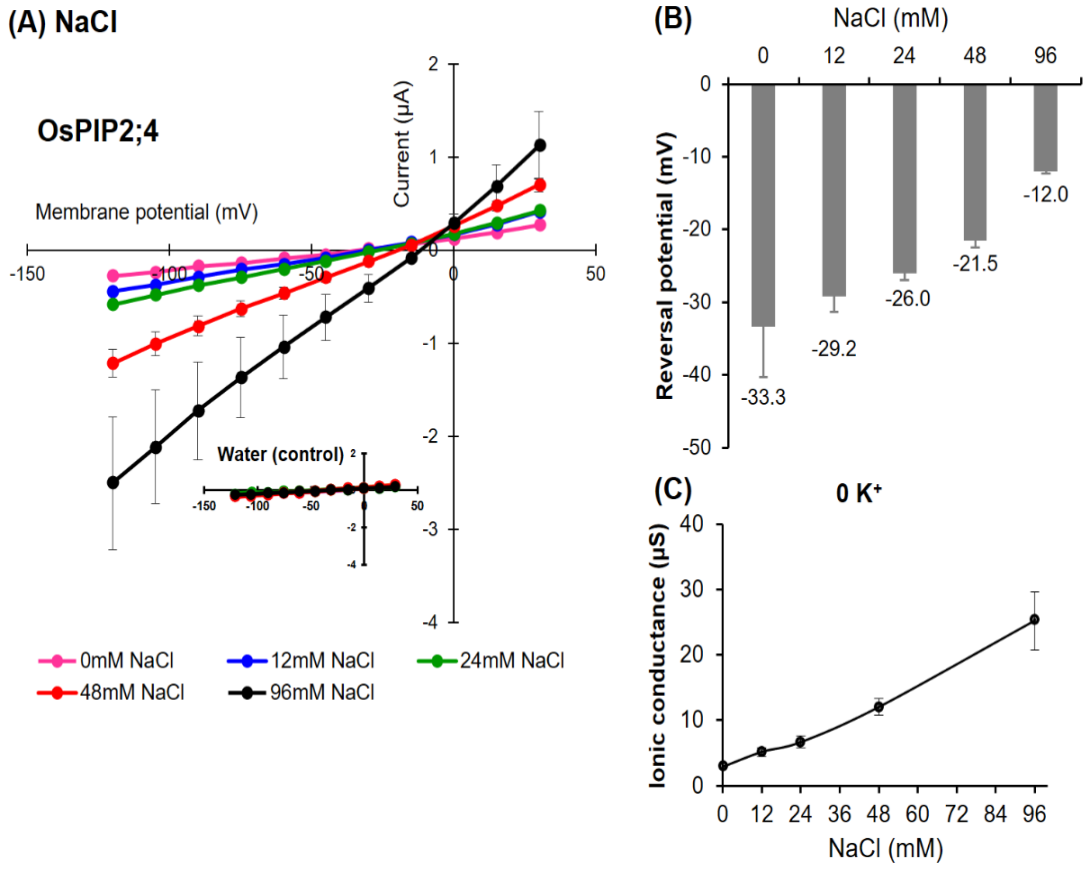

Figure 3.5. Na^+-permeability through OsPIP2;4-transporter. (A) Na^+ external concentration (chloride salt) were 5 different ratios bath solutions with low calcium condition contained a background (1.8 mM $MgCl_2$, 1.8 mM $CaCl_2$, 1.8 mM EGTA, 10mM HEPES pH 7.5 with Tris) with mannitol to adjust the osmotic potential. **(B)** Reversal potentials of currents flowing through OsPIP2;4 in A. **(C)** Ionic conductance was calculated based on the data obtained from V = −75 mV to −120 mV of the membrane potential. Steady-state current-voltage curves of *X. laevis* oocytes injected with 10 ng of cRNA per oocyte from the same batch. Data are means ± SE, n = 5 for control, n = 7 for *OsPIP2;4.*

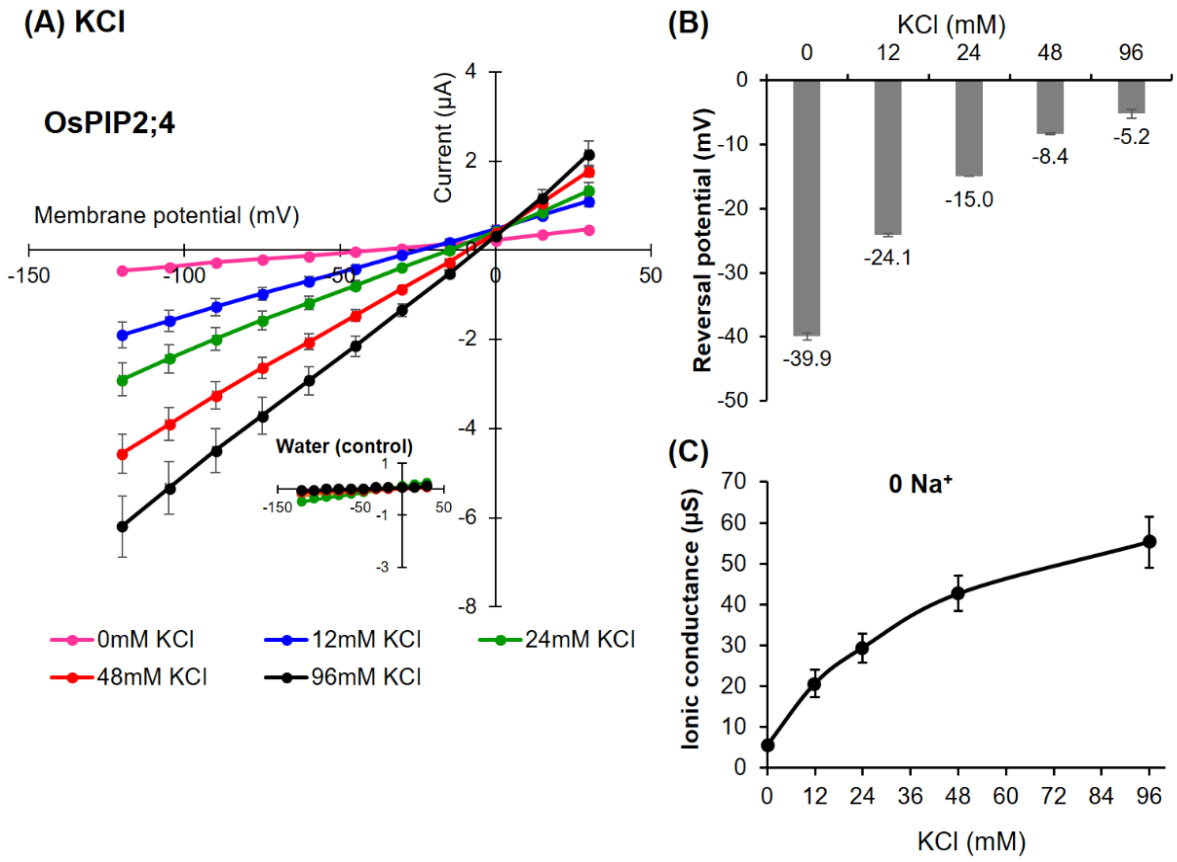

Figure 3.6. K^+-permeability through OsPIP2;4-transporter. **(A)** K^+ external concentration (chloride salt) were 5 different ratios bath solutions with low calcium condition contained a background (1.8 mM $MgCl_2$, 1.8 mM $CaCl_2$, 1.8 mM EGTA, 10mM HEPES pH 7.5 with Tris) with mannitol to adjust the osmotic potential. **(B)** Reversal potentials of currents flowing through OsPIP2;4 in A. **(C)** Ionic conductance was calculated based on the data obtained from V = −75 mV to −120 mV of the membrane potential. Steady-state current-voltage curves of *X. laevis* oocytes injected with 10 ng of cRNA per oocyte from the same batch. Data are means ± SE, n = 5 for control, n = 7 for *OsPIP2;4*.

3.3.2.3. OsPIP2;4 monovalent alkaline cation selectivity

OsPIP2;4 permeability to monovalent cations including Na^+, K^+, Rb^+, Cs^+, and Li^+ were compared in bath solutions containing 96 mM of one of these cations (as chloride salt) and fixed in low external free Ca^{2+} concentration (30 µM free Ca^{2+}) (Figure 3.7). OsPIP2;4-inward currents and ionic conductance depended on the monovalent cations present in the bath solution, indicating that the transporter discriminates between these cations. Especially, K^+ was the cation with which OsPIP2;4-currents was the largest and the reversal potential showed the less negative (approximately −10 mV), indicating that this cation is the most permeant one through OsPIP2;4, next Na^+ permeability among monovalent cations. On the other hand, in the presence of Cs^+, Rb^+, the reversal potential of OsPIP2;4 were the same as that in the presence of K^+ (no shift change), but the inward currents and conductance was strongly reduced compared with those in the presence of K^+ and Na^+ (by 70% and 60%, respectively).

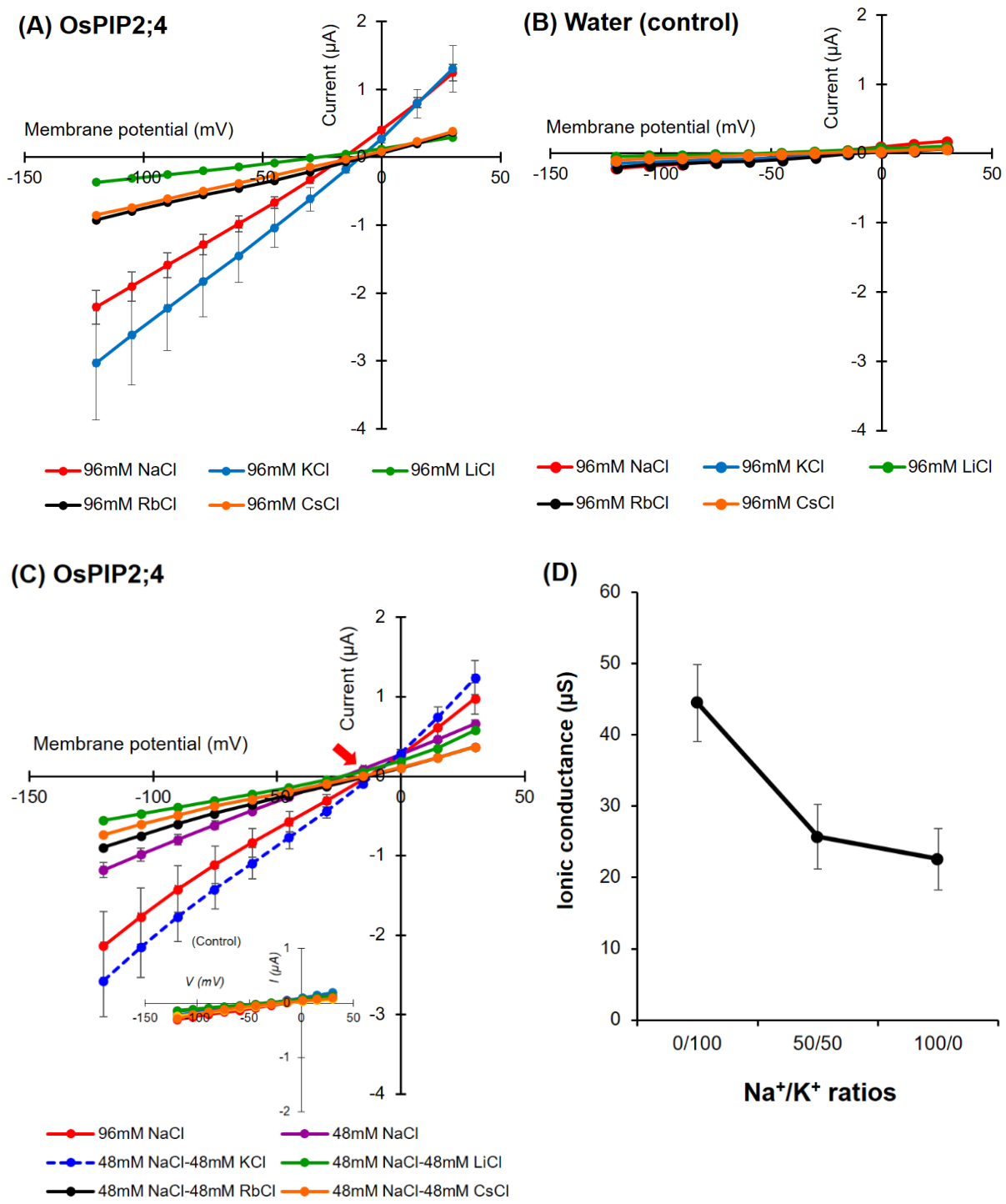

Figure 3.7. Monovalent alkaline cation selectivity of OsPIP2;4 and the effect of co-presence monovalent cations on OsPIP2;4-mediated ion channel activity. Current-voltage relationships obtained from oocytes either expressing OsPIP2;4 **(A)** or injected with water **(B)**. OsPIP2;4 displays different monovalent alkaline cation selectivity. Oocytes were successively immersed in bath solutions with a low calcium condition, supplemented with Na^+, K^+, Cs^+, Rb^+, Li^+ (as chloride salts) at the concentration of 96 mM. **(C)** Interaction of OsPIP2;4-mediated Na^+ transport by monovalent alkaline cations in the presence of 48 mM NaCl with 48 mM each alkaline cation. Red arrow indicated the reversal potential **(D)** The effect of external Na^+/K^+ concentration ratios on the ionic conductance of OsPIP2;4-expressing oocytes from V (membrane potential) = –75 mV to –120 mV. *X. laevis* oocytes were injected with 10 ng of *OsPIP2;4* cRNA for the recording of the channel in every experiment. Data are means ± SE (n = 7 for A, n = 5 for B, n = 6 to 7 for C, n = 7 for D).

Comparing OsPIP2;4 with other PIP2 transporters in cereals so far characterized and in particular with those described as K^+ permeable (HvPIP2;8 from barley) (Chapter 2), it could be noticed that OsPIP2;4 displayed the highest conductance to K^+ relative to that to Na^+. Indeed, the conductance to K^+ was higher than the conductance to Na^+ in OsPIP2;4 (in bath solutions comprising only K^+ or Na^+ as monovalent cations). When the oocytes were bathed in a 96 mM Li^+ solution, the OsPIP2;4-associated currents did not differ from the background currents recorded for the water-injected control oocytes (Figure 3.7A, B).

In addition, OsPIP2;4-associated currents were then tested in the co-presence of the solution with combinations of different monovalent cations. Experiments using solutions containing 48 mM NaCl in the co-presence of either 48 mM K^+, Cs^+, Rb^+ and Li^+ (as chloride salt), as shown in Figure 3.7C. Smaller OsPIP2;4-associated Na^+ inward currents was observed in Na^+ solutions co-presence of Rb^+, Cs^+ and Li^+ when compared with the solution containing with only 48 and 96 mM NaCl, respectively (Figure 3.7C). A positive shift in the reversal potential was observed in 96 mM NaCl (−13 mV) relative to 48 mM NaCl (−23 mV), consistent with OsPIP2;4 mediating Na^+ transport. Interestingly, in co-presence 48 mM NaCl and 48 mM KCl solution, there was larger Na^+ inward currents than in the solutions with only 48 mM NaCl, even though containing 96 mM NaCl (Figure 3.7C, D).

OsPIP2;4-injected oocytes were bathed in 86.4 mM NaCl and 9.6 mM KCl or 86.4 mM KCl and 9.6 mM NaCl solutions in low external free Ca^{2+} (free 30 μM Ca^{2+}) condition, the reversal potential for Na^+ (E_{Na+}) in the oocyte was −15 mV and the reversal potential for K^+ (E_{K+}) was −10 mV. In solutions containing 48 mM NaCl in the co-presence of either 48 mM Cs^+, Rb^+ and Li^+ (as chloride salt), as shown in Figure 3.7C, the reversal potential was −16 mV, −15 mV and −30 mV, respectively. The reversal potential in 96 mM NaCl solution was −13 mV. The ion permeability ratios through OsPIP2;4-transporter were calculated using Goldman equation (in Chapter 2), as Table 3.1.

Table 3.1. Ion permeability ratios of OsPIP2;4

ion	**Na^+**	**K^+**	**Rb^+**	**Cs^+**	**Li^+**
P_{ion}/P_{Na}	1	1.3	0.84	0.78	0

OsPIP2;4 preferred K^+ to Na^+ consistent with higher K^+ conductance than Na^+ conductance (Figure 3.5 and 3.6), with opposite relative selectivity between Na^+ and K^+ with HvPIP2;8. OsPIP2;4 was also permeable Cs^+, Rb^+, but not Li^+.

3.3.2.4. OsPIP2;4 ion transport activity was not affected by Cl^-

Exploring the selectivity of the OsPIP2;4-induced currents by anion Cl^- or not, the effect of the presence of the external anion Cl^- on OsPIP2;4 ion transport was tested using NaCl, Na-gluconate and Choline-Cl solutions (96 mM each).

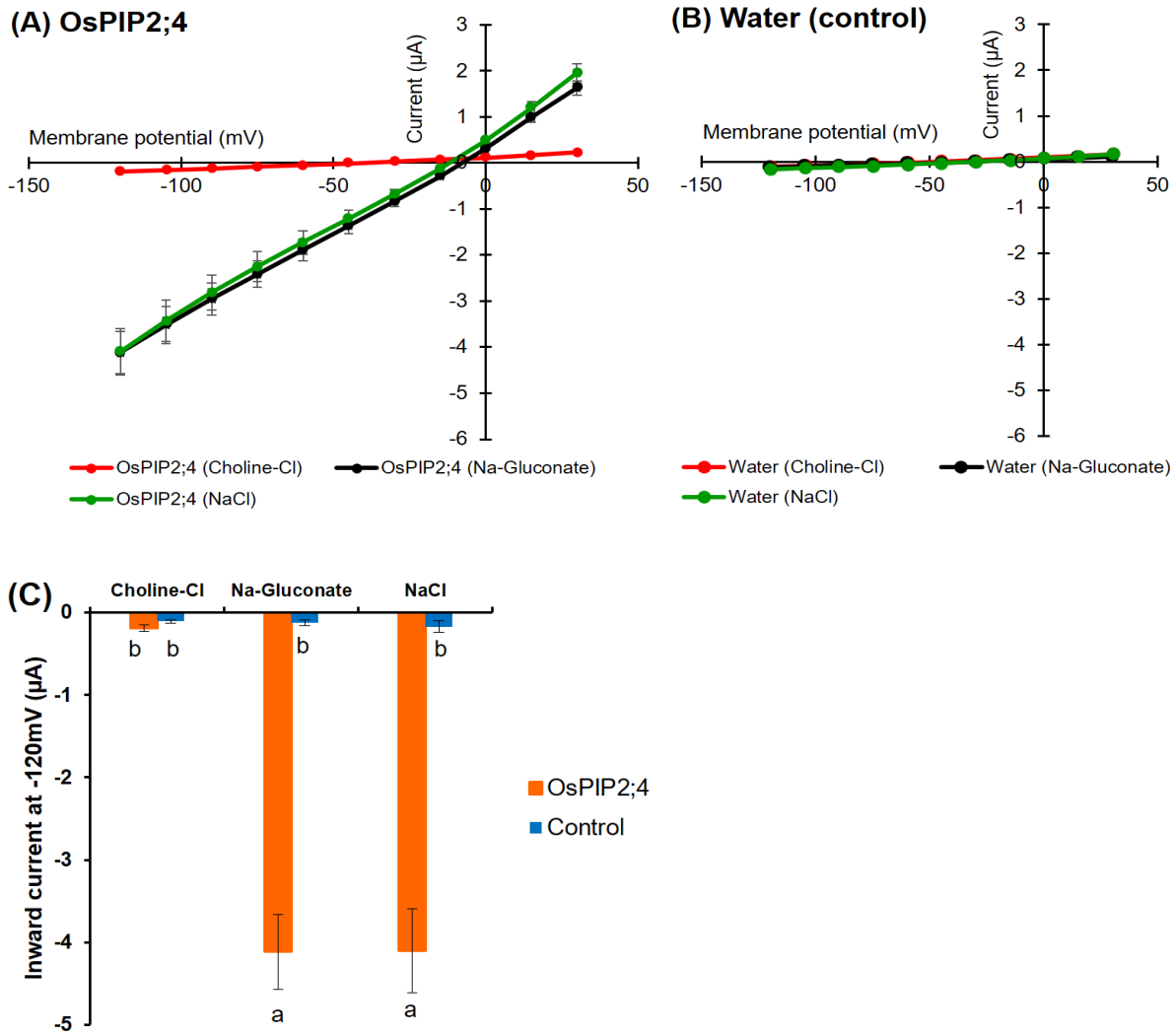

Figure 3.8. OsPIP2;4-mediated Na^+ transport is Cl^- independent. (A) Current-voltage relationships obtained from oocytes either expressing OsPIP2;4 or injected with water in the presence of either 96 mM NaCl, 96 mM Choline-Cl or 96 mM Na-gluconate. **(B)** Current-voltage relationships obtained from oocytes either expressing injected with water in the presence of either 96 mM NaCl, 96 mM Choline-Cl or 96 mM Choline-Cl. **(C)** Inward currents of OsPIP2;4 in the presence of the tested solutions. All solutions contained 30 µM Ca^{2+}. *X.laevis* oocytes were injected with 10 ng of *OsPIP2;4* cRNA for the recording of the channel. Significant differences ($P < 0.05$) are indicated by different letters using one-way ANOVA with Duncan's multiple comparisons test. Data are means ± SE (n = 7 to 8).

Similar current–voltage relationships for OsPIP2;4-expressing oocytes were observed regardless of whether there was Cl^- or gluconate solutions used in the bath (Figure 3.8A), and

there was slightly shifted change in the reversal potential (approximately −10 mV) and same inward currents was recorded for different solutions as well, indicating that the anion Cl^- had not effect on recorded inward currents of OsPIP2;4. In contrast, in the presence of 96 mM Choline-Cl, the OsPIP2;4-expressing oocytes elicited minor currents (−0.18 ± 0.03 µA at −120 mV), comparable to those of the water-injected control oocytes (−0.10 ± 0.02 µA at −120 mV), which was significantly different to the currents observed in the presence of 96 mM NaCl and Na-gluconate (Figure 3.8A-C). These results indicated clearly that the OsPIP2;4-associated Na^+-induced currents across the plasma membrane of the oocytes were not affected by the external Cl^-.

3.3.2.5. Effects of divalent cations on OsPIP2;4-mediated ion transport activity

As well as HvPIP2;8, the effect of different divalent cations on the ion conductance activity of OsPIP2;4 was examined. As shown in Figure 3.9, OsPIP2;4 currents were recorded maximal activation in divalent-free saline. After perfusion of bath saline with Ca^{2+}, Mg^{2+}, Ba^{2+}, and Cd^{2+} resulted in the reduction of OsPIP2;4-inward currents (Figure 3.9A).

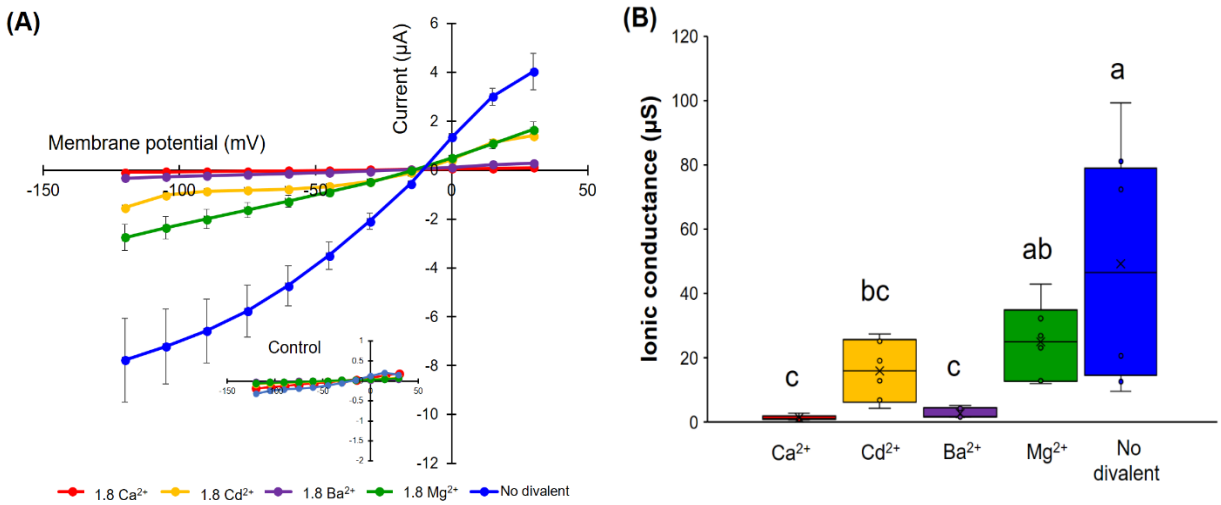

Figure 3.9. Effects of divalent cations on the ion current responses in oocytes expressing OsPIP2;4. Effect of divalent cations on the ion currents of the OsPIP2;4-transporter; bath solutions with a low 1.8 mM Ca^{2+} background calcium conditions were successively replaced with either 1.8 mM Ca^{2+}, Ba^{2+}, Cd^{2+}, and Mg^{2+} (as chloride salts), at concentrations of 86.4 mM NaCl and 9.6 mM KCl. (**B**) Box plot summary of the ionic conductance presented in (A); the ionic conductances were calculated from V = −75 mV to −120 mV. Steady-state current–voltage curves of the *X. laevis* oocytes injected with 10 ng of cRNA per oocyte were recorded. Currents from the oocytes injected with water were the negative controls from the same batch. Significant differences ($P < 0.05$) are indicated by different letters using one-way ANOVA with Duncan's multiple comparisons test. Data are the means ± SE of three independent experiments, (n = 7 to 8).

Indeed, the ionic conductance in OsPIP2;4-expressing oocytes was strongly blocked by Ca^{2+} and Ba^{2+}, lesser inhibited by Cd^{2+} but no significant difference. In contrast, the application of 1.8 mM $MgCl_2$ gave rise to a weeker inhibitory effect on the OsPIP2;4-mediated ion currents, the ion conducting of OsPIP2;4 in 1.8 mM $MgCl_2$ showed no significantly different with in divalent-free saline (Figure 3.9A, B).

3.3.2.6. Co-expression of OsPIP2;4 with OsPIP1s reduced OsPIP2;4 ion transport activity

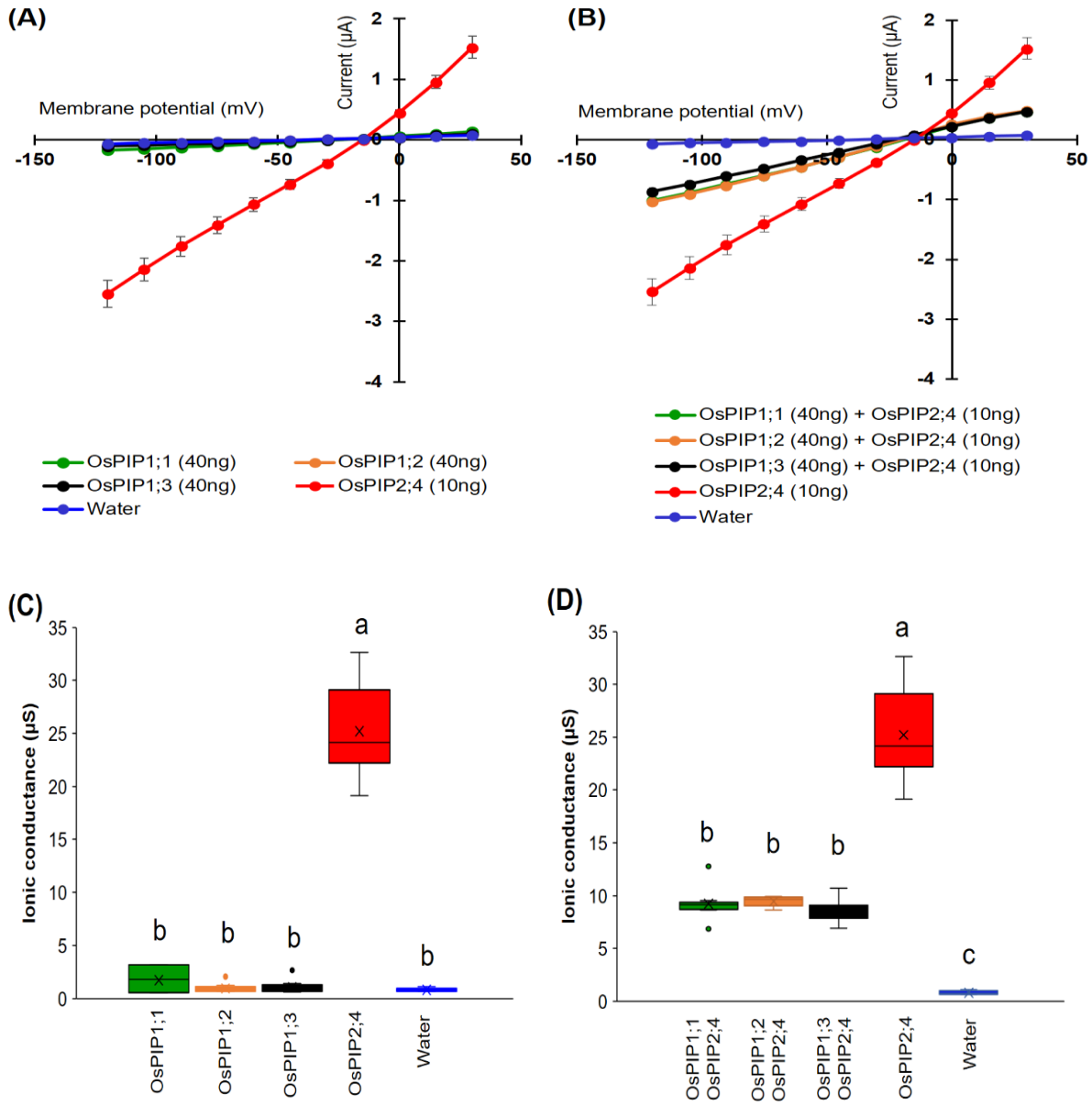

Figure 3.10. Co-expression of OsPIP1s and OsPIP2;4 reduces OsPIP2;4-dependent currents in *X. leavis* oocytes. (A) Current-voltage relationships obtained from oocytes either expressing OsPIP2;4 alone, each OsPIP1 alone or injected with water, each OsPIP1 of the three OsPIP1s did not show ion channel activity when expressed alone. **(B)** Co-expression OsPIP2;4 with each OsPIP1 largely inhibited ion channel activity of OsPIP2;4. **(C-D)** Box plot summary of the ionic conductance (the ionic conductances were calculated from V = −75 mV to −120 mV) for data shown in A and B, respectively. Oocytes were injected with 10 ng cRNA of *OsPIP2;4*, 40 ng cRNA

of each *OsPIP1* in both solo- and co-expression analyses. The bath solution included 86.4 mM NaCl, 9.6 mM KCl, 1.8 mM $MgCl_2$, 1.8 mM EGTA, 1.8 mM $CaCl_2$, 10 mM HEPES, pH 7.5 with Tris, and therefore the free Ca^{2+} concentration was 30 μM. Significant differences ($P < 0.05$) are indicated by different letters using one-way ANOVA with Duncan's multiple comparisons test. Data are means ± SE (n = 8 to 10 for OsPIP1 and OsPIP2;4, n = 5 for water).

As mentioned in Chapter 2, HvPIP1s co-expression with HvPIP2;8 resulted in greatly decreased ion inward currents of HvPIP2;8 but did not totally abolished for certain HvPIP1 combinations with HvPIP2;8 even though HvPIP1s had not ion transport activity. Therefore, I also examined the relationship interaction of OsPIP1s (OsPIP1;1 to OsPIP1;3) in co-expression with OsPIP2;4. Each OsPIP1 displayed similar currents and ionic conductance was no significant difference with the water-injected controls when expressed alone (Figure 3.10A, C).

The phenomenon of most PIP1 proteins failing to target to the plasma membrane and residing in intracellular membranes results from either missing plasma membrane trafficking signals or existing ER retention motifs (Chevalier and Chaumont, 2015). Actually, OsPIP1;3 was detected in ER-like membranes around nucleus of rice protoplast (Liu et al., 2020). The OsPIP2;4-associated inward currents were significant as expected (around −2,5 μA at −120 mV) in low external free Ca^{2+} concentration (Figure 3.10A, B). However, when each OsPIP1 was co-expressed with OsPIP2;4, the large OsPIP2;4-associated currents were reduced in the co-expression combinations examined (approximate −1 μA at −120 mV), and ionic conductance was significantly different with OsPIP2;4 expressing alone in oocyte (Figure 3B, D).

These results indicated that OsPIP1s might be interacting with OsPIP2;4 in hetero-tetramer formation expressed in *X. laevis* oocytes and that this either prevents and significantly reduces the OsPIP2;4 ion channel activity. In contrast, in water permeability, OsPIP1s co-expression with OsPIP2;4 showed no significantly difference with OsPIP2;4 expressed alone in oocytes even though OsPIP1s had no water transport observation (Figure 3.11) as Ding et al., (2019) and Matsumoto et al., (2009) reported. Thus, mechanism of ion and water transport might be different in PIP aquaporin tetramers. The frequency and variation of PIP2/PIP1 hetero-tetramers in planta remain important questions not only for the regulation of ion conductance but also for the regulation of water conductance until now.

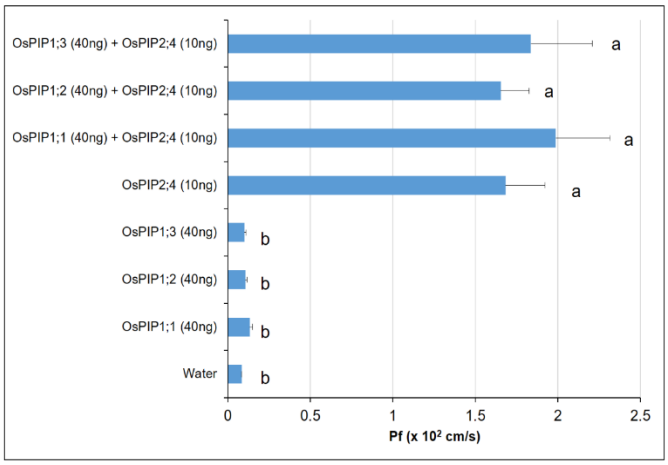

Figure 3.11. Water transport activity of co-expression OsPIP1s with OsPIP2;4. The amounts and kind of cRNAs injected were shown on the left of the graph. Significant differences ($P < 0.05$) are indicated by different letters using one-way ANOVA with Duncan's multiple comparisons test. Data are means ± SE (n = 7 to 10).

3.3.3. Expression pattern and tissue-specific expression of *OsPIP2;4*

Absolute quantitative qPCR analysis showed that *OsPIP2;4* was mainly expressed in root rather than in stem, leaf sheaths and leaf blades (Figure 3.12A). Especially, the expression of *OsPIP2;4* was higher in root tips (0-5 mm) than root elongation zone (5-15 mm) (Figure 3.12B). Immunostaining of the roots samples from 15 days-old seedlings with an *OsPIP2;4*-antibody showed that *OsPIP2;4* was expressed in epidermis and exodermis of root tips (0-5 mm) (Figure 3.12D). As a control without 1st antibody, no significant signal was observed from the root tip cells (Figure 3.12C). This localization implies important roles of OsPIP2;4 in the water and ion transport of rice plant under salinity stress. Further investigations are needed to reveal the exact physiological roles of OsPIP2;4 in salinity tolerance mechanism *in planta*.

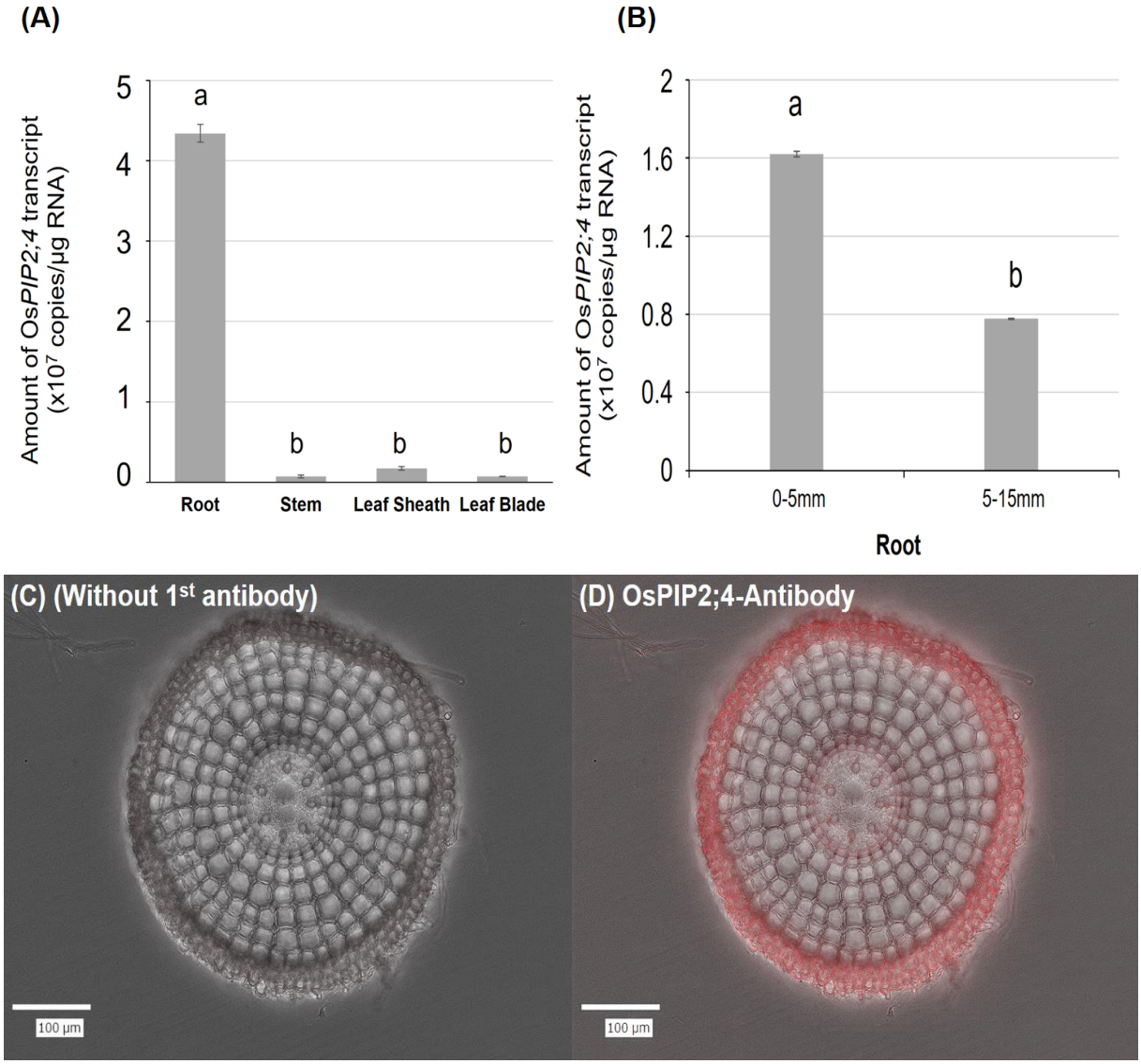

Figure 3.12. Localizations of OsPIP2;4 in rice root tissues. Rice plants were grown in a hydroponic culture solution (normal condition) and are placed in a growth chamber under the temperature was maintained at 28°C and 25°C in 12 h day (250 µmol s^{-1} m^{-2} illumination) and 12 h night, respectively for 8 days. **(A)** Absolute qPCR for *OsPIP2;4* in the root, stem, leaf sheaths, leaf blades tissues. **(B)** Absolute qPCR for *OsPIP2;4* in the root tips (0-5 mm) and basal root parts (5-15 mm) from 2 week-old seedlings of Nipponbare rice under normal conditions in A and B. Root sections at around 5 mm from the root tips were subjected to immunocytochemistry using the anti-*OsPIP2;4* anti-body. **(C)** Without 1st antibody; **(D)** Young root with antibody. Bars represent 100 µm. Significant differences ($P < 0.05$) are indicated by different letters using one-way ANOVA with Duncan's multiple comparisons test.

3.3.4. Phenotypic analysis of OsPIP2;4 transgenic plants in salinity stress conditions

3.3.4.1. Expression of the OsPIP2;4-gene in transgenic plants at reproductive stage

At the reproductive stage, *OsPIP2;4* transcripts were examined in the various tissues including flag leaf sheath (FLS), flag leaf blade (FLB), peduncle (P), node I (N I), node II (N

II), internode II (IN II) of wild types (WT) and transgenic lines response to salt stressed through absolute quantitative qPCR (Figure 3.13).

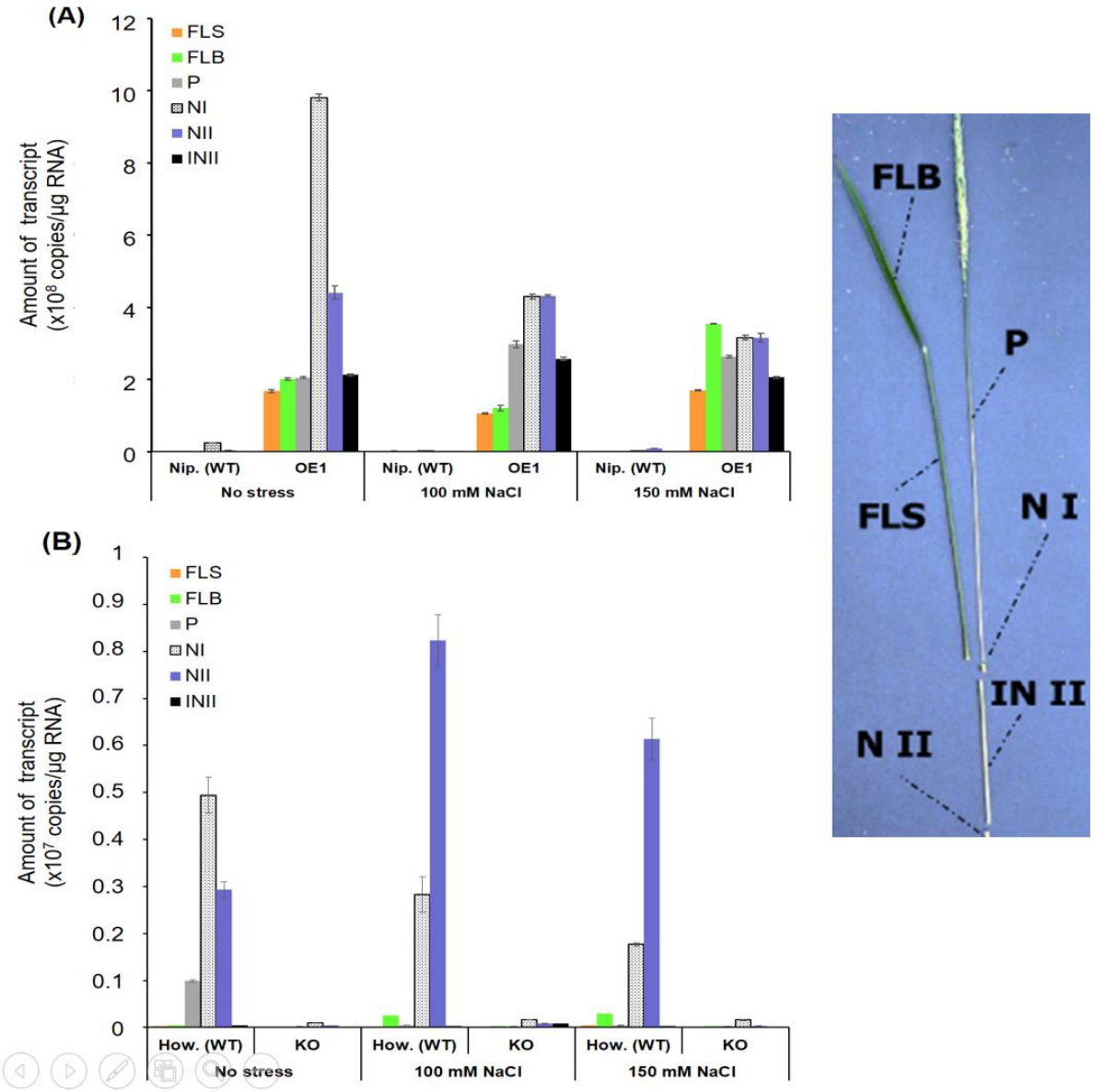

Figure 3.13. Expression profile of OsPIP2;4 in various tissues of transgenic rice lines. Quantitative real-time PCR analyses were performed using RNA samples derived from various tissues of soil-grown Nipponbare (wild type) and overexpressing line 1 (OE1) in A and Howayoung (wild type) and knockout (KO) line in B at the reproductive growth phase with or without NaCl treaments (25 – 150 mM NaCl) for more than a month is shown settings its expression in the flag leaf sheath (FLS), flag leaf blade (FLB), peduncle (P), node I (N I), node II (N II), internode II (IN II) (n = 4 ± SE).

The results showed that the *OsPIP2;4* transcript levels of overexpressing 1 (OE1) line was strongly higher than Nipponbare (WT) in response to salt stress and control conditions. *OsPIP2;4* transcripts of OE1 were relatively highly expressed in node I and II when compared with other tissues, but seemed similar in flag leaf blade, flag leaf sheath, peduncle, and internode

II (Figure 3.13A). On the other hand, the *OsPIP2;4* transcript levels of KO line were extremely lower than Howayoung (WT). *OsPIP2;4* transcripts in Howayoung (WT) were predominantly expressed in node I and node II under control and salinity stress conditions (Figure 3.13B). The node is an essential tissue for distributing minerals and toxic elements, which are transported from the roots (Yamaji et al., 2014). Therefore, the level of expression of *OsPIP2;4* was elevated in node I and node II response to salinity stress. This result revealed that the expression level of *OsPIP2;4* was stable for each transgenic plant both in seedlings and in reproductive growth stage, therefore, used for further analysis.

3.3.4.2. Na^+ and K^+ accumulation in over-expressing OsPIP2;4 plant under salt stress treatment

To investigate whether OsPIP2;4-mediated Na^+ and K^+ transport contributes to salt tolerance in rice plants, Na^+ and K^+ contents in various aerial tissues of overexpressing and knockout rice lines were measured. Wild type and transgenic plant were grown in the same pot filled with soil from paddy fields and grown in greenhouse.

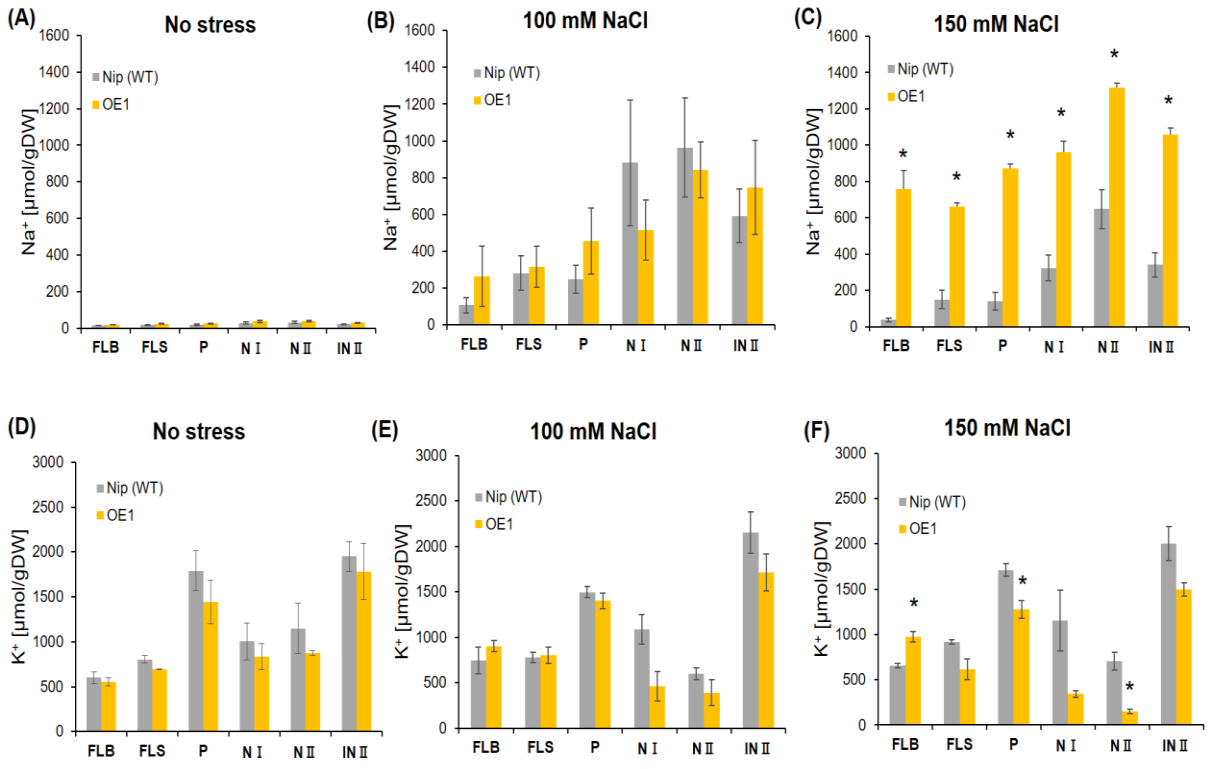

Figure 3.14. Accumulation of Na^+ and K^+ in over-expressing OsPIP2;4 plants at the reproductive growth stage. Nipponbare (wild type) and overexpressing line 1 (OE1) were planted in the same pot filled with paddy-filed soil and grown for approximately 3.5 months. When the plants started heading, NaCl treatment was initiated by gradually increasing the content of Na^+ in tap water from 25 mM to 150 mM for more than a month. Tissues of the upper parts were excised and washed briefly by the ultrapure water. Ion contents were determined using an inductively coupled plasma optical emission spectrometer. Flag leaf sheath (FLS), flag leaf blade (FLB), peduncle

(P), node I (N I), node II (N II), internode II (IN II) (n = 3, ± SE). Na^+ content (**A, B, C**); K^+ content (**D, E, F**). The Welch's-t test was used for the statistical analysis: * $P < 0.05$, vs. wild type (WT) in each NaCl concentration.

Under the control condition without NaCl, there was no significant difference observed in Na^+ or K^+ contents of all tissues between wild type and overexpressing plants (Figure 3.14A, D). Generally, under salt stress conditions, Na^+ accumulated higher in nodes (I and II) and internode II than flag leaves and peduncles. But, there was no significant difference in Na^+ content between wild type and overexpressing plants under 100 mM NaCl treatment (Figure 3.14B). However, under 150 mM NaCl treatment, overexpression of OsPIP2;4 resulted in accumulating more Na^+ in every organ tested with significantly different from wild type (Figure 3.14C). In particular, Na^+ content of node II was approximately 3-fold higher in OsPIP2;4-overexpressing plants than those in wild type (150 mM NaCl) and 35-fold higher than OE plants (no stress) (Figure 3.14A, C). For K^+ accumulation, there was no significant difference in K^+ accumulation between wild type and overexpressing plants in all organs tested under control and 100 mM NaCl (Figure 3.14D, E). Nevertheless, K^+ content was lower in overexpressing plants compared to wild type except in flag leaf blade under 150 mM NaCl treatment (Figure 3.14F). Significantly reduction of K^+ content was observed in peduncles and node II compared with wild type in 150 mM NaCl condition. Especially, K^+ content was the lowest accumulation in node II compared to other tissues and decreased around 1.3 fold compared to wild type, which was opposite to Na^+ content was the highest accumulation in node II under 150 mM NaCl treatment (Figure 3.14C, F).

On the other hand, less accumulation of Na^+ and more K^+ was observed in knockout (KO) in every aerial tissues tested in salt stress condition (Figure 3.15B, D). Generally, the Na^+ was highly accumulated in nodes (I and II) and internode II compared to other tissues in both wild type and KO. Under 150 mM NaCl treatment, Na^+ accumulated in KO plants was lower than wild type (Figure 3.15B). There was a significant difference in Na^+ content in all tissues except flag leaf sheath between wild-type and KO with approximately 8-fold in node I, 4.8-fold in node II, and a 9.1-fold decrease in KO compared to wild-type (Figure 3.15B). In contrast, there was higher K^+ accumulation in KO plants in all tissues tested compared with wild type under both conditions. K^+ content of KO in node II and internode II was significantly higher than wild type under 150 mM NaCl treatment (Figure 3.15D).

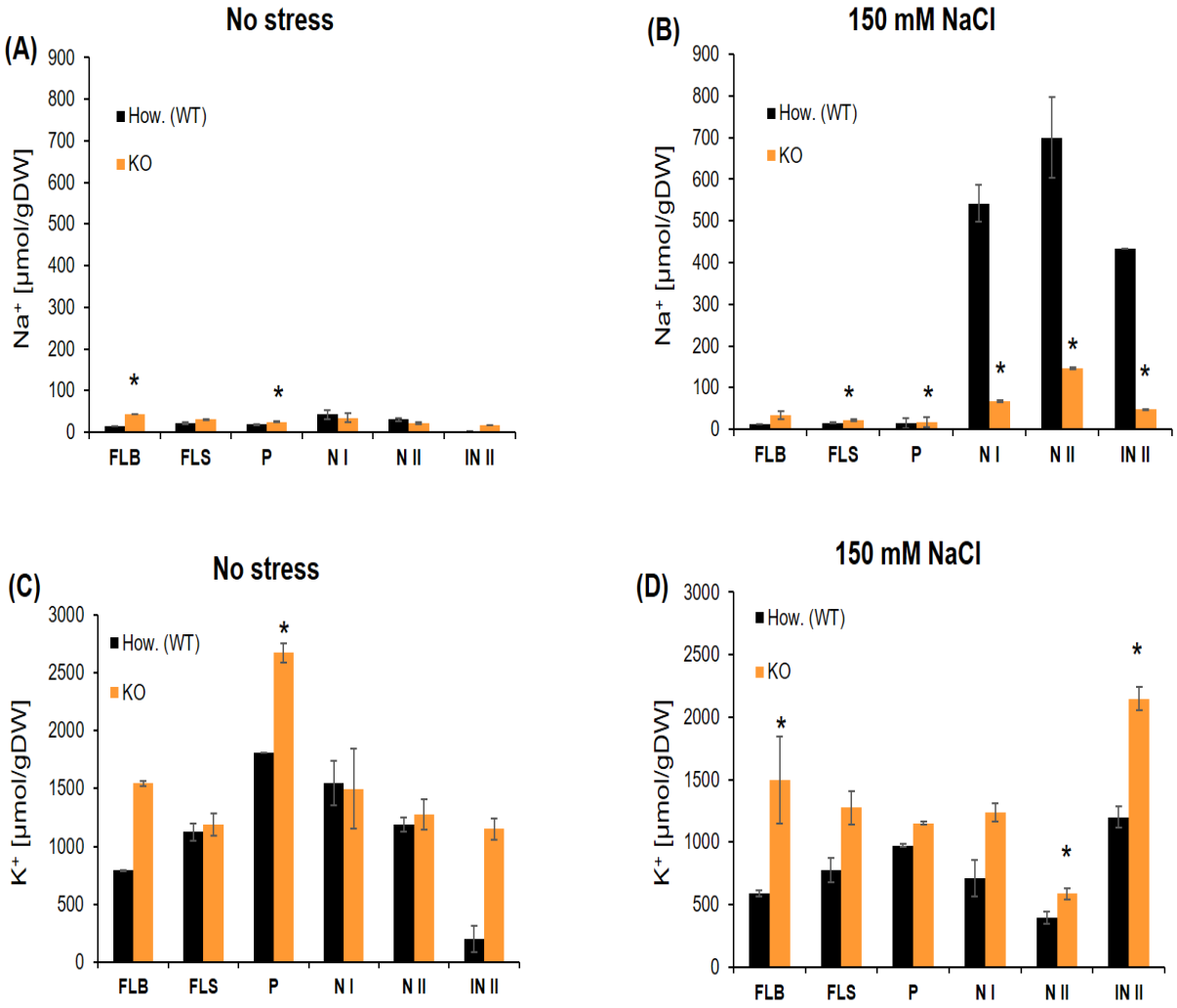

Figure 3.15. Accumulation of Na^+ and K^+ in knockout OsPIP2;4 plants at the reproductive growth stage. Howayoung (wild type) and knockout (KO) line were planted in the same pot filled with paddy-filed soil and grown for approximately 3.5 months. When the plants started heading, NaCl treatment was initiated by gradually increasing the concentration of Na^+ in tap water from 25 mM to 150 mM for more than a month. Tissues of the upper parts were excised and washed briefly by the ultrapure water. Ion contents were determined using an inductively coupled plasma optical emission spectrometer. Flag leaf sheath (FLS), flag leaf blade (FLB), peduncle (P), node I (N I), node II (N II), internode II (IN II) (n = 3, ± SE). Na^+ content (**A, B**); K^+ content (**C, D**). The Welch's-t test was used for the statistical analysis: * $P < 0.05$, vs. wild type (WT) in each NaCl concentration.

3.4. Discussion

3.4.1. Ion transport properties of OsPIP2;4 expressed in *X. laevis* oocytes

In this study, *OsPIP2;4* was predominantly expressed in root, especially in root tip rather than stem, leaf sheaths and leaf blades and others root part. In addition, *OsPIP2;4* was mainly localized at epidermis and exodermis of root tip (Figure 3.12), suggesting that *OsPIP2;4* may play important roles in transporting water and ion from the soil into plants. Actually, OsPIP2;4 conducted both water and ion when expressed in *X. laevis* oocytes (Figure 3.3 and

3.11; Ding et al., 2019). Here, I observed that only in *X. laevis* oocytes expressing OsPIP2;4 in low external free Ca^{2+} induced significant ionic conductance among other OsPIP2s and OsPIP1s (Figure 3.3A and 3.10A). Previous studies have been demonstrated water transport activity for OsPIP2;1, OsPIP2;2, OsPIP2;3, OsPIP2;4, OsPIP2;5 in yeast expressing (Ding et al., 2019). OsPIP2;4 showed a potential activity to permeate both Na^+ and K^+ with prefer K^+ to Na^+ and highly dependent on effect of external free Ca^{2+} concentration on the plasma membrane in *X. laevis* oocytes (Figures 3.5; 3.6 and 3.7). OsPIP2;4-associated Na^+ inward currents were not affected by Cl^- (Figure 3.8). Moreover, the present data showed that OsPIP2;4 was slightly transport Rb^+, Cs^+ but not to Li^+ under low external free Ca^{2+} condition (96 mM for each monovalent), and Na^+ transport was strongly inhibited by co-presence with Rb^+, Cs^+, Li^+ (Figure 3.7A, C). OsPIP2;4-ion conducting was inhibited by divalent cations (Ca^{2+}, Ba^{2+}, Cd^{2+} and lesser by Mg^{2+}) (Figure 3.9). On the other hand, co-expression of OsPIP2;4 and OsPIP1s (OsPIP1;1, OsPIP1;2, OsPIP1;3) proteins reduced the OsPIP2;4-induced ionic conductance but still remained a higher ionic conductance when compared with water-injected control, and significantly different comparable with OsPIP2;4-associated currents expressed in oocytes alone (Figure 3.10).

Previous studies have been revealed that heterologous expression of AtPIP2;1, categorized as a plasma membrane-localized aquaporin in *Arabidopsis thaliana*, is associated with non-selective cation conductance, and this ion transport function is sensitive to Ca^{2+} (Byrt et al., 2017), and a barley aquaporin HvPIP2;8-associated ionic conductance was highly dependent to external free Ca^{2+} concentration (Chapter 2). Recently, the Ca^{2+} sensitivity was revealed in ion conducting aquaporins like AtPIP2;1, AtPIP2;2, DmBIB, HsAQP1 (Kourghi et al., 2017). In this study, TEVC experiments were used for screening OsPIPs and water-injected control expressing in *X. laevis* ooyctes, and it was revealed that only OsPIP2;4-induced largest inward currents among the set of eleven OsPIPs tested under low external free Ca^{2+} concentration, but not in high Ca^{2+} condition (Figure 3.3A, B and Figure 3.10). However, OsPIP2;5 also showed small currents when expressed in oocytes, indicating that OsPIP2;5 might be capable of facilitating ionic conductance in low Ca^{2+} condition, but the OsPIP2;5-induced currents were significantly smaller than OsPIP2;4 associated-currents (Figure 3.3A, C). It could be noted that each plant ion conducting aquaporin shows different properties in term of cation selectivity in *X. laevis* oocytes.

OsPIP2;4 has been demonstrated to conduct water and ions transport activity when expressed in *X. laevis* oocytes (Figure 3.3 and 3.11; Ding et al., 2019), I hypothesize that OsPIP2;4 can transport both water and ion transport in plants. OsPIP2;4-Na^+, K^+ transport

activity was inhibited by raising the external free Ca^{2+}, and OsPIP2;4-induced currents were strongly blocked by application extracellular 1.8 mM Ca^{2+} concentration (Figure 3.4). This result has implications for the role of Ca^{2+} in alleviating Na^+ toxicity under saline conditions. Ca^{2+} has long been known to ameliorate the symptoms of salt stress in plants when supplied in concentrations more than the normally required concentration for growth in non-saline media (0.1 mM) (Hyder and Greenway, 1965). Similarly, AtPIP2;1, AtPIP2;2 were also inhibited by Ca^{2+}, and AtPIP2;1, AtPIP2;2 from *Arabidopsis thaliana* maximum inhibition was observed at 100μM, 10μM free Ca^{2+}, respectively (Kourghi et al., 2017). Another study demonstrated that AtPIP2;1 ionic conductance was also blocked by Ca^{2+} (Byrt et al., 2017). Na^+ influx through the nonselective cation (NSC) channel in wheat was sensitive to Ca^{2+}, and Ca^{2+} partially inhibited Na^+ influx into low-salt-grown roots (Romola Jane Davenport and Mark Tester, 2000). Ion transport of aquaporin HvPIP2;8 was also inhibited by extracellular Ca^{2+} (IC_{50} = 401 μM) (Chapter 2), which is less sensitive to Ca^{2+} than OsPIP2;4-transporter (IC_{50} = 92 μM) (https://www.aatbio.com/tools/ic50-calculator). Indeed, in my experiments, an increase in external Ca^{2+} from 1.0 to 1.8 mM was shown to be an inhibition OsPIP2;4 inward currents observed like water-injected control (Figure 3.4). In plants, where changes in free Ca^{2+} have important signaling roles particularly in response to stress (Sanders et al., 2002; Choi at el., 2014), the inhibition of ion conducting OsPIP2;4 by extracellular Ca^{2+} should be physiologically important under salinity condition.

Electrophysiological studies have suggested that Na^+ influx into cereals is mediated by voltage-independent, nonselective cation channels. Studies of Na^+ currents in the cortex of wheat (Tyerman et al., 1997), and suspension-cultured barley (Amtmann et al., 1997) indicated that Na^+ influx was predominantly via an instantaneous current of selectivity among monovalent cations (Amtmann and Sanders, 1999; Tyerman et al., 1999; White, 1999). However, in other studies, permeability sequence for monovalent cations of $Rb^+ > K^+ > Cs^+ > Na^+ > Li^+$ were observed in wheat (Tyerman et al., 1997). Meanwhile, OsHKT2;4 displayed a high permeability to K^+ compared with that to Na^+ (permeability sequence: $K^+ > Rb^+ \approx Cs^+ > Na^+ \approx Li^+ \approx NH_4^+$ (Sassi et al., 2012). Present study revealed that OsPIP2;4 was highly permeable K^+ than Na^+, although OsPIP2;4 also showed slightly permeate Rb^+ and Cs^+, but did not mediate Li^+ transport (Figure 3.7A, C). External Na^+ seemed inhibit K^+ transport activity of OsPIP2;4. This property was different from the other aquaporins. For example, Na^+-transport of HvPIP2;8 was inhibited by raising the external K^+ concentration, and also inhibited by co-presence of Rb^+, Cs^+ and Li^+ in the bath solutions (Chapter 2). In OsHKT2;2, extracellular K^+ stimulated the OsKHT2;2-mediate Na^+ transport (Yao et al., 2010). In contrast, Na^+ transport activity of HvHKT1;5 was inhibited by external K^+ (Huang et al., 2020). In addition, the influence of

divalent cations (Ca^{2+}, Ba^{2+}, Cd^{2+}, Mg^{2+}) inhibited the OsPIP2;4 ionic conductance compared with in divalent-free saline (Figure 3.9). These properties of OsPIP2;4-transporter were observed as well as HvPIP2;8, AtPIP2;1 and AtPIP2;2 (Chapter 2; Kourghi et al., 2017).

Since Cl^- ion is the most dominant anion in saline soil, plants accumulate high levels of Cl^- in the leaves when grown under saline condition. A lot of studies indicate Na^+ as an important ion highly correlated with high salt concentration. However, other studies demonstrated that handling of Cl^- might be very important for salt sensitive in some other crops. Cl^- uptake by roots must be restricted including *Hordeum* (Teakle and Tyerman, 2010; Tavakkoli et al., 2010). Here, the aquaporin OsPIP2;4-induced currents were not affected by Cl^- expressing in *X. laevis* oocytes, suggesting that OsPIP2;4-transporter had no permeability to Cl^- from experiments using Choline-Cl and Na-gluconate or NaCl (Figure 3.8). As a result, the presence or absence anion Cl^- was no effect on ion transport activity of OsPIP2;4-transporter, and ions uptake by OsPIP2;4 might not require the presence of Cl^-. This result was similar observation in HvPIP2;8-transporter in barley (Chapter 2).

Previous studies have already shown that the OsPIP1;3 protein expressed in *Xenopus* oocytes did not elicit significant water permeability but did interact with some OsPIP2 members (OsPIP2;2 and OsPIP2;4 but not OsPIP2;3) to increase water permeability (Matsumoto et al., 2009; Liu et al., 2020). Here, co-expression of OsPIP2;4 with OsPIP1s (OsPIP1;1, OsPIP1;2, OsPIP1;3) significantly decreased the ionic conductance compared with the expression of OsPIP2;4 alone. Meanwhile, OsPIP1s had not ion transport activity (Figure 3.10), revealed that OsPIP2;4-associated ion transport activity might be negatively regulated through hetero-tetramer formation with OsPIP1s. I also further observed that co-expression of OsPIP2;4 with OsPIP1s did not enhanced water permeability even though OsPIP1s had not also show water permeability (Figure 3.11). Similarly, co-expression of OsPIP2;1 with OsPIP1;1 and OsPIP2;2 with OsPIP1;3 significantly increased its water permeability, suggesting that the heteromerization of OsPIP1;1/OsPIP2;1, OsPIP1;3/OsPIP2;2 and re-localization might be required to modulate their water channel activity (Liu et al., 2013; Liu et al., 2020). The intracellular retentions of PIP1s are either caused by missing plasma membrane trafficking signals or by existing ER retention motifs, whereas the interaction and hetero-tetramer of certain pairs of PIP1s and PIP2s can significant enhanced water permeability like co-expression OsPIP1;1/OsPIP2;1 and OsPIP1;3/OsPIP2;2 as descried (Bienert et al., 2018). A previous study revealed that when co-expression of AtPIP2;1 with AtPIP1;2 enhanced the water permeability compared with the expression of AtPIP2;1 or AtPIP1;2 alone. However, the ionic conductance of AtPIP2;1 could be suppressed to the level of the water-injected controls when

AtPIP2;1 was co-expressed with AtPIP1;2, indicating that the ionic conductance was not associated with higher water permeability (Byrt et al., 2017). In addition, in case co-expression HvPIP2;8 with HvPIP1s also significantly reduced the ionic conductance when compared with HvPIP2;8-expressed alone in oocytes (Chapter 2). Taken together, mechanisms of water and ion transport are different from each other in heteromer with OsPIP2;4 and OsPIP1s. Monomer pores and central pore of heteromer may be involved.

3.4.2. The role of *OsPIP2;4* in salt tolerance mechanism in rice

All tissues of overexpression plants exhibited a significantly higher level of *OsPIP2;4* transcripts than Nipponbare (WT) (Figure 3.13A). In contrast, *OsPIP2;4* transcript levels of KO line were extremely lower than Howayoung (WT) (Figure 3.13B).

Long-term salinity stress treatment with gradual increases in NaCl led to enhancement of OsPIP2;4-expression in the nodes (I and II) of soil-grown rice plants from heading to ripening stages. Elevated expression of *OsPIP2;4* in node I and node II may be caused by salinity stress. Under 150 mM NaCl treatment, OsPIP2;4-overexpressing plants resulted in significantly higher Na^+ and lower K^+ contents in aerial tissues compared with wild type. Na^+ content was the highest accumulation in node II, followed by internode II, then node I compared with wild type. There was no significant difference in Na^+ and K^+ contents between overexpressing and wild type plants in both control and 100 mM NaCl conditions (Figure 3.14A, B, D, E). Knockout plant showed significantly lower Na^+ and higher K^+ contents in all tissues compared to wild type under salt-stressed (Figure 3.15B, D). These results suggested that OsPIP2;4 acts Na^+ absorption under salt stress, which leads to the reduction of the K^+ content. Together with Na^+ selective transport mediated by OsPIP2;4 aquaporin expressed in *X.laevis* oocytes (Figure 3.4 and 3.6) and *OsPIP2;4* were predominantly expressed in root, especially in epidermis and exodermis of root tip (Figure 3.12). It can be estimated that OsPIP2;4 may contribute to the transport of Na^+ from the root-soil boundary, then Na^+ moves radially to the stele, and is loaded into the xylem. Then Na^+ is taken up to the shoot in the transpiration stream and finally accumulated in aerial parts, especially in nodes (I and II) and internode (II) and lesser in flag leaf at the reproductive growth stage during salinity stress. On the other hand, other transporters/channels should also be involved in the Na^+ absorb ion in root then moves to the xylem (Munns and Tester, 2008). In a previous study, overexpressing of transgenic durum wheat TdPIP2;1 retained low Na^+ and high K^+ concentrations in their shoot under salt conditions (Ayadi et al., 2019). Imposition of salinity stress on the OsHKT1;4 RNAi plants in the reproductive growth stage caused significant Na^+ over accumulation in aerial organs, in particular, leaf blades and sheaths (Suzuki et al., 2016b).

Taken together, these findings suggest that mechanisms to regulate OsPIP2;4 aquaporin are one of a key mechanisms used by plants to ion transport, therefore ion homeostasis during salinity stress. New physiological function of OsPIP2;4 is recognized in response to salinity stress as the first investigated in rice plants. To fully understand the role of OsPIP2;4-mediated Na^+-selective transport in salt-tolerance and in the yield of salt-stressed rice plants, further experiments including the tissue specific function of OsPIP2;4 are required.

References

Alavilli H. Alavilli H., Awasthi J.P., Rout G. R., Sahoo L., Lee B., Panda S.K. **(2016)**. Overexpression of a Barley Aquaporin Gene, HvPIP2;5 Confers Salt and Osmotic Stress Tolerance in Yeast and Plants, *Frontiers in Plant Science*, 7(October), pp. 1–12. doi: 10.3389/fpls.2016.01566.

Ayadi M., Brini F., Masmoudi K. **(2019)**. Overexpression of a wheat aquaporin gene, TdPIP2;1, enhances salt and drought tolerance in transgenic durum wheat cv. Maali, *International Journal of Molecular Sciences*, 20(10). doi: 10.3390/ijms20102389.

Amtmann A., Laurie S., Leigh R., Sanders D. **(1997)**. Multiple inward channels provide flexibility in K^+/Na^+ discrimination at the plasma membrane of barley suspension culture cells. *J. Exp. Bot.,* 48: 431–440.

Amtmann A., Sanders D. **(1999)**. Mechanisms of Na^+ uptake by plant cells. *Adv. Bot. Res.,* 29: 75–112.

Bienert M.D., Diehn T.A., Richet N., Chaumont F., Bienert G.P. **(2018)**. Heterotetramerization of Plant PIP1 and PIP2 Aquaporins Is an Evolutionary Ancient Feature to Guide PIP1 Plasma Membrane Localization and Function. *Front. Plant Sci., 9*, 15.

Besse M., Knipfer T., Miller A.J., Verdeil J.L., Jahn T.P., Fricke W. **(2011)**. Developmental pattern of aquaporin expression in barley (*Hordeum vulgare* L.) leaves. *J. Exp. Bot.,* 62, 4127–4142.

Byrt C.S., Zhao M., Kourghi M., Bose J., Henderson S.W., Qiu J., Tyerman, S.D. **(2017)**. Non-selective cation channel activity of aquaporin AtPIP2;1 regulated by Ca^{2+} and pH. *Plant Cell Environ.,* 40, 802–815.

Chaumont F., Barrieu F., Wojcik E., Chrispeels M. J., Jung R. **(2001)**. Aquaporins constitute a large and highly divergent protein family in maize. *Plant Physiol.* 125, 1206–1215. doi: 10.1104/pp.125.3.1206.

Chaumont F., Tyerman S.D. **(2014)**. Aquaporins: Highly Regulated Channels Controlling PlantWater Relations. *Plant Physiol.*, 164, 1600–1618.

Coffey O., Bonfield R., Corre F., Althea Sirigiri J., Meng D., Fricke W. **(2018)**. Root and cell hydraulic conductivity, apoplastic barriers and aquaporin gene expression in barley (Hordeum vulgare L.) grown with low supply of potassium. *Ann. Bot.,* 122, 1131–1141.

Chinnusamy V., Jagendorf A., Zhu J. K. **(2005)**. Understanding and improving salt tolerance in plants. *Crop Sci.,* 45(2): 437–448.

Chevalier, A.S. and Chaumont, F. **(2015)**. Trafficking of plant plasma membrane aquaporins: multiple regulation levels and complex sorting signals. *Plant Cell Physiol.*, 56, 819–829.

Dynowski M., Mayer M., Moran O., Ludewig U. **(2008)**. Molecular determinants of ammonia and urea conductance in plant aquaporin homologs. *FEBS Letters*, 582, 2458–2462.

Danielson J.Å., Johanson U., **(2008)**. Unexpected complexity of the aquaporin gene family in the moss Physcomitrella patens. *BMC Plant Biol.,* 8, 45.

Ding L., Uehlein N., Kaldenhoff R., Guo S., Zhu Y., Kai L. **(2019)**. Aquaporin PIP2;1 affects water transport and root growth in rice (*Oryza sativa* L.). *Plant Physiology and Biochemistry,* 139,152-160.

Fox A.R., Maistriaux L.C., Chaumont F. **(2017)**. Toward understanding of the high number of plant aquaporin isoforms and multiple regulation mechanisms. *Plant Sci.,* 264, 179–187.

Forrest K.L., Bhave M. **(2007)**. Major intrinsic proteins (MIPs) in plants: a complex gene family with major impacts on plant phenotype. *F unct. Integr. Genomics.,* 7: 263 – 289.

Guo L., Zi Y. W., Lin H., Wei E. C., Chen J., Liu M., Zhang L.C., Li J.Q., Gu H. **(2006)**. Expression and functional analysis of the rice plasma-membrane intrinsic protein gene family, *Cell Research*, 16(3), pp. 277–286. doi: 10.1038/sj.cr.7310035.

Hakata M., Nakamura H., Iida-Okada K., Miyao A., Kajikawa M., Imai-Toki N., Pang J., Amano K., Horikawa A., Tsuchida-Mayama T., Song J., Igarashi M., Kitamoto H.K., Ichikawa T., Matsui M., Kikuchi S., Nagamura Y., Hirochika H., and Hiroaki Ichikawa H. **(2010)**. Production and characterization of a large population of cDNA-overexpressing transgenic rice plants using Gateway-based full-length cDNA expression libraries. *Breeding Sci.,* 60: 575–585.

Hove R. M., Ziemann M., Bhave M. **(2015)**. Identification and expression analysis of the barley (*Hordeum vulgare* L.) aquaporin gene family. *Plos One,* 10 (6): e0128025. doi:10.1371/journal. pone.0128025.

Huang L., Kuang L., Wu L., Shen Q., Han Y., Jiang L., Wu D., Zhang G. **(2020)**. The HKT transporter HvHKT1;5 negatively regulates salt tolerance, *Plant Physiology*, 182(1), pp. 584–596. doi: 10.1104/pp.19.00882.

Kourghi, M., Nourmohammadi S., Pei J.V., Qiu J., McGaughey S., Tyerman S.D.; Yool A.J. **(2017)**. Divalent cations regulate the ion conductance properties of diverse classes of aquaporins. *Int. J. Mol. Sci.,* 18, 2323.

Kumar, K., Mosa K.A., Chhikara S., Musante C., White J.C., Dhankher O.P. **(2014)**. Two rice plasma membrane intrinsic proteins, OsPIP2;4 and OsPIP2;7, are involved in transport and providing tolerance to boron toxicity, *Planta*, 239(1), pp. 187–198. doi: 10.1007/s00425-013-1969-y.

Kamiya T., Tanaka M., Mitani N., Ma J.F., Maeshima M., Fujiwara T. **(2009)**. NIP1;1, an aquaporin homolog, determines the arsenite sensitivity of Arabidopsis thaliana. *Journal of Biological Chemistry,* 284, 2114–2120.

Knipfer, T., Besse M., Verdeil, J.L., Fricke W. **(2011)**. Aquaporin-facilitated water uptake in barley (*Hordeum vulgare* L.) roots. *J. Exp. Bot.*, 62, 4115–4126.

Loqué D., Ludewig U., Yuan L. & Von Wirén N. **(2005)**. Tonoplast intrinsic proteins AtTIP2;1 and AtTIP2; 3 facilitate NH_3 transport into the vacuole. *Plant Physiology*, 137, 671–680.

Liu C., Fukumoto T., Matsumoto T., Gena P., Frascaria D., Kaneko T., Katsuhara M., Zhong S., Sun X., Zhu Y., Iwasaki I., Ding X., Calamita G., Kitagawa Y. **(2013)**. Aquaporin OsPIP1;1 promotes rice salt resistance and seed germination, *Plant Physiology and Biochemistry*. Elsevier Masson SAS, 63, pp. 151–158. doi: 10.1016/j.plaphy.2012.11.018.

Liu S.Y., Fukumoto T., Gena P., Feng P., Sun Q., Li Q., Ding X.D. **(2020)**. Ectopic expression of a rice plasma membrane intrinsic protein (OsPIP1;3) promotes plant growth and water uptake. *Plant J.*, 102, 779–796.

Mori I.C., Nobukiyo Y., Nakahara Y., Shibasaka M., Furuichi T., Katsuhara M. **(2018)**. A Cyclic Nucleotide-Gated Channel, HvCNGC2-3, Is Activated by the Co-Presence of Na^+ and K^+ and Permeable to Na^+ and K^+ Non-Selectively. *Plants*, *7*, 61.

Ma J.F., Tamai K., Yamaji N., Mitani N., Konishi S., Katsuhara M., Yano M. **(2006)**. A silicon transporter in rice. *Nature*, 440, 688–691.

Matsumoto T., Lian H.L., Su W.A., Tanaka D., Liu C.W. **(2009)**. Role of the aquaporin PIP1 subfamily in the chilling tolerance of rice. *Plant Cell Physiol*., 50:216–29.

Munns, R., Tester, M. **(2008)**. Mechanisms of salinity tolerance. *Ann. Rev. Plant Biol.*, *59*, 651–681.

Nada R.M., Abogadallah A.M. **(2020)**. Contrasting root traits and native regulation of aquaporin differentially determine the outcome of over expressing a single aquaporin (OsPIP2;4) in two rice cultivars. *Protoplasma*, 257:583-595.

Sassi A., Mieulet D., Khan I., Moreau B., Gaillard I., Sentenac H., and Anne-Aliénor V. **(2012)**. The Rice Monovalent Cation Transporter OsHKT2;4: Revisited Ionic Selectivity. *Plant Physiology*, Vol. 160, pp. 498–510.

Sakurai J., Ishikawa F., Yamaguchi T., Uemura M., Maeshima M. **(2005)**. Identification of 33 rice aquaporin genes and analysis of their expression and function, *Plant and Cell Physiology*, 46(9), pp. 1568–1577. doi: 10.1093/pcp/pci172.

Suzuki K., Yamaji N., Costa A., Okuma E., Kobayashi N.I., Kashiwagi T., Katsuhara M., Wang C., Tanoi K., Murata Y., Schroeder J.I., Ma J.F., and Horie T. **(2016b)**. OsHKT1;4-mediated Na^+ transport in stems contributes to Na^+ exclusion from leaf blades of rice at

the reproductive growth stage upon salt stress. BMC Plant Biology, pp.2-15. DOI 10.1186/s12870-016-0709-4

Takano J., WadaM., Ludewig U., Schaaf G., VonWirén N. & Fujiwara T. **(2006)**. The Arabidopsis major intrinsic protein NIP5;1 is essential for efficient boron uptake and plant development under boron limitation. *The Plant Cell*, 18, 1498–1509.

Todaka D., Nakashima K., Shinozaki K., Yamaguchi-Shinozaki K. **(2012)**. Towards understanding transcriptional regulatory networks in abiotic stress responses and tolerance in rice. *Rice*, 5(1): 6.

Tran S. T. H., Horie T., Imran S., Qiu J., McGaughey S., Byrt C.S., Tyerman S.D., Katsuhara M. **(2020)**. A survey of barley PIPc aquaporin ionic conductance reveals Ca^{2+}-sensitive HvPIP2;8 Na^+ and K^+ conductance. *Int. J. Mol. Sci.*, 21 (19), 1–20. doi: 10.3390/ijms21197135.

Tyerman S. D., Skerrett M., Garill A., Findlay G.P., Leigh R. **(1997)**. Pathways for the permeation of Na^+ and Cl_2 into protoplasts derived from the cortex of wheat roots. *J. Exp. Bot.*, 48: 459–480.

Tyerman S. D., Skerrett M. **(1999)**. Root ion channels and salinity. *Sci Hortic.*, 78: 175.235.

Verma H., Devi K., Baruah A.R., Sarma R.N. **(2020)**. Relationship of root aquaporin genes, OsPIP1;3, OsPIP2;4, OsPIP2;5, OsTIP2;1 and OsNIP2;1 expression with drought tolerance in rice, *Indian Journal of Genetics and Plant Breeding*, 80(1), 50–57. doi: 10.31742/IJGPB.80.1.6.

Uehlein N., Lovisolo C., Siefritz F., Kaldenhoff R. **(2003)**. The tobacco aquaporin NtAQP1 is a membrane CO_2 pore with physiological functions. *Nature*, 425, 734–737.

White P.J. **(1999)**. The molecular mechanism of sodium influx to root cells. *TIPS*, 4: 245–246.

Xu F., Wang K., Yuan W., Xu W., Liu S., Kronzucker H.J, Chen G., Miao R., Zhang M., Ding M., Xiao L., Kai L., Jianhua Zhang J., Zhu Y. **(2019)**. Overexpression of rice aquaporin *OsPIP1;2* improves yield by enhancing mesophyll CO_2 conductance and phloem sucrose transport. *Journal of Experimental Botany*, Vol. 70, No. 2, 671–681.

Yamaji N., Ma J.F. **(2014)**. The node, a hub for mineral nutrient distribution in graminaceous plants. *Trends Plant Sci.*,19(9):556–63.

Yao X., Horie T., Xue S., Leung H.Y., Katsuhara M., Brodsky D.E., Wu Y., Schroeder J.I. **(2010)**. Differential sodium and potassium transport selectivities of the rice OsHKT2,1 and OsHKT2;2 transporters in plant cells. *Plant Physiol.*, *152*, 341–355.

CHAPTER 4

Initial clarity of the molecular mechanism of ion selectivity of HvPIP2;8 and OsPIP2;4

HvPIP2;8 and OsPIP2;4 have dual function potential as both water and ion channel which are permeable to both Na^+ and K^+. To explore the molecular mechanism how HvPIP2;8 and OsPIP2;4 have ion selectivity functions, meanwhile, other PIP2s have not, amino acids of HvPIP2s and OsPIP2s were compared to find key amino acid. Then, artificial mutations were generated to check ion transport activity.

4.1. Materials and methods

4.1.1. Amino acid substitution

The amino acid replacement of HvPIP2;8 and OsPIP2;4 were carried out according to Multi Site-Directed Mutagenesis kit (Zheng et al., (2004) using a pair of primers as shown in Table 4.1.

Table 4.1. Gene-specific primer pairs used in the amino acid substitution

Gene name	Forward primer (5′-3′)	Reverse primer (5′-3′)
HvPIP2;8 A147G	ATCTGCGGCGCGGGGCTG GTGAGAGCC	GGCTCTCACCAGCCCCGCGCC GCAGAT
HvPIP2;8 F283K	AACAGCGCCATCAAGCGG TCCAACTAC	GTAGTTGGACCGCTTGATGGC GCTGTT
OsPIP2;4 T227M	CCGATCACCGGCATGGGC ATCAACCCG	CGGGTTGATGCCCATGCCGGT GATCGG
OsPIP2;4 A143G	ATCTGCGGCGTCGGGCTC GTCAAGGGG	CCCCTTGACGAGCCCGACGCC GCAGAT
OsPIP2;4 G278K	GCCAGTGCAAGGAAGTAC GGCTCCTTC	GAAGGAGCCGTACTTCCTTGC ACTGGC

Mutated nucleotides are underlined.

The 20 µl PCR reaction was carried out with 35 ng templates, 0.6 µl primer pair, 2 mM dNTPs, 25 mM $MgSO_4$, 2 µl 10 x PCR buffer, 0.4 µl enzyme KOD-plus-neo. The extension reaction was initiated by pre-heating the reaction mixture to 94ºC for 2 min; 18 cycles of 98ºC

for 10 s, T_m for 30 s and 68°C for 2 min, followed by incubation at 68°C for 3 min. The PCR-amplification products were evaluated by agarose gel electrophoresis. After PCR add 1 µl restriction enzyme *DpnI* (Takara) to each tube and digest templates at 37°C for 1 hour. 5 µl of digested PCR products is used for transformation to *E.coli*. The full length DNA sequence of HvPIP2;8 artificial mutants A147G or F283K and OsPIP2;4 mutants T227M, A143G or G278K in pXβG-ev1 plasmids were confirmed by Sanger's sequencing.

4.1.2. Water transport activity assay in *X. laevis* oocytes

The coding regions of *HvPIP2;8; HvPIP2;8 A147G; HvPIP2;8 F283K* and *OsPIP2;4; OsPIP2;4 T227M; OsPIP2;4 A143G; OsPIP2;4 G278K* cDNA were sub-cloned into the pXβG-ev1 expression vector. The constructs were linearlized with *PstI*, and capped cRNA were synthesized using the mMESSAGE mMACHINE T3 *in vitro* transcription kit (Ambion). Oocytes were isolated from adult female *Xenopus laevis* frogs and maintained as described previously (in Chapter 2). Oocytes were injected with 50 nL of a cRNA solution containing 10 ng of each mutants as described above. As a negative control, nuclease-free water-injected oocytes were used. The osmotic water permeability coefficient of oocytes was measured according to the procedures as described in part 2.2.6 of Chapter 2.

4.1.3. Statistical analysis

Statistical analysis was conducted using SPSS statistics software (version 20). Analysis of variance was identified by one-way ANOVA followed by the least significant difference (LSD) test at the *0.05* level; or one-way ANOVA followed by Duncan's multiple comparisons test.

4.2. Results

4.2.1. Identification Phenylalanine (Phe283) in C-terminal tail as an essential amino acid for ion transport activity of HvPIP2;8

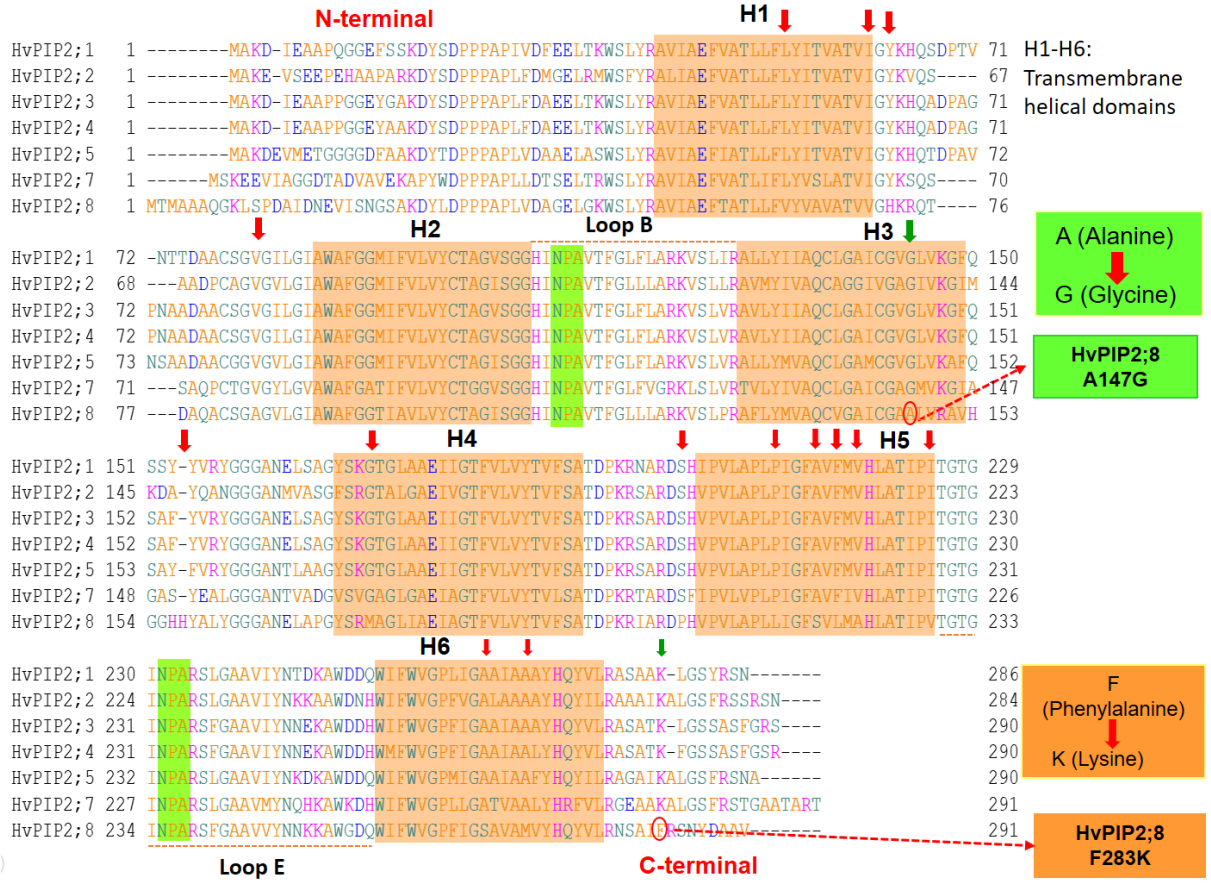

Figure 4.1. Comparison of HvPIP2;8 with other HvPIP2s amino acid sequences. Sequences alignment of the putative transmembrane (H1 to H6) and selectivity pore-forming regions are underlined with dotted blue lines (Loop B and loop E), NPA residues are in the green box, amino acids different position between OsPIP2;4 and others PIP2 is pointed with the red arrow (not yet generated mutants) and green arrow (generated mutants); N- and C-terminal tails are noted with red letter.

Sixteen amino acid of HvPIP2;8 are shown to be completely different with other HvPIP2s as shown in Figure 4.1. HvPIP2;8 has unique alanine (A147) instead of glycine (G) amino acid of other HvPIP2s in transmembrane 3 (H3). On the other hand, phenylalanine (F283) instead of a lysine (K) of other PIP2s in the C-terminal region. Therefore, I hypothesized that one of these amino acid results in unique ion selectivity. To test this hypothesis, I generated HvPIP2;8 A147G and HvPIP2;8 F283K that replaced alanine (A) at position 147 with glycine (G), phenylalanine (F) at position 283 with lysine (K), respectively, and characterized its electrophysiological properties by TEVC.

The currents of HvPIP2;8 A147G or HvPIP2;8 F283K-injected oocytes were examined in the in 86.4 mM NaCl; 9.6 mM KCl and 86.4 mM KCl; 9.6 mM NaCl in low external free Ca^{2+} (Figure 4.2A, B).

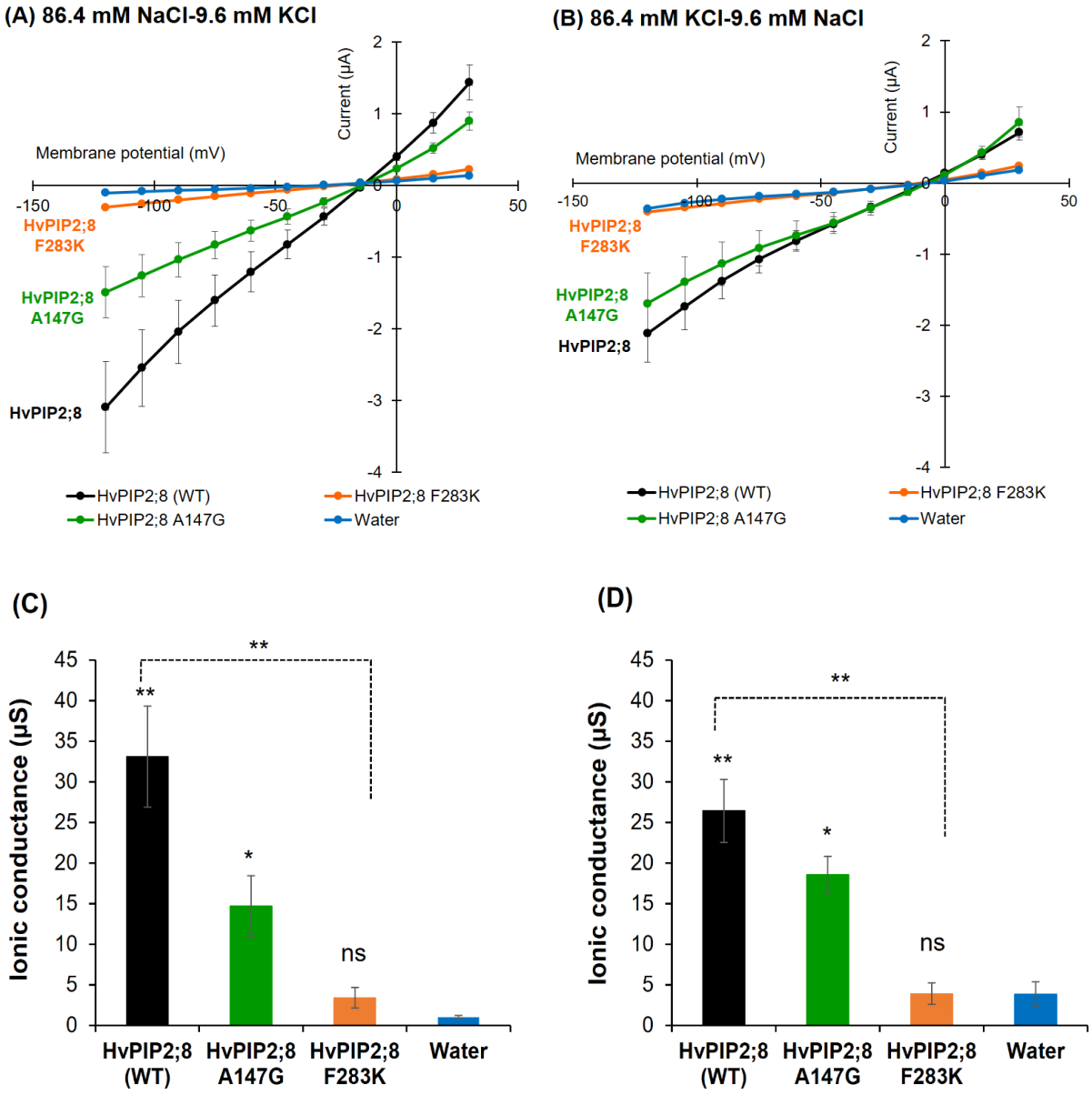

Figure 4.2. Ion permeability of HvPIP2;8 mutants. Current-voltage relationships of *X. leavis* oocytes expressing each mutant in the presence of 86.4 mM NaCl; 9.6 mM KCl **(A)** 86.4 mM KCl; 9.6 mM NaCl with 30 µM Ca^{2+} contained a background (1.8 mM $MgCl_2$, 1.8 mM $CaCl_2$, 1.8 mM EGTA, 10mM HEPES, pH 7.5 with Tris) (**B**). **(C, D)** The ionic conductances were calculated from V = −75 mV to −120 mV for data shown in A and B, respectively. The free Ca^{2+} concentrations are given in Methods. A step pulse protocol of −120 mV to +30 mV with a 15 mV increment was applied on every oocyte. Steady-state current-voltage curves of *X.laevis* oocytes injected with 10 ng of cRNA per oocyte from the same batch. Data are means ± SE, n = 7 to 8 (for A and B) with three independent experiments performed on different oocytes batch. The Welch's-t test was used for the statistical analysis: ** $P < 0.01$, * $P < 0.05$, ns: not significant *vs.* water (control).

Smaller currents were observed in HvPIP2;8 A147G when compared with HvPIP2;8 (WT) in both solutions. Since glycine amino acid at transmembrane 3 interacted with other residues, A147 could be related to change in the pore dimensions. Furthermore, HvPIP2;8 A147G mutant was also highly permeable more Na^+ than K^+ as same tendency with HvPIP2;8 (WT). No current was observed in HvPIP2;8 F283K in contrast to wild type HvPIP2;8. The inward conductance of HvPIP2;8 F283K showed significant different from HvPIP2;8 (WT) but no significantly difference was observed between HvPIP2;8 F283K and water (control) (Figure 4.2C, D). Regarding to water transport function both HvPIP2;8 mutants, HvPIP2;8 A147G and HvPIP2;8 F283K showed water permeable with no significant different from HvPIP2;8 (WT) (Figure 4.3). This suggests that phenylalanine (F283) has a crucial role in the ion permeability or the activation mechanism of HvPIP2;8 and substitution of lysine (K) at the same position in C-terminal blocked ion conductance. On the other hand, HvPIP2;8 F283K showed water permeability, suggesting that the mechanism of ion and water transport are different in the HvPIP2;8.

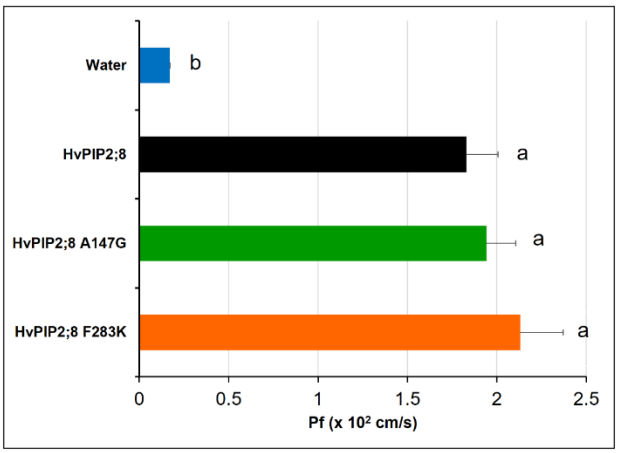

Figure 4.3. Water permeability of HvPIP2;8 mutants

Data are means ± SE, n = 10 with three independent experiments performed on different oocytes batch. Significant differences ($P < 0.05$) are indicated by different letters using one-way ANOVA with Duncan's multiple comparisons test.

4.2.2. Identification Glycine (Gly278) in C-terminal tail as an essential amino acid for ion transport activity of OsPIP2;4

OsPIP2;4 and OsPIP2;5 have different three unique amino acids among conserved domains of OsPIP2s (red and green arrows as shown in Figure 4.4). Mutants OsPIP2;4 A143G (Transmembrane 3); OsPIP2;4 G278K (C-terminal) were generated: alanine (A) at position 143 was replaced by glycine (G), glycine (G) at position 278 was replaced by lysine (K), respectively. Besides, a previous study showed that HvPIP2;4 T229M had not water/ion

transport activities (unpublished data). Therefore, I also created OsPIP2;4 T227M (loop E) mutant with replaced threonine (T) at position 227 with methionine (M) and characterized its electrophysiological properties by TEVC (Figure 4.5).

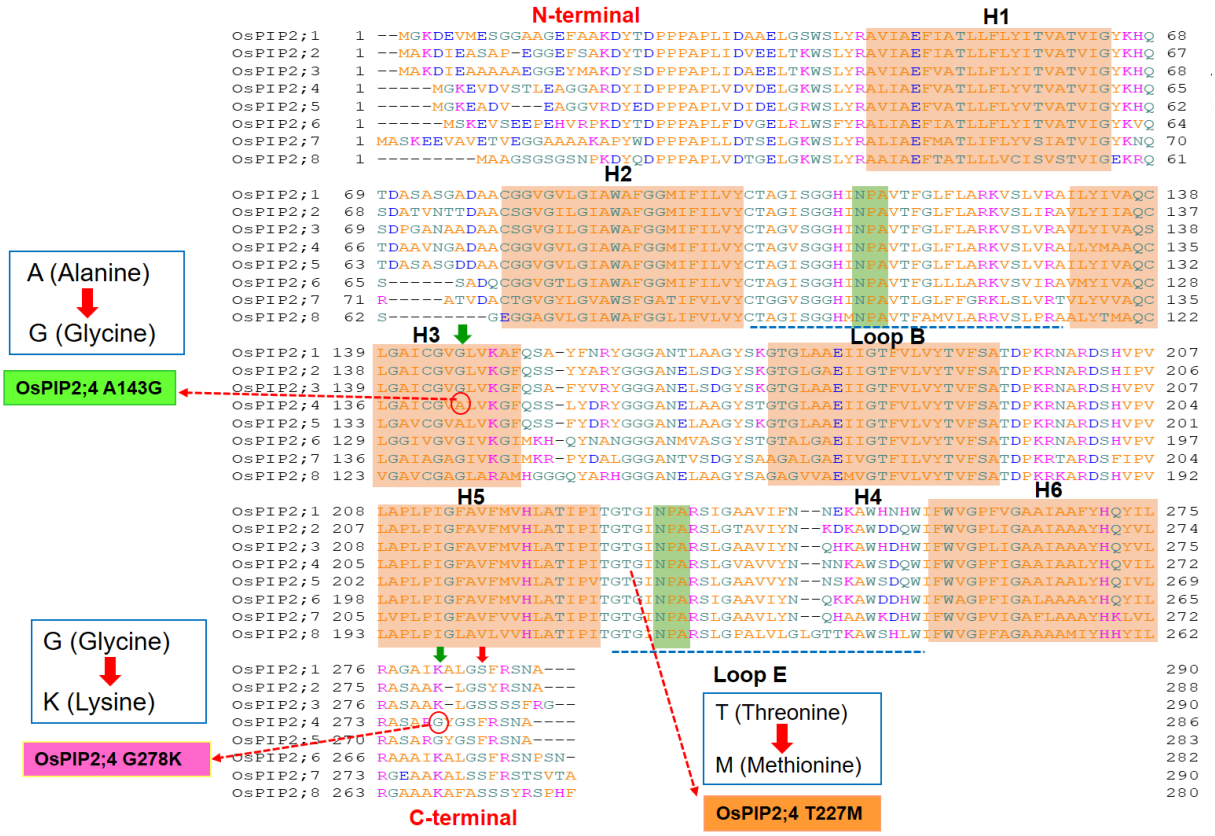

Figure 4.4. Comparison of OsPIP2;4 with other OsPIP2s amino acid sequences. Sequences alignment of the putative transmembrane (H1 to H6) and selectivity pore-forming regions are underlined with dotted blue lines (Loop B and loop E), NPA residues are in the green box, amino acids different position between OsPIP2;4 and others PIP2 is pointed with the red arrow (not yet generated mutants) and green arrow (generated mutants); N- and C-terminal regions are noted with red letter.

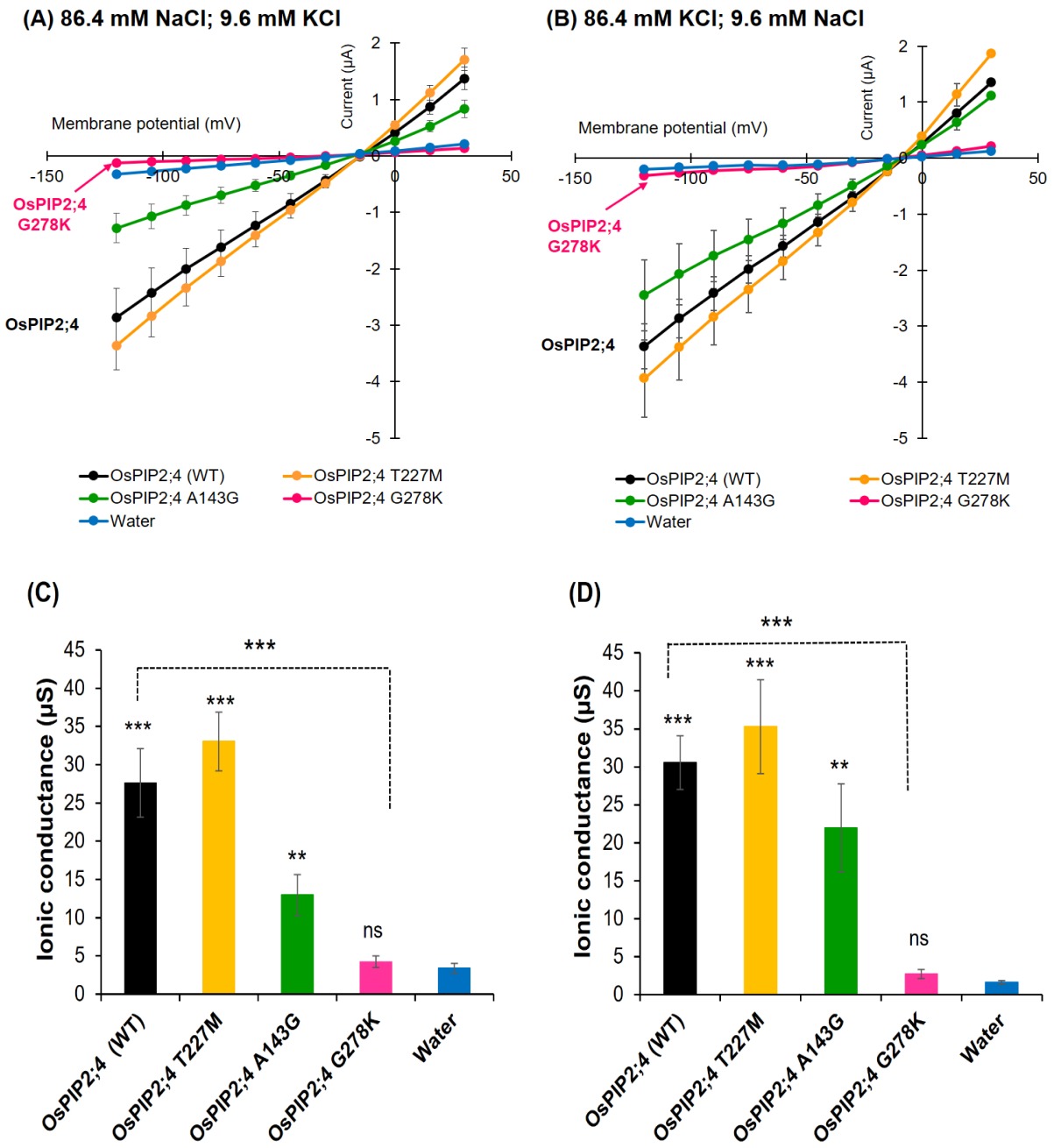

Figure 4.5. Ion permeability of OsPIP2;4 mutants. Current-voltage relationships of *X. leavis* oocytes expressing each mutant in the presence of 86.4 mM NaCl; 9.6 mM KCl **(A)** 86.4 mM KCl; 9.6 mM NaCl (**B**) contained a background (1.8 mM $MgCl_2$, 1.8 mM $CaCl_2$, 1.8 mM EGTA (free Ca^{2+} is calculated as 30 µM (given in 2.2.5 part in Chapter 2)), 10mM HEPES, pH 7.5 with Tris). **(C, D)** The ionic conductances were calculated from V = −75 mV to −120 mV for data shown in A and B, respectively. A step pulse protocol of −120 mV to +30 mV with a 15 mV increment was applied on every oocyte. Steady-state current-voltage curves of *X.laevis* oocytes injected with 10 ng of cRNA per oocyte from the same batch. Data are means ± SE, n = 7 to 8 (for A and B) with three independent experiments performed on different oocytes batch. The Welch's-t test was used for the statistical analysis: *** $P < 0.001$, ** $P < 0.01$, * $P < 0.05$, ns: not significant *vs.* water (control).

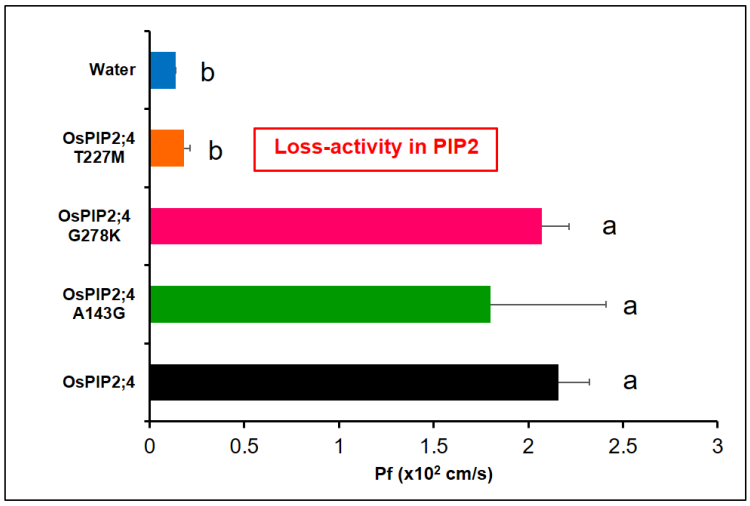

Figure 4.6. Water permeability of OsPIP2;4 mutants

Data are means ± SE, n = 10 with three independent experiments performed on different oocytes batch. Significant differences ($P < 0.05$) are indicated by different letters using one-way ANOVA with Duncan's multiple comparisons test.

As shown in Figures 4.5A and B, OsPIP2;4 A143G showed smaller currents when compared with OsPIP2;4 (WT). Meanwhile, OsPIP2;4 T227M showed larger currents than OsPIP2;4 (WT) in both 86.4 mM NaCl; 9.6 mM KCl and 86.4 mM KCl; 9.6 mM NaCl. Two mutants OsPIP2;4 A143G and OsPIP2;4 T227M were prefer K^+ to Na^+ as same as a tendency with OsPIP2;4 (WT) and was significantly different from water (control). OsPIP2;4 G278K did not show any currents leading to its ionic conductance no significant difference with water-injected control in both solutions (Figure 4.5A, B). Furthermore, the water permeability of mutants was examined by osmosis-based oocyte assays. OsPIP2;4 A147G showed water permeable with no significant difference from wild type OsPIP2;4 (Figure 4.6). The OsPIP2;4 T227M and OsPIP2;4 G278K showed an inverse role between water and ion transport activity. In particular, OsPIP2;4 T227M showed no water permeability as well as water-injected control, meanwhile, this mutant was permeable ion with larger than wild type OsPIP2;4-transporter. In contrast, the mutant OsPIP2;4 G278K showed water permeability with no significantly different from OsPIP2;4 (WT), but its ion transport activity was lost. These results suggest that a glycine (G278) in the C-terminal tail might be an essential amino acid for ion transport function of OsPIP2;4 and lysine (K278) was also key amino acid leading to lose of ion transporting function of OsPIP2;4. Moreover, this evidence reinforces the mechanism of ion and water transport are different in OsPIP2;4.

Table 4.2. Water permeability and ion transport activity of mutants

Mutations	Water permeability	Ion activity	Domain position
HvPIP2;8 (WT)	Yes	Yes	-
HvPIP2;8 A147G	Yes	Yes	Transmembrane 3
HvPIP2;8 F283K	Yes	No	C-terminal
OsPIP2;4 (WT)	Yes	Yes	-
OsPIP2;4 A143G	Yes	Yes	Transmembrane 3
OsPIP2;4 T227M	No	Yes	Loop E
OsPIP2;4 G278K	Yes	No	C-terminal

4.3. Discussion

The gating of aquaporins (the opening and closing pore) can be regulated by multiple factors. Some previous studies have reported for gating mechanism mainly focused on water transport function of human aquaporin 5 (HsAQP5) (Janosi et al., 2013); in plant *Spinacia oleracea* SoPIP2;1 (To¨rnroth-Horsefield et al., 2006); *Beta vulgaris* BvPIP2;2 (Fortuna et al., 2019); yeast AQY1 and *E. coli* AQPZ (Janosi et al., 2013). In-plant SoPIP2;1 the pore is closed by loop D, in yeast AQY1 by the longer N-terminal (Tyr31 is an inserted amino acid in AQY1 as compared to the sequence of HsAQP5), and in HsAQP5 by the coil connecting the second transmembrane helix to the first half helix. However, the evidence focus on the gating mechanism for ion transport is limited.

The major aim of this work is characterizing the structure of HvPIP2;8 and OsPIP2;4. This study clarified that HvPIP2;8 and OsPIP2;4 showed the largest ion dependent current, but other PIP2s did not reveal the current. My results showed that HvPIP2;8 F283K and OsPIP2;4 G278K were lost of ion transport function compared with wild type HvPIP2;8 and OsPIP2;4, respectively (Figure 4.2 and 4.5; Table 4.2). These results suggest that phenylalanine (F283) of HvPIP2;8 and a glycine (G278) of OsPIP2;4 in C-terminal region might be an essential amino acid for ions transport function of HvPIP2;8 and OsPIP2;4, respectively. Lysine (K283 of HvPIP2;8 and K278 of OsPIP2;4) were also the key amino acid leading to loss of ion transport function for both aquaporins. In contrast, both mutants showed water permeability with no significant difference from wild type (Figure 4.3 and 4.6), suggesting that the water and ion are

transported via different pathway. By comparison amino acid sequences of HvPIP2;8 and OsPIP2;4, we found phenylalanine (F283) of HvPIP2;8 and glycine (G278) of OsPIP2;4 at the same position in the C-terminal region. Moreover, lysine (K) is an amino acid which conserved in all other HvPIP2s and OsPIP2s. These results suggest the hypothesis that common ionic pathway in both HvPIP2;8 and OsPIP2;4. Mori et al., (2018) reported that HvCNGC2-3 has an alanine instead of a glycine amino acid different among other amino acid sequences of the putative pore-forming region of the group-II CNGCs, and HvCNGC2-3A394G showed no current both in the presence and absence of 8Br-cAMP which is required to active the channel protein. In addition, Kourghi et al., (2018) have also been reported that substitution of residues in loop D with proline showed effects on ion conductance amplitude that varied with position, suggesting that the structural conformation of loop D is important for gating of human AQP1 channel.

I focus on why do change of phenylalanine (F283) to lysine (K) in HvPIP2;8 and replace glycine (G278) to lysine (K) in OsPIP2;4 at the C-terminal domain (CTD) led to loss of ion transport function. Crystal structure analyses have provided views of the transmembrane (TM) regions of tetrameric prokaryotic sodium channels, but not of the CTD, because this domain is dynamically disordered. To explain, I speculate that two possible reasons: (1) Lysine belongs to basic amino acid (positive charged), it might be coiled-coil domain couples inactivation with channel opening, and is enabled by positive charged residues in the linker region. (2) When change of F283/HvPIP2;8 or G278/OsPIP2;4 to lysine (K) with longer R-chain making a longer C-terminal region, it could make a coil connecting with others C-terminal or connecting with another transmembrane of monomers leading to the cytoplasmic end of the channel can closed state completely blocks ion flow through the central or intrasubunit pore.

Bagnéris et al., (2013) have reported that the transmembrane domain is connected by a defined but flexible linker region to a C-terminal consisting of a stable four-helix coiled-coil bundle, with one helix contributed by each of the monomers in the tetramer, the length of the coiled-coil regions of the different prokaryotic channels may account for the different kinetics of their activation and inactivation processes. The linker and the coiled-coil regions have different roles in the processes of inactivation channel gating and maintenance of tetramer integrity. This type of structure could enable the opening and closing of the bottom of the pore during gating without disrupting the quaternary structure of the four-helix bundle, a process that would otherwise be energetically very costly. The movement of the transmembrane 6 (H6) helices is also accompanied by a slight alteration in the orientation of the amino-acid terminal of the transmembrane 5 (H5) helices, producing a minor displacement where they would meet

the H4–H5 linker to the voltage sensor domain. Therefore, I think the replacement of phenylalanine F283 in HvPIP2;8 or glycine G278 in OsPIP2;4 by lysine (K) might be change interaction with the amino-acid residues of the transmembrane 6 (H6) because of nearest to C-terminal region leading to change the movement of H6 and others transmembrane relative to the pore gating in the cytoplasmic end (CE). Actually, a gating mechanism that completely blocks the water flux at the cytoplasmic end (CE) of the pore has been reported for plant and yeast aquaporins (Chaumont et al., 2005; Fischer, et al., 2009; Tornroth-Horsefield et al., 2010). The protein-protein coupling might play a crucial role in regulating the water flow through the channels, especially at the CE gating site. The closed state of the CE completely blocks the water passage by a gating mechanism characterized by the translation of the key residue His67 inside the pore (Janosi et al., 2013), and also possible for ion transport mechanism. The closing mechanism is usually caused by displacement of an aquaporin-specific key residue (Tornroth-Horsefield et al., 2010).

While I am unable to know exactly the ion transporting mechanism of HvPIP2;8 and OsPIP2;4 until now, I could use *in silico* studies to reveal their underlying protein structure-function relationship. The significant increase in computer power currently allows us to study water and ion channels using molecular dynamics (MD) simulations, I hope that experimental methods will be able to confirm my hypothesis. However, as shown in Figure 4.1 and 4.3, I found 16 positions of HvPIP2;8 are different from other HvPIP2s and 3 positions of OsPIP2;4 are different from other OsPIP2s, still 14 positions for HvPIP2;8 and 1 position for OsPIP2;4 have not yet examined. As an initial clarity ion transport mechanism of HvPIP2;8 and OsPIP2;4, I have found phenylalanine F283 of HvPIP2;8 and glycine G278 of OsPIP2;4 in C-terminal tail are an essential amino acid for ion transporting function, and lysine (K) is a key residue leading to loss ion transporting activity in both HvPIP2;8 and OsPIP2;4 but not water permeability.

References

Bagnéris, C., DeCaen P.G., Hall B.A, Naylor C.E, Clapham D.E., Kay C.W.M., Wallace B.A. **(2013)**. Role of the C-terminal domain in the structure and function of tetrameric sodium channels. *Nature Communications*, 4. doi: 10.1038/ncomms3465.

Chaumont F., Moshelion M., Daniels M.J. **(2005)**. Regulation of plant aquaporin activity. *Biology of the Cell*, 97: 749–764.

Fischer G., Kosinska-Eriksson U., Aponte-Santamaria C., Palmgren M., Geijer C. **(2009).** Crystal structure of a yeast aquaporin at 1.15 angstrom reveals a novel gating mechanism. *Plos Biology*, 7: e1000130

Fortuna C. A., Zerbetto De Palma G., Aliperti Car, L., Armentia L., Vitali V., Zeida A., Estrin D.A., Alleva K. **(2019)**. Gating in plant plasma membrane aquaporins: the involvement of leucine in the formation of a pore constriction in the closed state. *FEBS Journal*, 286 (17), 3473–3487. doi: 10.1111/febs.14922.

Mori I.C., Nobukiyo Y., Nakahara Y., Shibasaka M., Furuichi T., Katsuhara M. **(2018)**. A cyclic nucleotide-gated channel, HvCNGC2-3, is activated by the co-presence of Na^+ and K^+ and permeable to Na^+ and K^+ non-selectively, *Plants*, 7, 61; doi:10.3390/plants7030061.

Janosi L., Ceccarelli M. **(2013)**. The gating mechanism of the human aquaporin 5 revealed by molecular dynamics simulation. *PLoS ONE*, 8 (4). doi: 10.1371/journal.pone.0059897.

Kourghi M., De Ieso M.L., Nourmohammadi S., Pei J.V, Yool A.J. **(2018)**. Identification of Loop D domain amino acids in the human aquaporin-1 channel involved in activation of the ionic conductance and inhibition by AqB011. *Front. Chem.,* 6:142. doi: 10.3389/fchem.2018.00142.

To¨rnroth-Horsefield S., Wang Y., Hedfalk K., Johanson U., Karlsson M., Tajkhorshid E., Neutze R., Kjellbom P. **(2006)**. Structural mechanism of plant aquaporin gating. *Nature*. Vol 439. doi:10.1038/nature04316

Tornroth-Horsefield S., Hedfalk K., Fischer G., Lindkvist-Petersson K., Neutze R. **(2010)**. Structural insights into eukaryotic aquaporin regulation. *Febs Letters*, 584, 2580–2588.

Zheng L., Baumann U., Reymond J.L. **(2004)**. An efficient one-step site-directed and site-saturation mutagenesis protocol. *Nucleic Acids Res.,* Vol. 32, No. 14.

CHAPTER 5

General discussion

Ionic stress is one of the most important components of salinity and caused by excess Na^+ accumulation, especially in the aerial parts of plants. The transport mechanisms involve Na^+ and/or K^+ transporters/channels as well as non-selective cation channels (NSCC). Uptake of Na^+ at the root-soil boundary is believed to occur mainly through NSCC, including the cyclic nucleotide-gated channels (CNGCs) and glutamate receptors (GLRs), as well as through some high affinity K^+ transporters (HKTs) and K^+ channels including the Arabidopsis K^+ transporter (AKT1), and the high-affinity K^+ uptake transporter (HAK) (Tester and Davenport, 2003; Hanin et al., 2016, Mori et al., 2018). It is reported that aquaporins are also implicated in Na^+ uptake in plants (Byrt et al., 2017). In this study, twelve barley PIPs (5 PIP1 and 7 PIP2) and eleven rice PIPs (3 PIP1 and 8 PIP2) examined by the heterogenous expression system in *Xenopus laevis* oocytes using two electrode voltage clamp (TEVC) experiment. Then, HvPIP2;8 and OsPIP2;4 were first identified as ion-conducting aquaporin in barley and rice with permeability to Na^+ and K^+, but the ion transport activities were inhibited by external free Ca^{2+} condition with different levels in both aquaporins. Through detailed analyses, two PIP aquaporins display as NSCC when expressed in *X. laevis* oocytes and localized at the plasma membrane.

5.1. Different roles of HvPIP2;8 and OsPIP2;4 in ion transport activity

HvPIP2;8 and OsPIP2;4 have dual function as both water and cation channel, where the channel characteristics can be influenced by K^+ and divalent cation, and protein interactions. I observed that *X. laevis* oocytes expressing HvPIP2;8 and OsPIP2;4 displayed significant ionic conductance relative to the controls and relative to the oocytes expressing any of other six HvPIP2 and five HvPIP1; eight OsPIP2 and three OsPIP1 proteins, respectively (Figure 2.2 and Figure 3.3). One of interesting feature of HvPIP2;8 and OsPIP2;4 are inhibited by some divalent cations (Ca^{2+}, Ba^{2+}, and Cd^{2+}). But, the cation conductance of OsPIP2;4 proved to have a higher inhibitory constant of external Ca^{2+} (IC_{50} = 92 µM) compared to that of HvPIP2;8 (IC_{50} = 401 µM) similar to AtPIP2;2 and AtPIP2;1, respectively. External calcium blocks the inward currents of both HvPIP2;8 and OsPIP2;4, but, an increase the Mg^{2+} concentrations in the presence of Ca^{2+} seemed to ameliorate the inhibitory effect of the Ca^{2+}. It might be a competitive interaction between Ca^{2+} and Mg^{2+} at the same binding site. There was also an interaction between Ca^{2+} inhibition and Ba^{2+} relief of block for AtPIP2;1 and AtPIP2;2 (Kourghi et al., 2017) that is similar to the interaction seen here for Ca^{2+} and Mg^{2+} in case of HvPIP2;8 and OsPIP2;4.

Byrt et al., (2017), McGaughey et al., (2018) and Muns et al., (2020) have proposed that AtPIP2;1 and AtPIP2;2 could be molecular candidates for the elusive non-selective cation channels (NSCC) observed *in planta*. AtPIP2;1 facilitated the transport of K^+ transport *in vivo* and this result supports the NSCC hypothesis. On the other hand, the NSCC observed by Demidchik et al., (2002) had greater K^+ conductance relative to Na^+ conductance (with a selectivity ratio of 1.49:1) similar to that observed for K^+ relative to Na^+ conductance for AtPIP2;1 expressed in *X.laevis* oocytes (Qiu et al., 2020). HvPIP2;8 and OsPIP2;4 in this study also revealed as a NSCC when expressed in *X.laevis* oocytes. HvPIP2;8 and OsPIP2;4 permeated both Na^+ and K^+ but ion selectivity characteristics were opposite. HvPIP2;8 prefers Na^+ to K^+ ($Na^+ > K^+$) and the Na^+ permeability of HvPIP2;8 was inhibited in the presence of external K^+ (Figure 2.4). Indeed, there was also an interaction between Na^+ and K^+ for HvPIP2;8 where a mix of the two ions at a ratio of 1:1 significantly inhibited the current. Meanwhile, OsPIP2;4 prefers K^+ to Na^+ ($K^+ > Na^+$), and a mix of the two ions at a ratio of 1:1 enhanced the current compared with Na^+ alone (Figure 3.7C, D). Such properties were observed in some transporters expressed in *X. laevis* oocytes. For example, *Triticum aestivum* TaHKT1;5-D and *Triticum monococcum* TmHKT1;5-A encode dual affinity Na^+-transporters and their dual affinity Na^+ transport was inhibited by raising the external K^+ concentration (Byrt et al., 2008; Xu et al., 2018) or HvHKT1;5 was permeable to Na^+ and its Na^+ transport activity was also inhibited by external K^+ (Huang et al., 2020); whereas, for OsHKT2;2, extracellular K^+ stimulated the OsHKT2;2-mediated Na^+ transport (Yao et al., 2010). Additional research is needed to establish the model how different monovalent ions are recognized by ion channel aquaporins towards understanding the interaction between K^+ and Na^+ in HvPIP2;8 and OsPIP2;4 channel activity. Additionally, K^+ or Na^+ uptake in roots was facilitated by an NSCC mechanism sensitive to divalent cations, that could be contributed to by ion channel aquaporins sensitive to divalent cations (Kourghi et al., 2017).

On the other hand, other monovalent cations (Rb^+, Cs^+, Li^+) did not elicit currents in case of HvPIP2;8, meanwhile, OsPIP2;4 showed small currents with Rb^+ and Cs^+, but not Li^+ same as HvPIP2;8. According Tyerman et al., 2021, the feature of HvPIP2;8 is different from AtPIP2;1, that shows significant currents with Rb^+, Cs^+, and Li^+ (J.Qiu, unpublished data) and also has opposite relative selectivity between Na^+ and K^+ (Qiu et al., 2020). In contrast, OsPIP2;4 prefers K^+ to Na^+ as AtPIP2;1.

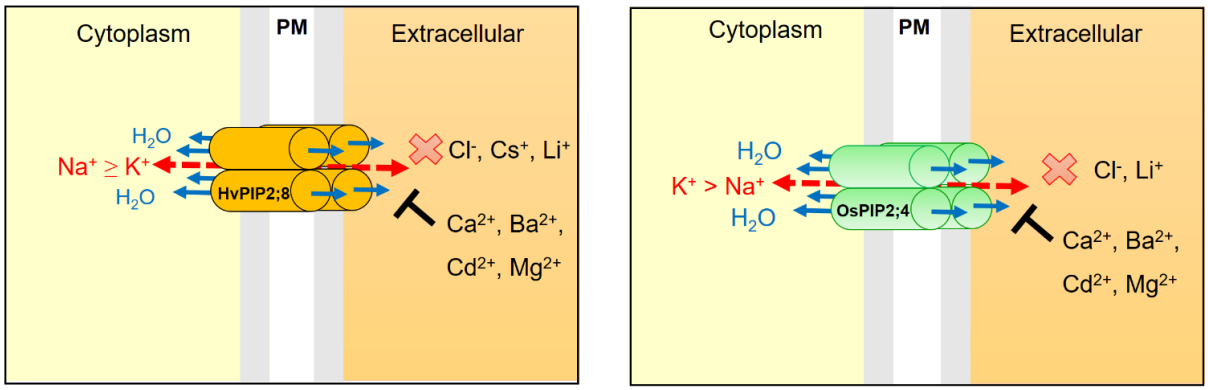

Figure 5.1. The functions of HvPIP2;8 and OsPIP2;4 (PM: plasma membrane)

Moreover, *HvPIP2;8* transcript increased in barley shoot tissues following salt treatments in a salt-tolerant cultivar Haruna-Nijo and K305, but not in salt-sensitive I743 (Figure 2.9). There is potential for HvPIP2;8 to be involved in barley salt-stress responses, and HvPIP2;8 could facilitate both water and Na^+/K^+ transport activity. The implications of Ca^{2+} sensitivity could be different according to what kind of physiological role HvPIP2;8 has *in planta*: if the HvPIP2;8 mediated the Na^+ influx into the cytosol of mesophyll cells in leaves, then a Ca^{2+}-dependent inhibitory effect might be a positive feature as it could prevent excess Na^+ influx.

In contrast, *OsPIP2;4* was predominantly expressed in root, especially in roots tips rather than stem, leaf sheath and leaf blade and other root parts. In addition, *OsPIP2;4* was mainly localized at epidermis and exodermis of root tip (Figure 3.12), suggesting that *OsPIP2;4* may play an important role in transporting water and ion from the soil into plants, then Na^+ moves radially to the stele, and is loaded into the xylem and the implications of Ca^{2+} sensitivity could be happened at the root-soil boundary.

The feature of HvPIP2;8 and OsPIP2;4-ion transporting physiologically suggests potential roles for PIP2s in nutrient acquisition under salt stress or normal condition and their also worthy of testing *in planta.*

5.2. Relationship between water and ion transport in homo- and hetero-tetramer

Co-expression of HvPIP2;8 and HvPIP1 proteins reduced the HvPIP2;8-induced ionic conductance with differences between the PIP1 isoforms; HvPIP1;3 and HvPIP1;4 co-expressed with HvPIP2;8 showed ionic conductance (Figure 2.7D). Shibasaka et al., (2012) and present result showed that co-expression of HvPIP2;8 with HvPIP1;2 in *X. laevis* oocytes did not enhance the water transport activity compared to that of the expression of HvPIP2;8 alone. In contrast, co-expression of HvPIP1;2 with other HvPIP2s (2;1 to 2;5) increased the water permeability coefficient (Horie et al., 2011). This indicates that heteromerization of each HvPIP2

and HvPIP1;2 may modulate water channel activity differently. Similarly, in rice PIPs, co-expression of OsPIP2;4 with OsPIP1s (OsPIP1;1, OsPIP1;2, OsPIP1;3), significantly decreased the ionic conductance relative to single of OsPIP2;4 and still remaining significantly higher conductance when compared with water injected control, meanwhile, OsPIP1s could not ions transport activity (Figure 3.10). On the other hand, co-expression of HvPIP2;8/HvPIP1s and OsPIP2;4/OsPIP1s did not enhanced water permeability (Figure 2.8 and Figure 3.11). Co-expression of OsPIP2;1 with OsPIP1;1 and OsPIP2;2 with OsPIP1;3 significantly increased its water permeability, suggesting that the heteromerization of OsPIP1;1/OsPIP2;1, OsPIP1;3/OsPIP2;2 and re-localization might be required to modulate their water channel activity (Liu et al., 2013; Liu et al., 2020). The intracellular retention of PIP1s is either caused by missing plasma membrane targeting signals or by existing ER retention motifs, whereas the interaction and hetero-tetramer of certain pairs of PIP1s and PIP2s can significantly enhance water permeability as co-expression OsPIP1;1/OsPIP2;1 and OsPIP1;3/OsPIP2;2 were mentioned above (Bienert et al., 2018). A previous study revealed that AtPIP2;1 was co-expressed with AtPIP1;2 the water permeability was greater than when AtPIP2;1 or AtPIP1;2 was expressed alone. However, the ionic conductance of AtPIP2;1 could be suppressed to the level of the water-injected control when AtPIP2;1 was co-expressed with AtPIP1;2, indicating that the ionic conductance was not associated with higher water permeability (Byrt et al., 2017) as well as HvPIP2;8 and OsPIP2;4 in this study.

How are water and ion transports in PIP1:PIP2 hetero-tetramer (when co-expressed in *X.laevis* oocytes) regulated different?. It is hypothesized that monomer pore and central pore are involved in water and ion transport, respectively.

From early study, the molecular basis of water permeation indicates that P_f values are dependent on the number of hydrogen bonds (H-bonds) that water molecules form with pore-lining residues (Horner et al., 2015). The pore radius increases changing the angle of the conical shape of the cytoplasmic entrance (Tong et al., 2016), where H-bond forming glycine residues are located (Tani et al., 2009). Horner et al., (2015) reported that the number of H-bonds between water molecules and pore-lining residues determines the permeability of the monomeric water pathway (P_f). In addition, the charge effect at the pore entrance can account for small P_f changes, constituting a fine-tuning over the hundred-fold change of P_f that the number of H-bond forming pore-lining residues can account for (Horner et al., 2018). While negative charges at the pore entrance or exit do not affect P_f, positive charges increase P_f, possibly because positively charged residues are weakly hydrated in comparison to negatively charged residues (Horner et al., 2018). In contrast, the mechanism of proton exclusion was

predicted by an electrostatic barrier centered on the fingerprint NPA motif, and not by the interruption of the H-bonded water chain (De Groot et al., 2003). Further studies using AQP1-mutants expanded this conception, enhancing the idea that the NPA and the Ar/R constriction regions are two concerted cation filters (Wu et al., 2009). In particular, the asparagine residues of the NPA region are postulated to repel positive charges by electrostatic interactions (Wree et al., 2011; Rothert et al., 2017). Since the electrostatic profile of AQP monomers is key in selectivity (Oliva et al., 2010), then, the translocation of positive charged ions through AQP1 monomers should be restricted (Wu et al., 2009).

A simple gating model is proposed in Figure 5.2 by Tyerman et al., (2021) to account for the inverse relationship observed between ion and water conductance in AtPIP2;1. It is based on the open and closed structures of SoPIP2;1 and the assumption that each intrasubunit (monomer) water pore gates independently. It is also possible that cooperativity between the gating of each intrasubunit/ subunit pore will affect the central pore in homo-tetramer/ hetero-tetramer.

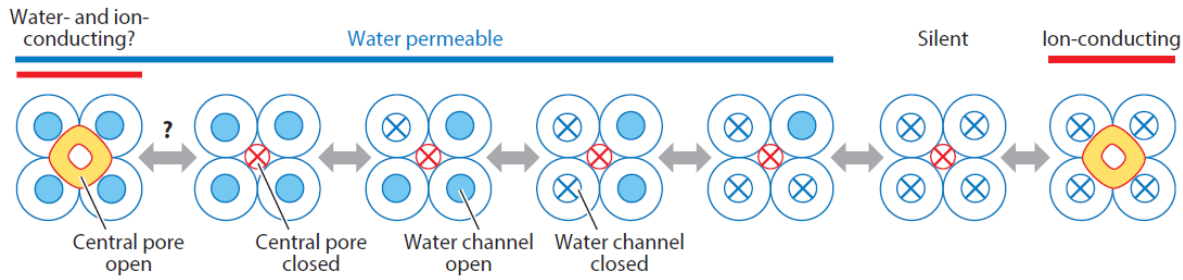

Figure 5.2. Possible transitions in gating between water-conducting monomers to the ion-conducting central pore (Tyerman et al., 2021)

The movement and half turn of transmembrane domain 5 (TM5) during the gating of the intrasubunit pore of SoPIP2;1 is expected to alter the central pore diameter in some regions and to expose polar side chains to be pore lumen, which is conducive of ion conductance. Also, the movement of transmembrane domain 1 (TM1) of SoPIP2;1 may also affect the orientation of loop A (LA) that caps the external entrance to the central pore. In addition, constrictions in the central pore are different between AQP1, SoPIP2;1, AtPIP2;4, and AtPIP2;1 (based on SWISS-MODEL homology model P43286 using AtPIP2;4 as a template). PIPs have additional constriction at the extracellular side formed by the four Cys residues of loop A, not present in AQP1, that form two disulfide link between monomers (Bienert et al., 2012). Moreover, four Cys residues of loop A form the cap over the entrance of the central pore. Interestingly, corresponding four Cys residues are present in HvPIP2;8 and OsPIP2;4. In this study, when co-expressed with HvPIP1s/HvPIP2;8 or OsPIP1s/OsPIP2;4 in *X.laevis* oocytes, the ionic

conductances of HvPIP2;8 or OsPIP2;4 were greatly reduced. From such result, central pore of hetero-tetramer might close by interaction among monomers. Each monomer could be affected by the interactions with its neighbors, ion transport could cooperativelly decrease. Similarly, AtPIP2;1-AtPIP1;2 hetero-tetramers blunt the ion transport but not the water permeability (Byrt et al., 2017). It is discussed that the central tetrameric pore is the favored pathway for ion conductance through human AQP1 (Yool et al., 2002). AQP1 ion channels are proposed to conduct solutes and water through pharmacologically distinct pathways. That is water transport mediated through the monomer pores, and ion transport is mediated by the central pore of the tetramer following activation by intracellular cGMP (Kourghi et al., 2018). However, the molecular basis of ion permeation and the role of the central pore have not been well investigated.

Refferences

Bellati J., Alleva K., Soto G., Vitali V., Jozefkowicz C., Amodeo, G. **(2010)**. Intracellular pH sensing is altered by plasma membrane PIP aquaporin co-expression. *Plant Mol. Biol.*, 74, 105–118.

Bienert G.P., Cavez D., Besserer A., Berny M.C., Gilis D. **(2012)**. A conserved cysteine residue is involved in disulfide bond formation between plant plasma membrane aquaporin monomers. *Biochem. J.* 445:101–111.

Bienert M.D., Diehn T.A., Richet N., Chaumont F., Bienert G.P. **(2018)**. Heterotetramerization of plant PIP1 and PIP2 aquaporins is an evolutionary ancient feature to guide pip1 plasma membrane localization and function. *Front. Plant Sci.*, *9*, 15.

Byrt C.S. **(2008)**. Genes for sodium exclusion in wheat. Ph.D. Thesis, University of Adelaide, Adelaide, Australia. Available online: https://digital.library.adelaide.edu.au/dspace/handle/2440/56208 (accessed on).

Byrt C.S., Zhao M., Kourghi M., Bose J., Henderson S.W., Qiu J., Tyerman S. **(2017)**. Non-selective cation channel activity of aquaporin AtPIP2;1 regulated by Ca^{2+} and pH. *Plant Cell Environ.*, *40*, 802–815.

De Groot B.L., Frigato T., Helms V., Grubmüller H. **(2003)**. The mechanism of proton exclusion in the aquaporin-1water channel. *J. Mol. Biol.*, 333, 279–293.

Fetter K., Van Wilder V., Moshelion M., Chaumont F. **(2004)**. Interactions between plasma membrane aquaporins modulate their water channel activity. *Plant Cell*, 16, 215–228.

Hanin M., Ebel C., Ngom M., Laplaze L., Masmoudi K. **(2016)**. New insights on plant salt tolerance mechanisms and their potential use for breeding. *Front. Plant Sci.*, 7, 1787.

Horie T., Kaneko T., Sugimoto G., Sasano S., Panda S.K., Shibasaka M., Katsuhara M. **(2011)**. Mechanisms of water transport mediated by PIP aquaporins and their regulation via phosphorylation events under salinity stress in Barley roots. *Plant Cell Physiol., 52*, 663–675.

Horner A., Zocher F., Preiner J., Ollinger N., Siligan, C., Akimov S.A., Pohl P**. (2015)**. The mobility of single-file water molecules is governed by the number of H-bonds they may form with channel-lining residues. *Sci. Adv.*, 1, e1400083.

Horner A., Siligan C., Cornean A., Pohl P. **(2018)**. Positively charged residues at the channel mouth boost single-file water flow. *Faraday Discuss.*

Huang L., Kuang L., Wu L., Shen Q., Han Y., Jiang L., Wu D., Zhang G. **(2020)**. The HKT transporter HvHKT1;5 negatively regulates salt tolerance, *Plant Physiology*, 182(1), pp. 584–596. doi: 10.1104/pp.19.00882.

Kitchen P., Conner M.T., Bill R.M., Conner A.C. **(2016)**. Structural determinants of oligomerization of the aquaporin-4 channel. *J. Biol. Chem.*, 291, 6858–6871.

Kourghi M., Nourmohammadi S., Pei J.V., Qiu J., McGaughey S., Tyerman S.D., Yool A.J. **(2017)**. Divalent cations regulate the ion conductance properties of diverse classes of aquaporins. *Int. J. Mol. Sci., 18*, 2323.

Kourghi M., De Ieso M.L., Nourmohammadi S., Pei J.V, Yool A.J. **(2018)**. Identification of Loop D domain amino acids in the human aquaporin-1 channel involved in activation of the ionic conductance and inhibition by AqB011. *Front. Chem.,* 6:142. doi: 10.3389/fchem.2018.00142.

Liu C., Fukumoto T., Matsumoto T., Gena P., Frascaria D., Kaneko T., Katsuhara M., Zhong S., Sun X., Zhu Y., Iwasaki I., Ding X., Calamita G., Kitagawa Y. **(2013)**. Aquaporin OsPIP1;1 promotes rice salt resistance and seed germination. *Plant Physiol. and Bio.* Elsevier Masson SAS, 63, pp. 151–158. doi: 10.1016/j.plaphy.2012.11.018.

Liu S.Y., Fukumoto T., Gena P., Feng P., Sun Q., Li Q., Ding X.D. **(2020)**. Ectopic expression of a rice plasma membrane intrinsic protein (OsPIP1,3) promotes plant growth and water uptake. *Plant J*., *102*, 779–796.

Mahdieh M., Mostajeran A. **(2009)**. Abscisic acid regulates root hydraulic conductance via aquaporin expression modulation in Nicotiana tabacum. *J. Plant Physiol.,*166, 1993–2003.

McGaughey S.A., Qiu J., Tyerman S.D., Byrt C.S. **(2018)**. Regulating root aquaporin function in response to changes in salinity. *Ann. Plant Rev. Online, 1*, 381–416.

Möller C., Fotiadis D., Suda K., Engel A., Kessler M., Müller D.J. **(2003)**. Determining molecular forces that stabilize human aquaporin-1. *J. Struct. Biol.,* 142, 369–378.

Mori I.C., Nobukiyo Y., Nakahara Y., Shibasaka M., Furuichi T., Katsuhara M. **(2018)**. A cyclic nucleotide-gated channel, HvCNGC2-3, is activated by the co-presence of Na^+ and K^+ and permeable to Na^+ and K^+ non-selectively. *Plants, 7*, 61.

Munns R., Day D. A., Fricke W., Watt M., Arsova B., Barkla, B. J. **(2020)**. Energy costs of salt tolerance in crop plants. *New Phytologist*, 255, 1072–1090.

Murata K., Mitsuoka K., Hirai T., Walz T., Agre P., Heymann J.B., Engel A., Fujiyoshi Y. **(2000)**. Structural determinants of water permeation through aquaporin-1. *Nature,* 407, 599–605.

Oliva R., Calamita G., Thornton J.M., Pellegrini-Calace M. **(2010)**. Electrostatics of aquaporin and aquaglyceroporin channels correlates with their transport selectivity. *Proc. Natl. Acad. Sci.,* USA, 107, 4135–4140.

Qiu J., McGaughey S.A., Groszmann M., Tyerman S.D., Byrt C.S. **(2020)**. Phosphorylation influences water and ion channel function of AtPIP2,1. *Plant Cell Environ.*, in press.

Rothert M., Rönfeldt D., Beitz E. **(2017)**. Electrostatic attraction of weak monoacid anions increases probability for protonation and passage through aquaporins. *J. Biol. Chem.*, 292, 9358–9364.

Shibasaka M., Sasano S., Utsugi S., Katsuhara M. **(2012)**. Functional characterization of a novel plasma membrane intrinsic protein2 in barley. *Plant Sigal. Behav., 7*, 1648–1652.

Sutka M., Amodeo G., Ozu M. **(2017)**. Plant and animal aquaporins crosstalk: what can be revealed from distinct perspectives. *Biophys. Rev.*, 9, 545–562.

Tani K., Mitsuma T., Hiroaki Y., Kamegawa A., Nishikawa K., Tanimura Y., Fujiyoshi Y. **(2009)**. Mechanism of aquaporin-4's fast and highly selective water conduction and highly selective water conduction and proton exclusion. *J. Mol. Biol.* 398 (4), 694-706.

Temmei Y., Uchida S., Hoshino D., Kanzawa N., Kuwahara M., Sasaki S., Tsuchiya T. **(2005)**. Water channel activities of Mimosa pudica plasma membrane proton exclusion. *J. Mol. Biol.*, 389, 694–706. intrinsic proteins are regulated by direct interaction and phosphorylation. *FEBS Lett.*, 579, 4417–4422.

Tester M., Davenport R. **(2003)**. Na^+ tolerance and Na^+ transport in higher plants. *Ann. Bot.*, 91, 503–527.

Tong J., Wu Z., Briggs M.M., Schulten S., Mc Intosh T.J. **(2016)**. The water permeability and pore entrance structure of Aquaporin-4 depend on lipid bilayer thickness. *Biophys. J.*, 111, 90–99.

Tyerman S.D., McGaughey S.A., Qiu J., Yool A.J., Byrt C.S. **(2021)**. Adaptable and multifunctional ion-conducting aquaporins. *Annu. Rev. Plant Biol.*, 72:703–736

Vandeleur R. K., Mayo G., Shelden M. C., Gilliham M., Kaiser B. N., Tyerman, S. D. **(2009)**. The role of plasma membrane intrinsic protein aquaporins in water transport through roots: diurnal and drought stress responses reveal different strategies between isohydric and anisohydric cultivars of grapevine. *Plant Physiol.*, 149, 445–460.

Wree D., Wu B., Zeuthen T., Beitz E. **(2011)**. Requirement for asparagine in the aquaporin NPA sequence signature motifs for cation exclusion. *FEBS J.*, 278, 740–748.

Wu B., Steinbronn C., Alsterfjord M., Zeuthen, T., Beitz E. **(2009)**. Concerted action of two cation filters in the aquaporin water channel. *EMBO J.*, 28, 2188–2194.

Xu B., Hrmova M., Gilliham M. **(2018)**. High affinity Na^+ transport by wheat HKT1;5 is blocked by K^+. *BioRxiv*. Available online: https://www.biorxiv.org/content/10.1101/280453v2.abstract (accessed on).

Yaneff A., Sigaut L., Marquez M., Alleva K., Pietrasanta L.I., Amodeo G. **(2014)**. Heteromerization of PIP aquaporins affects their intrinsic permeability. *Proc. Natl. Acad. Sci.*, USA, 111, 231–236.

Yao X., Horie T., Xue S., Leung H.Y., Katsuhara M., Brodsky D.E., Wu Y., Schroeder J.I. **(2010)**. Differential sodium and potassium transport selectivities of the rice OsHKT2;1 and OsHKT2;2 transporters in plant cells. *Plant Physiol.*, *152*, 341–355.

Yool A. J., and Weinstein A. M. **(2002)**. New roles for old holes: ion channel function in aquaporin-1. News Physiol. Sci. 17, 68–72. doi: 10.1152/nips.01372.2001

SUMMARY

Because Na^+ is the main contributing factor to salt stress, Na^+ transporters/channels have been the major targets for engineering salt stress tolerance. In the present study, I functionally identified HvPIP2;8 and OsPIP2;4 firstly from barley and rice, Na^+ and K^+-permeable PIP aquaporin under salt stress. Although, its clearly molecular mechanism is still unknown.

Twelve barley PIPs (5 PIP1 and 7 PIP2) and eleven rice PIPs (3 PIP1 and 8 PIP2) were examined by the heterogenous expression system in *X. laevis* oocytes using two electrode voltage clamp (TEVC) experiment. Then, HvPIP2;8 and OsPIP2;4 were first identified as ion-conducting aquaporin in barley and rice with permeability to Na^+ and K^+, but the ion transport activities were inhibited by external free Ca^{2+} condition with different levels in both aquaporins.

HvPIP2;8 has a dual function as both water and cation channel. Ion channel characteristics are influenced by K^+ and divalent cation, and protein interactions. HvPIP2;8-associated ion currents were detected with Na^+ and K^+ ($Na^+ > K^+$) but not Cs^+, Rb^+, or Li^+, and were inhibited by Ca^{2+}, Ba^{2+}, Cd^{2+} and lesser by Mg^{2+}, which also interacted with Ca^{2+}. Currents were reduced in the presence of K^+, Cs^+, Rb^+, or Li^+ relative to Na^+ alone. Five HvPIP1 isoforms co-expressed with HvPIP2;8 inhibited the ion conductance relative to HvPIP2;8 alone but HvPIP1;3 and HvPIP1;4 with HvPIP2;8 showed the ion conductances at a lower level. *HvPIP2;8* transcript increased in barley shoot tissues after salt treatments in a salt-tolerant cultivar Haruna-Nijo and K305, but not in salt-sensitive I743.

OsPIP2;4 in rice (*Oryza Sativa* L. cv. Nipponbare) was expressed dominantly in the root, and OsPIP2;4-protein was detected in young root epidermis and exodermis. OsPIP2;4 permeated both Na^+ and K^+ in low external free Ca^{2+} concentration (permeability sequence: $K^+ > Na^+ > Rb^+ \approx Cs^+ > Li^+$), but the ion transport activity was inhibited by high Ca^{2+} condition and other divalent cations such as Ba^{2+}, Cd^{2+} and Mg^{2+}. OsPIP2;4-associated ion currents were decreased in the presence of Rb^+, Cs^+, Li^+ relative Na^+ alone. Three OsPIP1 (OsPIP1;1 to OsPIP1;3) isoforms inhibited the OsPIP2;4 ionic conductance when they were co-expressed with OsPIP2;4. OsPIP2;4-overexpressing plant at the reproductive growth stage accumulated more Na^+ in all tissues of the upper parts with a significant difference from wild type, meanwhile, K^+ content was lower under 150 mM NaCl treatment. However, the imposition of salinity stress on the knockout (KO) plants caused a significant reduction of Na^+ accumulation in aerial organs, in particular, nodes (I, II) and internode II. K^+ content exhibited higher in KO than wild type.

The artificial mutants HvPIP2;8 F283K and OsPIP2;4 G278K were lost ions transporting function compared with wild type HvPIP2;8 and OsPIP2;4, respectively. In contrast, both mutants showed water permeability with no significant difference from wild type, suggesting that the water and ion transport activity are different in mutants HvPIP2;8 F283K and OsPIP2;4 G278K. A phenylalanine (F283) of HvPIP2;8 and glycine (G278) of OsPIP2;4 in C-terminal tails are an essential amino acid for ion transport function, and lysine (K) is a key residue leading to losing ion transport activity in both HvPIP2;8 and OsPIP2;4 but not water permeability.

Detail mechanisms for the channel gating and the link between water and ion transport depending on the interaction between monomers have not been well investigated as well as activation mechanisms of the central pore, too. Further studies of how ion channel gating is related to water flow will reveal the molecular relationships between water and ion flows in plant.

In conclusion, our electrophysiological analyses of barley HvPIP and rice OsPIP aquaporins expressed in *X. laevis* oocytes have shown that HvPIP2;8 and OsPIP2;4 facilitates an ionic conductance at the plasma membrane in the presence of Na^+ and/or K^+ with external Ca^{2+}-sensitive manner, respectively. Co-expression of HvPIP1s/HvPIP2;8 and OsPIP1s/OsPIP2;4 significantly reduced the HvPIP2;8 or OsPIP2;4-dependent ionic conductances. HvPIP2;8 and OsPIP2;4 are likely to be subject to complex regulation involving heteromerization and post-translational modification. As a physiological role, it was demonstrated that Na^+ uptake by OsPIP2;4 and HvPIP2;8, and different accumulation in every aerial part at the reproductive growth stage of transgenic rice plants. These findings indicate a newly recognized function of OsPIP2;4 in response at first in rice plants with insight into the potential roles of plant aquaporins under salt stress. Future research will uncover the molecular and structural mechanisms that control the dual permeability of aquaporins for ion and water, and more testing of the physiological role of HvPIP2;8 and OsPIP2;4 *in planta*.

Acknowledgements

Undertaking this Ph.D. study has been a truly life-changing experience for me, and it would have been impossible without the support and guidance that I have received from many organizations and people.

First and foremost, I would like to express my deepest and sincerest gratitude thanks to my supervisor Professor Dr. Maki Katsuhara. I am grateful to him for allowing me to study in his laboratory. I do appreciate his patient, valuable and professional instructions, and advice in my experiments and my thesis. And I also sincerely appreciate his great help in my daily life.

Secondly, I would like to express my sincere thanks to my co-supervisors Professor Dr. Jian Feng Ma and Associate Professor Dr. Takayuki Sasaki for their useful suggestions and insightful comments on my experiments and my thesis. I want to express my deep thanks to Associate Professor Dr. Tomoaki Horie, Shinshu University, Japan for providing materials for my experiments and supporting me with good opportunities to join in his research project. I would like to express my deep thanks to the Australian research group for co-laboratory in my first paper. I also want to give my sincere thanks to Yoshiyuki Tsuchiya for his kind help during my experiments. Many thanks to all of my lab members for their warmhearted help and encouragement not only in the laboratory but also in daily life in Japan.

Thirdly, I would like to express thank the Ministry of Education, Culture, Sports, Science, and Technology (MEXT) scholarship for the financial support during my study in Japan. I would like to thank the Faculty of Agronomy, Hue University of Agriculture and Forestry, Hue University, Vietnam for their support time, and encouragement for my Ph.D. study in Japan.

Last but not the least, I would like to thank my beloved parents and family for their warmest support, patience, and encouragement for all of my pursuits, without their support, I would not go that far. Especially, I would like to thanks to my twin nephew, Tran Duy Kien and Tran Duy Khoi, who always provide me the positive energy to help me pass all difficulties.

September, 2021

Tran Thi Huong Sen